TSUNAMI ANALYSIS OF $(Th, Pu)O_2$ BENCHMARK EXPERIMENTS IN ZED-2

SENSITIVITY AND UNCERTAINTY ANALYSIS OF $(Th, Pu)O_2$ BENCHMARK EXPERIMENTS IN ZED-2 USING TSUNAMI

BY

TING ZHU, B.A.Sc.

A THESIS

SUBMITTED TO THE DEPARTMENT OF ENGINEERING PHYSICS

AND THE SCHOOL OF GRADUATE STUDIES

OF MCMASTER UNIVERSITY

IN PARTIAL FULFILMENT OF THE REQUIREMENTS

FOR THE DEGREE OF

MASTER OF APPLIED SCIENCE

Master of Applied Science (2011) McMaster University

(Engineering Physics) Hamilton, Ontario, Canada

TITLE:	Sensitivity and Uncertainty Analysis of $(Th, Pu)O_2$ Benchmark Experiments in ZED-2 Using TSUNAMI
AUTHOR:	Ting Zhu Bachelor of Applied Science in Engineering Science (Physics) University of Toronto, Toronto, Canada
SUPERVISOR:	Dr. Adriaan Buijs
NUMBER OF PAGES:	x, 88

Abstract

In 1984, the ZED-2 research reactor was used to study five $(Th, Pu)O_2$ fuel bundles with the goal to provide both benchmark tests for future reactor code validation and experimental measurements for a possible thorium fuel cycle in CANDU. In this work, the neutronic models of these critical experiments were investigated by TSUNAMI, a sensitivity and uncertainty (S/U) analysis tool, part of the SCALE6 reactor physics package from the Oak Ridge National Laboratory.

TSUNAMI consists of different modules that are capable of calculating the values of k_{eff} and the uncertainties in k_{eff} due to uncertainties in the nuclear data. It generates energy-dependent sensitivity coefficients from which the percentage change in k_{eff} due to perturbations in nuclear data values can be determined. The calculated k_{eff} has a bias which is the difference between calculation and measurement. Several sources of uncertainties are responsible for the observed k_{eff} bias. But the most dominant and universal contributor is the uncertainties in the nuclear data. Because of the shared nature of nuclear data in all simulations, correlations among the calculated k_{eff} values exist and can be measured in terms of the correlations in the nuclear data uncertainties. TSUNAMI provides a consistent and systematic approach to examine these correlations and their effect on k_{eff} biases. It also offers an interesting application of the Generalized Linear Least Squares (GLLS) methodology which applies adjustments to the original nuclear data so that k_{eff} biases are reduced.

Using TSUNAMI, the computed k_{eff} values agree with the experimental k_{eff} up to a bias of 2.3mk or lower. It is also found that the list of top uncertainty contributors in k_{eff} is identical among the simulations, confirming a high degree of correlation in the nuclear data uncertainties. An illustrative example demonstrated the application of TSUNAMI to coolant void reactivity. In this particular simulation, the coolant density was reduced to mimic the loss of coolant condition. Positive reactivity was induced as the simulation predicted. Through S/U analysis, the uncertainty in the computed reactivity was determined in a similar fashion as the k_{eff} uncertainty. Top reactivity uncertainty contributors were also identified. Finally the GLLS procedure was explored using the coolant void example along with the experiments.

Even though the results are not conclusive on the applicability of these $(Th, Pu)O_2$ ZED-2 benchmark experiments to future thorium CANDU reactors, they have called attention to the need for a larger number and better designs of relevant benchmark experiments. It is proposed that they should be designed to maximize the sensitivity information of thorium and plutonium in order to offer more meaningful S/U analysis and establish good confidence in the future investigation of $(Th, Pu)O_2$ fuel in CANDU reactors.

Acknowledgements

I would like to express my gratitude to my thesis supervisor Dr. Adriaan Buijs for the opportunity of entering the interesting field of reactor physics. I owe the productive and stimulating experience during my Master's studies to Dr. Buijs' recommendation, support and guidance.

I am also grateful to Dr. Jimmy Chow from the Atomic Energy of Canada Limited, with whom I was always able to have lively discussions and benefited greatly from his working experience of TSUNAMI.

This work would not have been possible without the financial support from Dr. David Novog and I appreciate his insights and feedback for making this thesis a better piece of work.

Tremendous thanks to my fellow graduate students and my summer student Russell Truesdell. It has been a really fun ride!

Finally, I can never be more thankful to my parents and Ben Schmidt for supporting me in my selfish pursuit of knowledge.

Contents

List of Tables

List of Figures

Chapter 1

Introduction

1.1 Motivation

Between mid-1950s and 1970s, experiments were conducted for thorium-based fuel designs in several types of reactors, as part of the international endeavour in developing a thorium-based fuel cycle (see IAEA, 2005). In Canada, headed by the Atomic Energy of Canada Limited (AECL), there were similar efforts to investigate the physics parameters of thorium-based fuels, specifically by utilizing heavy water-moderated reactors. Given the greater abundance of thorium (Th) in nature than uranium (U), thorium combined with plutonium (Pu) in particular has been found to show significant promises in many aspects. The $(Th, Pu)O_2$ fuel provides an attractive solution for the incineration of weapon- or civilian-grade plutonium. In contrast to $(Th, U)O_2$, there is no further production of plutonium associated with $(Th, Pu)O_2$. Fertile ^{232}Th breeds fissile ^{233}U whose fission neutron yield per neutron absorbed is higher than that of U^{235} in thermal reactors. $(Th, Pu)O_2$ fuel is also considered proliferation-resistant due to the formation of ^{232}U which has strong gamma radiation daughter products (IAEA, 2005).

1.2 Problem Statement

In reactor physics, the value of the multiplication factor k_{eff} characterizes the state of a system under three conditions:

$$k_{eff} \begin{cases} > 1 & \text{supercritical} \\ = 1 & \text{critical} \\ < 1 & \text{subcritical} \end{cases}$$

If a nuclear fission experiment is performed and measured to have a steady state of neutron population, the experiment is by definition a critical experiment. Furthermore, a benchmark experiment is a critical experiment which is well-characterized in order to provide a reliable basis for the comparison between its experimental measurements and computational results from simulations (CNSC, 2009). One of the most frequently cited computational results is the value of k_{eff}. Since the benchmark experiment is critical by design, the experimental k_{eff} is equal to 1. The k_{eff} calculation of the benchmark

experiment however, may not duplicate the exact value of 1 due to several uncertainty sources. The difference between the experimentally measured and the computed values of k_{eff} is defined as the computational bias:

$$\beta_c = |k_m - k_c| = |1 - k_c|$$

The types of uncertainties which could interfere with the k_{eff} computation and hence contribute to the k_{eff} bias include (Williams *et al.*, 2009b):

1. *numerical approximations* which consist of computer rounding and truncation errors, as well as intelligent approximations used to solve the neutron transport equation;

2. *system modelling approximations* that come from deliberate simplifications of the computer replica of the physical system and experimental uncertainties in material compositions, densities, dimensions, purities, and so forth;

3. *input data uncertainties* which are uncertainties in the evaluated nuclear data such as microscopic cross sections, fission spectra, neutron yield, and scattering distributions that are contained in ENDF/B (nuclear data library). This type of uncertainties is universal in the sense that it is consistently affecting all simulations regardless of the model complexity or computational method (stochastic or deterministic), as long as the same nuclear data are used.

The aforementioned uncertainty sources not only contribute to the computational bias for benchmark experiments, but also more importantly, they result in unknown computational biases to systems that do not have experimental measurements such as for new bundle or lattice configuration designs. Suppose a series of benchmark experiments were performed on a new fuel design. Computer simulations could indicate the extent of bias and uncertainty in the calculated k_{eff} values. If we can understand the propagation of uncertainties from the different uncertainty sources into the known computational bias β_c, we can extend the understanding to the computed k_{eff} for design systems (aka. without experimental measurements) that are simulated using the same computer code and nuclear data library as the benchmark experiment simulation.

In order to achieve this, we first have to determine an appropriate suite of benchmark experiments and quantify their applicability to the design system. Traditionally, the selection is based on similarity in physical characteristics and through expert judgment. However, this approach can be limited

by more complex designs for which it could be expensive to perform adequate benchmark experiments and measurements. Also, some benchmark experiments could have been done decades ago such that there is a lack of rigorous documentation on the sources of uncertainties, thus resulting in biases that are difficult to account for. In this work, a set of critical experiments involving five $(Th, Pu)O_2$ bundles were selected. Even though they were performed as benchmark experiments, due to the small number of $(Th, Pu)O_2$ bundles and the age of the experiments, their applicability to be used adequately by the traditional approach is more challenging to assess.

The scope of this work is focused on modelling the benchmark experiments using a Monte Carlo code called KENO from the SCALE6 package from Oak Ridge National Laboratory, followed by a sensitivity and uncertainty analysis using the TSUNAMI modules also from SCALE6. Through systematic and consistent sensitivity/uncertainty approaches, the sources of biases in the calculated k_{eff} values can be identified, as well as in other parameters such as the coefficient of Coolant Void Reactivity. The scope of this work is not to establish applicability of the $(Th, Pu)O_2$ benchmark experiments for future thorium CANDU reactors using the TSUNAMI techniques. That would be another Master's project which could apply the results from this work to examine similar isotopic sensitivities, the biases due to the same Monte Carlo computational method and nuclear data used.

Chapter 2

Methodology

Neutron transport problems have long rooted in the study of the Boltzmann transport equation whose derivation is intuitive but whose solution is more difficult to obtain. Until the development of computers having sufficient computing capabilities, the study of neutron behaviour in complicated systems such as nuclear reactors was quite limited, leading to highly simplified models such as those using only two neutron energy groups. The increasing sophistication of reactor systems requires the transport equation to be solved in three dimensions and using multigroups (more than two) or even continuous energy structures in order to be accurate. Two state-of-art reactor physics codes suitable for this purpose are based on the method of Monte Carlo: (1) MCNP (Monte Carlo N-Particles) by Los Almos National Laboratory and (2) KENO in the SCALE6 (Standard Computer Analyses for Licensing Evaluation V.6) package by Oak Ridge National Laboratory. However, only the SCALE6 package has the built-in capability of sensitivity and uncertainty analysis by perturbation. In Section 2.1 of this chapter, several important Monte Carlo features are explained while the complete theory can be found in numerous works such as by Spanier and Gelbard (1969), Carter and Cashwell (1975) and Lewis and Miller (1984). Section 2.2 unfolds how perturbation theory and adjoint-flux method together provide an extremely efficient means to determine reactivity changes. Finally in Section 2.3 and Section 2.4, the definitions and calculations of the sensitivity coefficient and k_{eff} uncertainty are presented.

2.1 Monte Carlo Techniques

The inspiration for the term *Monte Carlo* comes from the Monte Carlo casino in Monaco. It is a natural reminder of the characteristics of this increasingly popular computational method, which are randomness and probability. They can be illustrated by the example of rolling an ordinary die. Even though the outcome of each roll is randomly generated, the distribution of the outcomes should follow the predicted probability: equal for each of the six faces of the die. There are numerous physical processes that can be simulated using the Monte Carlo method. In our case, we are interested in simulating and determining the motion of neutrons in a nuclear reactor.

2.1.1 Simulating Neutron Motion

Monte Carlo technique treats the motion of a single neutron as a random walk process governed by probabilities. As the neutron travels through a medium, it interacts with other particles. The probabilities dictating these different interactions are related to a variable called cross section. The probability density, $p(s)$ of a neutron is the product of its probability to have travelled through a distance from 0 to s without interaction and then to have an interaction at s (see Hébert, 2009, chapt. 2.4). It is:

$$p(s) = e^{-\int_0^s \Sigma_t(s')ds'} \cdot \Sigma_t(s) \tag{2.1}$$

where Σ_t is called the total macroscopic cross section with a unit of cm^{-1} and $\Sigma_t(s)$ represents the total probability of all kinds of interactions at s. Thus the probability of the neutron having an interaction at x is:

$$P(x) = \int_0^x p(s)ds = 1 - e^{-\int_0^x \Sigma_t(s')ds'} \tag{2.2}$$

Suppose we randomly generate the probability to be $P = 1 - \xi$, where $\xi \in \Re$ and $0 \leq \xi \leq 1$:

$$P = 1 - \xi = 1 - e^{-\int_0^x \Sigma_t(s')ds'} \tag{2.3}$$

We can obtain the length x of the neutron flight path in terms of the probability P by calculating the value of x such that Equation (2.4) is satisfied:

$$\int_0^x \Sigma_t(s')ds' = -\ln \xi \tag{2.4}$$

If Σ_t is constant along the neutron flight path, it can be taken out of the integral and the neutron path length calculation is simplified as:

$$x = -\frac{\ln \xi}{\Sigma_t} \tag{2.5}$$

Otherwise, it can be very time consuming to compute the value of x which would satisfy Equation (2.4). Various methods are compared by Brown and Martin (2003).

2.1.2 Neutron Flux Estimators

In the previous section, the motion of neutrons was shown to be simulated rather easily and quickly. However, as the number of neutron simulations increases, the speed and memory requirements call for intelligent methods to manage the vast amount of information on these neutron trajectories. Furthermore, knowing the detailed trajectories, we can technically determine the number of neutrons passing through any location $\vec{r}$, any surface or volume in the system at any given time, which is more useful information. The neutron flux ϕ which is the long-sought solution to the neutron transport problem (Section 2.2.1) is obtained using **estimators**, a statistic concept adopted in Monte Carlo method. Several estimators have been developed using different estimation approaches. In the following, three common neutron flux estimators are explained.

Track Length Estimator

As its name suggests, the track length estimator calculates fluxes by summing all distances which are covered by neutrons in volume V. Equation (2.5) shows an individual neutron path length x_1 as a result of Σ_t and a preselected probability ξ. The neutron undergoes an interaction at the end of x_1 and travels for another x_2, still inside volume V but with a different Σ_t' and probability ξ'. This process continues until the neutron leaves the volume V or is absorbed. Let l_n be the sum of path lengths traversed by a single neutron:

$$l_n = \sum_i x_i \tag{2.6}$$

The total flight distance L covered by N neutrons inside the volume V in one unit of time (one second) can then be found as:

$$L = \sum_n^N l_n \tag{2.7}$$

In a unit time, the distance l_n is the same as the speed $|\vec{v}_n|$ of the neutron. Therefore, $L = \sum_n^N |\vec{v}_n|$. It will be shown in Section 2.2.1 that, the definition of groupwise scalar flux allows it to be equated to the total distance travelled in one second by all of the N particles with the same speed $|\vec{v}_n|$:

$$\phi(\vec{r}, E, t) = \int_{4\pi} d\hat{\Omega} \left(N(\vec{r}, E, \hat{\Omega}, t) \cdot \vec{v}_n(\hat{\Omega}, \mathrm{v_n}) \right) = \sum_n^N |\vec{v}_n| = \sum_n^N l_n \tag{2.8}$$

Hence, the track length estimator calculates the groupwise scalar flux inside a unit volume to be:

$$\phi_{g,V} = \frac{1}{V}\sum_{n}^{N} l_n \tag{2.9}$$

Some references (such as by Lewis and Miller (1984)) continue to normalize flux $\phi_{g,V}$ to a source strength of one neutron:

$$\tilde{\phi}_{g,V} = \frac{1}{V}\frac{1}{N}\sum_{n}^{N} l_n \tag{2.10}$$

Collision Estimator

The collision estimator uses the rate of collision (R) resulted from a flux of neutrons interacting with target particles with Σ_t per unit volume:

$$R = \Sigma_t(\vec{r}, E)\phi(\vec{r}, \hat{\Omega}, E, t) \tag{2.11}$$

Let C be the number of collisions in a unit time ($\triangle t$ = one second) and a unit volume (V):

$$C = R\triangle tV = \Sigma_t\phi\triangle tV \tag{2.12}$$

Since Monte Carlo keeps track of neutron trajectories, the number of collisions for each user-defined mesh volume V is readily available. Scalar flux ϕ per unit time can be easily calculated as:

$$\phi = \frac{C}{\Sigma_t V} \tag{2.13}$$

Equation (2.13) can also be normalized to a source strength of one neutron:

$$\phi = \frac{1}{N}\frac{C}{\Sigma_t V} \tag{2.14}$$

The downside of the collision estimator is that when the medium is "optically thin", meaning there are few collision events in the medium. The scalar flux result can especially suffer from large variances if not allowed to be computed using a sufficiently large number of simulations.

Last-event Estimator

This estimator records events of neutron capture as opposed to events of collision in the collision estimator (see Carter and Cashwell, 1975, chapt. 4, p. 50). This method can underestimate the flux in medium consisting of low neutron capture isotopes and result in large variances.

2.1.3 Analog vs. Non-Analog

It is generally true that the standard deviation (σ) of the estimator is proportional to $1/\sqrt{N}$ where N is the number of repeated trials of the estimator calculation (see Lewis and Miller, 1984, chapt. 7.4, p. 317). This implies that an acceptable variance (σ^2) is to be supported by a large number of Monte Carlo runs, which proceed in cycles or generations. A generation is defined from the "birth" of S_i number of neutrons to their "death" (by absorption or escape). At the end of the i^{th} generation, the S_{i+1} number of neutrons become the "seeds" (source distribution) for the next generation $i+1$. The number of randomly generated neutrons (called histories) per generation and the number of generations are two important quantities which ideally should be as large as possible. Clearly this ideal situation is limited by the available computation time and memory. In order to achieve a well-balanced computational time and result variance, the method of **importance sampling** is often applied in Monte Carlo simulations by changing the neutron transport process from **analog** to **non-analog**.

From its birth to its death, if the neutron's history is calculated using "natural" probabilities, the entire process is called analog. This means the simulation of neutron random walk is faithfully following the physics of neutron interaction with matter. On the other hand, the non-analog process does not follow the physical neutron transport process exactly. It involves several sampling schemes which either reduce the computing time or the variance of the estimator calculations.

The motivation behind the non-analog process can be explained well using an example of shielding calculation (see Lewis and Miller, 1984, chapt. 7.6, p. 327-334). The flux value at the outside of the shield is contributed by a relatively small number of neutrons that succeed in penetrating the shield. The probability density function describing this shielding case is:

$$f(x) = c \cdot \delta(x - x_o) + g(x) \tag{2.15}$$

where the $c \cdot \delta(x - x_o)$ term represents the large fraction of neutrons which fail to penetrate the shield at x_o and $g(x)$ represents the distribution of distances

x that neutrons make after escaping from absorption in the shield. Since the total probability is 1 and we can obtain the following relations:

$$\int f(x)dx = c \cdot \int \delta(x - x_o)dx + \int g(x)dx \tag{2.16}$$

$$\int g(x)dx = 1 - c \tag{2.17}$$

On one hand, $g(x)$ is a continuous probability density function and can be represented by the track length estimator. On the other hand, the last-event estimator is suitable for describing the $c \cdot \delta(x - x_o)$ probability. Clearly the track length estimator alone cannot provide the complete representation of the physical process due to the relatively smaller contribution from the escaped neutrons. As shown, a proper and realistic sampling scheme should be a combination of both probability densities. However, if following an analog simulation, the number of neutron histories generated would have to be large enough to give a good sample of neutrons passing through the shielding due to its low probability (calculated by $1 - c$). Since using a very large number of neutrons and keeping track of their histories can lead to very time consuming computation, an alternative was proposed.

Let $\tilde{f}(x)$ be the modified probability density function to the original $f(x)$. A weight function can be defined as:

$$\mathrm{w}(x) = \frac{f(x)}{\tilde{f}(x)} \tag{2.18}$$

It follows that the expectation of the estimator is unchanged:

$$E[x] = \int x f(x)dx = \int x \frac{f(x)}{\tilde{f}(x)} \tilde{f}(x)dx = \int x \mathrm{w}(x) \tilde{f}(x)dx \tag{2.19}$$

$\tilde{f}(x)$ can be derived from physical experience. Using the example of shielding calculation again, we should focus on those surviving neutrons by sampling the $g(x)$ part of the distribution more. One approach of achieving this modified sampling scheme is to raise the number of these "important" neutrons, while appropriately lowering their respective weights. This can be seen in Equation (2.19) that the overall effect is unchanged in the product of $\mathrm{w}(x)\tilde{f}(x)$, meaning the estimator is maintained unbiased. This sampling scheme is one of the **Russian roulette** methods. Another common Russian roulette sampling scheme replaces the $c \cdot \delta(x - x_o)$ estimator with a multi-step termination process. First the neutron weight is compared to a threshold

value. A random number ξ between 0 and 1 is generated. Another user-defined input number Ξ is compared with ξ, followed by the choice of termination of neutron history: if $\xi > 1/\Xi$, the history is terminated; otherwise, the history is continued with a new weight which is equal to the product of Ξ and the initial weight.

Comparing the two types of Russian roulette, they have opposite effects on the estimator variance. The splitting-neutron (first) type improves the variance in that a larger number of more important contributors is available. But this method can suffer from longer computational time since for each additional neutron, there has to be a simulation of its flight and interaction history. On the other hand, the termination (second) type gains in faster computational time in exchange with a larger variance. Neither schemes should be used alone since they can be more suitable in different situations and media respectively.

2.2 Perturbation theory

2.2.1 Neutron Transport Equation

> The transport equation is introduced to describe a population of neutral particles such as neutrons or photons, in a closed domain, under transient (i.e., time-dependent) or steady state (i.e., stationary) conditions. Its derivation is based on the principle of particle conservation. - Hébert (2009)

Compared to the elaborate schemes of Monte Carlo method shown in the previous section, the derivation of the neutron transport equation is intuitive and deterministic. Instead of describing each and every neutron's motion, it considers a group of neutrons N inside a control volume V at some location $\vec{r}$ in space, travelling in a cone of $d\hat{\Omega}$ about the direction $\hat{\Omega}$ with energies between E and dE at time t. Equation (2.20) is the time dependent, integro-differential form of the neutron transport equation whose left hand side represents the net rate of mass flow and the three terms on the right sum up the three mechanisms that can gain or lose neutrons.

$$\frac{\partial}{\partial t}N(\vec{r},\hat{\Omega},E,t) = -\hat{\Omega}\cdot\nabla\phi(\vec{r},\hat{\Omega},E,t) - \Sigma(\vec{r},E)\phi(\vec{r},\hat{\Omega},E,t) + Q(\vec{r},\hat{\Omega},E,t) \tag{2.20}$$

where $\phi(\vec{r},\hat{\Omega},E,t)$ is the angular flux in phase space $(\vec{r},\hat{\Omega},E,t)$. By definition,

it is equal to:

$$\phi(\vec{r}, \hat{\Omega}, E, t) = N(\vec{r}, E, \hat{\Omega}, t) \cdot \vec{v}_n(\hat{\Omega}, \mathrm{v_n}) \tag{2.21}$$

where $\mathrm{v_n} = \sqrt{2E/\text{mass of neutron}}$. The scalar flux can be obtained by:

$$\phi(\vec{r}, E, t) = \int_{4\pi} d\hat{\Omega}\phi(\vec{r}, \hat{\Omega}, E, t) \tag{2.22}$$

If all of the conditions are time-independent, Equation (2.20) can be reduced to:

$$\hat{\Omega} \cdot \nabla\phi(\vec{r}, \hat{\Omega}, E) + \Sigma(\vec{r}, E)\phi(\vec{r}, \hat{\Omega}, E) = Q(\vec{r}, \hat{\Omega}, E) \tag{2.23}$$

Equation (2.23) says that the loss of neutrons in phase space due to neutrons leaving the control volume, and neutrons undergoing collisions in the volume V which has a total cross section Σ, is equal to the gain of neutrons from some neutron source Q. Under this perfect balance, the state of the system is at equilibrium and thus time-independent. The solution to Equation (2.23), ϕ can be solved analytically or iteratively in very simple geometries. But the Monte Carlo method described previously has huge advantage in terms of implementation and computations in computer codes for sophisticated systems.

2.2.2 Neutron Transport in Operator Notation

At steady state, the creation and destruction rates of neutrons are equal and have been described by Equation (2.23). In a multiplying system, the source term Q can be explicitly written out to reflect the fission mechanism:

$$Q(\vec{r}, \mathsf{E}) = \chi(E) \int d\mathsf{E}'\nu\Sigma_f(\vec{r}, \mathsf{E}')\phi(\vec{r}, \mathsf{E}') \tag{2.24}$$

where $\mathsf{E} = (\hat{\Omega}, E)$, $\nu\Sigma_f(\vec{r}, \mathsf{E}') = \nu(\vec{r}, E')\Sigma_f(\vec{r}, \mathsf{E}')$ and $\nu(\vec{r}, E')$ is the number of secondary neutrons per fission at energy E'. $\chi(E)$ is the fission distribution dependent of neutron energy E in unit of $1/E$. The second term of Equation (2.23) can also be separated into absorption and scattering reactions:

$$\begin{aligned}\Sigma(\vec{r}, E)\phi(\vec{r}, \mathsf{E}) =& \Sigma_t(\vec{r}, E)\phi(\vec{r}, \mathsf{E}) \\ &- \int d\mathsf{E}'\Sigma_s(\vec{r}, E' \to E, \hat{\Omega}' \to \hat{\Omega})\phi(\vec{r}, \mathsf{E}')\end{aligned} \tag{2.25}$$

Therefore, the steady state neutron transport equation with fission,

absorption and scattering reactions can be re-written using the operator notation:

$$\mathbf{L}\phi(\vec{r},\mathsf{E}) = [\hat{\Omega}\cdot\nabla + \Sigma_t(r,E)]\phi(\vec{r},\mathsf{E}) - \int d\mathsf{E}'\Sigma_s(\vec{r},E'\to E,\hat{\Omega}'\to\hat{\Omega})\phi(\vec{r},\mathsf{E}') \tag{2.26}$$

$$\mathbf{M}\phi(\vec{r},\mathsf{E}) = \chi(E)\int d\mathsf{E}'\nu\Sigma_f(\vec{r},\mathsf{E}')\phi(\vec{r},\mathsf{E}') \tag{2.27}$$

It should be noted that the above derivation is based on certain simplifications and assumptions. First of all, the fission spectrum notation $\chi(E)$ is for the total spectrum since we must be reminded that there are prompt and delayed neutrons resulted from fission and fission products (see Rozon, 1998, chapt. 2.3.1, p. 46-47):

$$\chi(E) = \frac{\nu_p\chi_p(E) + \sum_j \nu_{dj}\chi_{dj}(E)}{\nu} \tag{2.28}$$

where subscripts p and d denote prompt and delayed neutron quantities. Secondly, we have equated the source term Q in Equation (2.24) to fission only. This is equivalent to assuming that the steady transport equation is only valid in the absence of external sources.

For a critical system, $\mathbf{L}\phi$ is equal to $\mathbf{M}\phi$ which means the production of neutrons by fission is the same as the destruction from leakage (streaming), absorption and scattering. The effective multiplication factor, $\mathrm{k_{eff}}$ is introduced as shown in Equation (2.29) such that we can still write the neutron transport equation in operator notations even if the system is not critical:

$$\mathbf{L}\phi(\vec{r},\mathsf{E}) = \frac{1}{\mathrm{k_{eff}}}\mathbf{M}\phi(\vec{r},\mathsf{E}) \tag{2.29}$$

Equation (2.29) is essentially an eigenvalue problem after some algebraic arrangements:

$$\mathbf{L}^{-1}\mathbf{M}\phi = \mathrm{k_{eff}}\phi \tag{2.30}$$

where $\mathbf{L}^{-1}$ is the inverse of $\mathbf{L}$. In order for the flux to have a non-trivial solution, the required condition is:

$$\det(\mathbf{L}^{-1}\mathbf{M} - \mathrm{k_{eff}}\mathbf{I}) = 0 \tag{2.31}$$

where $\mathbf{I}$ is the identity operator. The solution ϕ which is the flux and the

eigenfunction, can only be positive, in the physical sense. Since only the fundamental eigenmode can satisfy this condition, it is the only physical solution.

2.2.3 Adjoint-based First-order Linear Perturbation

Perturbation

If we introduce some small perturbations into the system described by Equation (2.29), such as by changing the amount of absorbing or fissile materials, the behaviour of k_{eff} is expected to change, as well as the flux. The very simply case of these perturbations is assumed to be first-order and linear, meaning that we can add the perturbations ($\triangle$) directly to the unperturbed operators, the flux and k_{eff} as shown below:

$$\mathbf{L} = \mathbf{L_o} + \triangle\mathbf{L} \tag{2.32}$$

$$\mathbf{M} = \mathbf{M_o} + \triangle\mathbf{M} \tag{2.33}$$

$$\phi = \phi_o + \triangle\phi \tag{2.34}$$

$$k_{eff} = k_o + \triangle k \tag{2.35}$$

Therefore, the equation for the eigenvalue problem becomes:

$$(\mathbf{L_o} + \triangle\mathbf{L}) \cdot (\phi_o + \triangle\phi) = \frac{1}{k_o + \triangle k}(\mathbf{M_o} + \triangle\mathbf{M}) \cdot (\phi_o + \triangle\phi) \tag{2.36}$$

The assumption that the perturbation is very small and consequently the change in k_{eff} is also small, leads to $\triangle k/k_o \ll 1$ and we can apply the binomial approximation:

$$\frac{1}{k_o + \triangle k} = \frac{1}{k_o(1 + \triangle k/k_o)} \approx \frac{1}{k_o}(1 - \triangle k/k_o) = \frac{1}{k_o} - \frac{\triangle k}{k_o^2} \tag{2.37}$$

Given the definition of reactivity being $\rho = (k - 1)/k$, the following substitution is made:

$$\triangle\rho \approx \frac{\triangle k}{k_o^2} \tag{2.38}$$

$$\frac{1}{k_o + \triangle k} \approx \frac{1}{k_o} - \triangle\rho \tag{2.39}$$

We can combine equations (2.36) and (2.39) and arrive at Equation (2.40). The second and third order terms are grouped together and shall be

omitted in the first-order perturbation approximation.

$$(\triangle\mathbf{L} - \frac{1}{\mathrm{k_o}}\triangle\mathbf{M})\phi_o + (L_o - \frac{1}{\mathrm{k_o}}\mathbf{M_o})\triangle\phi + \triangle\rho\mathbf{M_o}\phi_o = \mathcal{O}(\triangle^2, \triangle^3) \approx 0 \quad (2.40)$$

$$\mathcal{O}(\triangle^2, \triangle^3) = \frac{1}{\mathrm{k_o}}\triangle\mathbf{M}\triangle\phi - \triangle\rho(\triangle\mathbf{M}\phi_o + \mathbf{M_o}\triangle\phi + \triangle\mathbf{M}\triangle\phi) \quad (2.41)$$

After re-arranging Equation (2.40), the change in reactivity is found:

$$\triangle\rho \approx -\frac{(\triangle\mathbf{L} - \frac{1}{\mathrm{k_o}}\triangle\mathbf{M})\phi_o + (L_o - \frac{1}{\mathrm{k_o}}\mathbf{M_o})\triangle\phi}{\mathbf{M_o}\phi_o} \quad (2.42)$$

While the perturbations in the operators are known, the perturbed flux ($\triangle\phi$) needs to be calculated to determine $\triangle\rho$. This could potentially lead to intensive computations because each time a perturbation is made, the neutron transport equation has to be solved (using Monte Carlo or transport codes) to acquire $\triangle\phi$. This can become tedious. A better approach for faster computation is explained in the following.

Adjoint-based Perturbation

Suppose there exists some particle flux $\phi_o^\dagger$, operators $\mathbf{M_o}^\dagger$, $\mathbf{L_o}^\dagger$ as well as a multiplication factor $\mathrm{k_o^\dagger}$ in their unperturbed states. They satisfy the following relation and form the same eigenvalue problem:

$$\mathbf{L_o}^\dagger\phi_o^\dagger = \frac{1}{\mathrm{k_o^\dagger}}\mathbf{M_o}^\dagger\phi_o^\dagger \quad (2.43)$$

When the following relations are also satisfied, the terms with the $\dagger$ superscript are said to be the adjoint of the original terms in Equation (2.29):

$$\langle\phi_o^\dagger, \mathbf{L_o}\phi_o\rangle = \langle\mathbf{L_o}^\dagger\phi_o^\dagger, \phi_o\rangle \quad (2.44)$$

$$\langle\phi_o^\dagger, \frac{1}{\mathrm{k_o}}\mathbf{M_o}\phi_o\rangle = \frac{1}{\mathrm{k_o}}\langle\phi_o^\dagger, \mathbf{M_o}\phi_o\rangle = \frac{1}{\mathrm{k_o^\dagger}}\langle\mathbf{M_o}^\dagger\phi_o^\dagger, \phi_o\rangle \quad (2.45)$$

It is shown in chapter 2.4.1, pages 64-65 of Rozon (1998) that $\mathrm{k_o} = \mathrm{k_o^\dagger}$. The $\langle\cdots\rangle$ notation is the same as that for the inner product operation:

$$\langle f, h\rangle = \int_{\mathrm{V}} d^3r \int dE d\hat{\Omega} f(\vec{r}, E, \hat{\Omega}) h(\vec{r}, E, \hat{\Omega}) \quad (2.46)$$

In Equation (2.42), if we apply the adjoint flux as a weighting function

in the following manner:

$$\triangle\rho \approx -\frac{\langle\phi_o^\dagger, (\triangle\mathbf{L} - \frac{1}{\mathrm{k_o}}\triangle\mathbf{M})\phi_o\rangle + \langle\phi_o^\dagger, (\mathbf{L_o} - \frac{1}{\mathrm{k_o}}\mathbf{M_o})\triangle\phi\rangle}{\langle\phi_o^\dagger, \mathbf{M_o}\phi_o\rangle} \tag{2.47}$$

It can be shown that the knowledge of $\triangle\phi$ is not required to compute $\triangle\rho$. Let us focus on the inner product with $\triangle\phi$:

$$\begin{aligned}\langle\phi_o^\dagger, (\mathbf{L_o} - \frac{1}{\mathrm{k_o}}\mathbf{M_o})\triangle\phi\rangle &= \langle\phi_o^\dagger, \mathbf{L_o}\triangle\phi\rangle - \frac{1}{\mathrm{k_o}}\langle\phi_o^\dagger, \mathbf{M_o}\triangle\phi\rangle \\ &= \langle\mathbf{L_o}^\dagger\phi_o^\dagger, \triangle\phi\rangle - \frac{1}{\mathrm{k_o^\dagger}}\langle\mathbf{M_o}^\dagger\phi_o^\dagger, \triangle\phi\rangle \\ &= \langle(\mathbf{L_o}^\dagger - \frac{1}{\mathrm{k_o^\dagger}}\mathbf{M_o}^\dagger)\phi_o^\dagger, \triangle\phi\rangle = 0 \end{aligned} \tag{2.48}$$

The inner product with $\triangle\phi$ in Equation (2.48) makes no difference due to:

$$(\mathbf{L_o}^\dagger - \frac{1}{\mathrm{k_o^\dagger}}\mathbf{M_o}^\dagger)\phi_o^\dagger = 0 \tag{2.49}$$

Therefore, the change in reactivity has been derived by the adjoint-based first-order linear perturbation method as:

$$\triangle\rho = -\frac{\langle\phi_o^\dagger, (\triangle\mathbf{L} - \frac{1}{\mathrm{k_o}}\triangle\mathbf{M})\phi_o\rangle}{\langle\phi_o^\dagger, \mathbf{M_o}\phi_o\rangle} \tag{2.50}$$

Adjoint Flux

We have seen from Equation (2.50), the need for the adjoint flux in solving perturbation problems. The adjoint integro-differential neutron transport equation is shown here using the $L^\dagger$ operator on the adjoint flux $\phi^\dagger$:

$$\left[-\hat{\Omega}\cdot\nabla + \Sigma_t(\vec{r}, E)\right]\phi^\dagger(\vec{r}, \mathsf{E}) - \int d\mathsf{E}'\Sigma_s(\vec{r}, \mathsf{E}\rightarrow\mathsf{E}')\phi^\dagger(\vec{r}, \mathsf{E}') = S^\dagger(\vec{r}, \mathsf{E}) \tag{2.51}$$

where $S^\dagger$ is used to denote the general adjoint source for simplicity. Irving (1971) showed that the adjoint flux is the *importance* of a particle leaving a collision. Irving's derivation and the concept of *importance* can be found in Irving (1971) and Lewins (1965) respectively. The steps to simulate the adjoint equation in Monte Carlo are similar to those of the forward equation. First coined by Irving (1971), *adjunctons* are artificial particles that satisfy Equation (2.51). Analogous to the neutrons, adjunctons are made to travel a certain distance governed by Equation (2.1), then undergo an interaction.

The forward and adjoint calculations differ in the values of cross sections which dictate the type of interaction and the consequent trajectory (see Irving, 1971).

2.3 k_{eff} Sensitivity Coefficients

As mentioned, perturbations on the system can be caused by the change in absorbing or fissile material concentration for example. A sensitivity coefficient is defined as a measure for the system k_{eff} change due to specific parameter changes. It has been found that for some parameters, there are both explicit and implicit effects which must be considered at the same time. The determination of the sensitivity coefficients can help identify those parameters to which k_{eff} value is sensitive and to what extent.

2.3.1 Explicit Sensitivity

Previously, the derivation of the perturbation method has been first-order and linear. Suppose there is a change in the macroscopic cross section (Σ) and this change leads to a change in the k_{eff} value. To characterize the relative change in k_{eff} due to a small perturbation in Σ, a factor called the sensitivity coefficient $S_{k,\Sigma}$ is defined to be used such that:

$$\frac{\triangle k}{k} = S_{k,\Sigma}\left(\frac{\triangle \Sigma}{\Sigma}\right) \tag{2.52}$$

Rearranging the terms and changing the finite $\triangle$ differences to partial derivatives, the sensitivity coefficient of k_{eff} to macroscopic cross section $\Sigma(\vec{r})$ at some point in phase-space $\vec{r}$ becomes (see Rearden, 2004):

$$S_{k,\Sigma(\vec{r})} = \frac{\Sigma(\vec{r})}{k}\frac{\triangle k}{\triangle \Sigma(\vec{r})} = \frac{\Sigma(\vec{r})}{k}\frac{\partial k}{\partial \Sigma(\vec{r})} \tag{2.53}$$

where the $\partial k/\partial \Sigma$ term can be further modified using Equation (2.38):

$$S_{k,\Sigma(\vec{r})} = \frac{\Sigma(\vec{r})}{k}\frac{k^2 \partial \rho}{\partial \Sigma(\vec{r})} \tag{2.54}$$

Using Equation (2.50), the reactivity change with respect to macroscopic cross section becomes:

$$\frac{\triangle \rho}{\triangle \Sigma} = \frac{\partial \rho}{\partial \Sigma} = -\frac{\langle \phi_o^\dagger, (\partial \mathbf{L}/\partial \Sigma - \frac{1}{k_o}\partial \mathbf{M}/\partial \Sigma)\phi_o \rangle}{\langle \phi_o^\dagger, \mathbf{M_o}\phi_o \rangle} \tag{2.55}$$

Finally substitute $\partial\rho/\partial\Sigma$ into Equation (2.54) and the sensitivity coefficient can be calculated as:

$$\begin{aligned} S_{\mathrm{k},\Sigma(\vec{r})} &= \frac{\Sigma(\vec{r})}{\mathrm{k}}\frac{\partial\rho\cdot\mathrm{k}^2}{\partial\Sigma(\vec{r})} \\ &= \frac{\Sigma(\vec{r})}{\mathrm{k}}\left(-\frac{\left\langle\phi_o^\dagger(\vec{\xi})\left[\frac{\partial\mathbf{L}[\Sigma(\vec{\xi})]}{\partial\Sigma(\vec{r})}-\frac{1}{\mathrm{k}}\frac{\partial\mathbf{M}[\Sigma(\vec{\xi})]}{\partial\Sigma(\vec{r})}\right]\phi_o(\vec{\xi})\right\rangle}{\left\langle\phi_o^\dagger(\vec{\xi})\frac{1}{\mathrm{k}^2}\mathbf{M_o}[\Sigma(\vec{\xi})]\phi_o(\vec{\xi})\right\rangle}\right) \end{aligned} \tag{2.56}$$

where $\vec{\xi}$ is the phase-space vector for ($\vec{r}$,E). The flux perturbation due to cross section perturbation is taken into account by $\triangle\phi$ and it has been shown that it is not required for the adjoint-based first-order linear approximation in Equation (2.48).

While $S_{\mathrm{k},\Sigma(\vec{r})}$ is energy group- , space- and direction-integrated (from $\langle\cdots\rangle$), the sensitivity coefficient for reaction x, isotope i, energy group g and mesh region z is computed as the following (see Rearden, 2004):

$$S_{\mathrm{k},\Sigma^i_{x,g,z}} = \frac{1}{D}\left(T^i_{1,x,g,z}+T^i_{2,f,g,z}+T^i_{3,x,g,z}\right) \tag{2.57}$$

where $T^i_{1,x,g,z}$, $T^i_{2,f,g,z}$, and $T^i_{3,x,g,z}$ compute the perturbation effects in the three processes: (1) neutron loss, (2) fission production and (3) scattering to group of interest. They are expanded to be:

$$T^i_{1,x,g,z} = -\Sigma^i_{x,g,z}V_z\sum_{j=0}^{\mathrm{NMOM}}(2l+1)\tilde{\phi}^{\dagger j}_{g,z}\tilde{\phi}^{j}_{g,z} \tag{2.58}$$

$$T^i_{2,f,g,z} = \frac{1}{\mathrm{k}}V_z\bar{\nu}^i_{g,z}\Sigma^i_{f,g,z}\phi_{g,z}\sum_{g'=1}^{G}\phi^\dagger_{g',z}\chi_{g',z} \tag{2.59}$$

$$T^i_{3,x,g,z} = \sum_{j=0}^{\mathrm{NMOM}}V_z\sum_{g'=1}^{G}\tilde{\phi}^{\dagger j}_{g',z}\tilde{\phi}^{j}_{g,z}\Sigma^{l,i}_{x,g'\to g,z} \tag{2.60}$$

where $\tilde{\phi}^{\dagger j}_{g,z}$ is the j-th component real-valued adjoint flux moment for energy group g and region z. l is the Legendre order that corresponds to the j-th real-valued flux moment. NMOM is the number of real-valued flux moments matching to the desired Legendre order of expansion. $\chi^i_{g',z}$ represents the average fraction of fission neutrons emitted into energy group g' from fission of isotope i in region z, and $\bar{\nu}^i_{g,z}$ represents the average number of fission neutrons emitted from fission of isotope i in energy group g and in region z.

The macroscopic cross section is denoted by $\Sigma^i_{x,g,z}$ where x can be replaced by f to indicate specifically the fission reaction. $\Sigma^{l,i}_{x,g'\to g,z}$ in $T^i_{3,x,g,z}$ is a component of the group-to-group scattering matrix for the l'th scattering moment of reaction x (see Rearden, 2004). D is the denominator portion of Equation (2.56):

$$\begin{aligned} D &= \mathrm{k}\left\langle \phi_o^\dagger(\vec{\xi})\frac{1}{\mathrm{k}^2}\mathbf{M_o}[\Sigma(\vec{\xi})]\phi_o(\vec{\xi})\right\rangle \\ &= \frac{1}{\mathrm{k}}\sum_{i=1}^{I}\sum_{z=1}^{R}V_z\sum_{g=1}^{G}(\bar{\nu}^i_{g,z}\Sigma^i_{f,g,z}\phi_{g,z})\sum_{g'=1}^{G}(\chi^i_{g',z}\phi^\dagger_{g',z}) \end{aligned} \tag{2.61}$$

2.3.2 Implicit Sensitivity

For a fast reactor system, the definition of sensitivity coefficient from Equation (2.53) is generally sufficient. However, for a thermal reactor system where resonance shielding becomes important in the sensitivity of $\mathrm{k_{eff}}$, *implicit* sensitivity coefficients are required (Williams *et al.*, 2001) in addition to the *explicit* sensitivity coefficients described above. For example, perturbation in hydrogen isotope will affect $\mathrm{k_{eff}}$ explicitly, as well as the resonance escape probability of uranium isotopes implicitly. To represent this implicit effect, we can denote the sensitivity coefficient of the uranium isotope due to the hydrogen isotope as $S_{\mathrm{u,h}}$, while using α_{u} and ω_{h} to denote general parameters for these two isotopes such as number density or cross section:

$$S_{\mathrm{u,h}} = \frac{\omega_{\mathrm{h}}}{\alpha_{\mathrm{u}}}\frac{\triangle\alpha_{\mathrm{u}}}{\triangle\omega_{\mathrm{h}}} \tag{2.62}$$

Also, the $\mathrm{k_{eff}}$ sensitivity coefficient due to α_{u} is:

$$S_{\mathrm{k,u}} = \frac{\alpha_{\mathrm{u}}}{\mathrm{k}}\frac{\triangle\mathrm{k}}{\triangle\alpha_{\mathrm{u}}} \tag{2.63}$$

Together, the implicit sensitivity of $\mathrm{k_{eff}}$ due to perturbation in parameter ω_{h} is:

$$S_{\mathrm{k,h}} = \left(\frac{\alpha_{\mathrm{u}}}{\mathrm{k}}\frac{\triangle\mathrm{k}}{\triangle\alpha_{\mathrm{u}}}\right)\left(\frac{\omega_{\mathrm{h}}}{\alpha_{\mathrm{u}}}\frac{\triangle\alpha_{\mathrm{u}}}{\triangle\omega_{\mathrm{h}}}\right) = S_{\mathrm{k,u}}S_{\mathrm{u,h}} \tag{2.64}$$

The above expression illustrates the general method of determining the implicit sensitivity coefficient. Detailed mathematical derivation of implicit sensitivity coefficient is provided by Rearden (2004) and several calculation

methods are presented by Williams *et al.* (2001). Finally, the complete group-wise, reaction-, nuclide- specific k_{eff} sensitivity coefficient is a sum of the explicit and implicit coefficients:

$$\left(S_{k,\Sigma^i_{x,g}}\right)_{\text{total}} = \left(S_{k,\Sigma^i_{x,g}}\right)_{\text{explicit}} + \left(S_{k,\Sigma^i_{x,g}}\right)_{\text{implicit}} \tag{2.65}$$

2.4 k_{eff} Uncertainty

The Monte Carlo method is based on probabilities and we have seen its statistic characteristics in terms of estimators, expectation values, etc. The value of k_{eff} calculated using the Monte Carlo method is taken as the mean value of a set of Monte Carlo calculations which are stabilizing and approaching convergence. Associated with the mean k_{eff} value, the standard deviation of the mean k_{eff} is another statistic feature. However, it is not to be confused with the uncertainty in k_{eff} as a result of uncertainties in the three sources discussed in Chapter 1.2: (1) method simplifications, computer's numerical and rounding errors, (2) computer model's uncertainties and (3) nuclear data uncertainties. The first and second types of uncertainty vary according to the computational method, computer capability and the degree of accuracy of the models respectively. On the other hand, uncertainties in the nuclear data are propagated to the k_{eff} value from experimental uncertainties when nuclear data were measured. The treatment of the nuclear data uncertainties is explained in the following.

To begin, let us study the propagation of uncertainty which determines the variance of function $\mathcal{F}(a,b)$ with two dependent variables a and b for simplicity. It is calculated as:

$$\sigma^2_{\mathcal{F}} = \left(\frac{\partial \mathcal{F}}{\partial a}\right)^2 \sigma^2_a + \left(\frac{\partial \mathcal{F}}{\partial b}\right)^2 \sigma^2_b + 2\left(\frac{\partial \mathcal{F}}{\partial a}\right)\left(\frac{\partial \mathcal{F}}{\partial b}\right)\sigma^2_{ab} \tag{2.66}$$

$$= \begin{pmatrix} \frac{\partial \mathcal{F}}{\partial a} & \frac{\partial \mathcal{F}}{\partial b} \end{pmatrix} \begin{pmatrix} \sigma^2_a & \sigma^2_{ab} \\ \sigma^2_{ab} & \sigma^2_b \end{pmatrix} \begin{pmatrix} \frac{\partial \mathcal{F}}{\partial a} \\ \frac{\partial \mathcal{F}}{\partial b} \end{pmatrix} \tag{2.67}$$

where σ^2_a and σ^2_b are the variances of a and b, and σ^2_{ab} is their covariance. Also, the first-order Taylor expansion of $\mathcal{F}$ is assumed:

$$\mathcal{F}(a,b) \approx \mathcal{F}(a_o,b_o) + \left[\frac{\partial \mathcal{F}(a_o,b_o)}{\partial a}\triangle a + \frac{\partial \mathcal{F}(a_o,b_o)}{\partial b}\triangle b\right] \tag{2.68}$$

Extending the formulation of Equation (2.66) to the calculation of k_{eff} uncertainty[1], it is obvious that the value of k_{eff} is a function of the nuclear data $\Sigma^i_{x,g}$. The sensitivity coefficients $S_{k,\Sigma^i_{x,g}}$ are essentially the partial derivatives in Equation (2.66). If we know the nuclear data uncertainty information, specifically the variances and covariances, the propagation of uncertainty leads to Equation (2.69) which defines the variance of k_{eff} to be the quadratic product of the groupwise sensitivity coefficient vectors and a covariance matrix:

$$\sigma_k^2 = \vec{S_k} \mathbf{C}_{\alpha\alpha} \vec{S_k^T} \tag{2.69}$$

where matrix $\mathbf{C}_{\alpha\alpha}$ is the nuclear data covariance matrix. The subscript $\alpha\alpha$ is used as a reminder that $\mathbf{C}_{\alpha\alpha}$ has the dimension of a matrix.

The variance of the nuclear data (α) can be easily determined as the expected square of the difference between the measured α value and its expected value (equivalent to *mean*):

$$\mathrm{V}(\alpha) \equiv \langle \delta\alpha^2 \rangle = \int (\alpha - \langle \alpha \rangle)^2 \, d\alpha \tag{2.70}$$

In the case of two variables α_n, α_p, they can have a covariance which is defined as:

$$\mathrm{COV}\,(\alpha_n, \alpha_p) = \langle \delta\alpha_n, \delta\alpha_p \rangle = \int (\alpha_n - \langle \alpha_n \rangle)(\alpha_p - \langle \alpha_p \rangle) d\alpha_n d\alpha_p \tag{2.71}$$

When we speak of nuclear data α, the term in fact encompasses reaction cross sections (σ), neutron energy distribution from fission (χ) and the average number of neutrons emitted per fission ($\bar{\nu}$). Using one single vector, α can store M elements:

M = I number of isotopes×X number of reactions×G number of energy groups

While the dimension of $\vec{S_k}$ is $1 \times M$, $\mathrm{COV}\,(\alpha_n, \alpha_p)$ is a matrix of the size $M \times M$. The nuclear data covariance matrix $\mathbf{C}_{\alpha\alpha}$ is constructed such that the relative variances are along the matrix diagonal and the relative covariances are the off-diagonal elements:

$$\mathbf{C}_{\alpha\alpha} \equiv \frac{\mathrm{COV}\,(\alpha_n, \alpha_p)}{\alpha_n \alpha_p} \tag{2.72}$$

[1] In order to avoid confusing it with the statistic variance, the term "uncertainty" is used to denote the k_{eff} variance due to uncertainties in the nuclear data.

By convention, the sensitivity vector $\vec{S_k}$ and the covariance matrix $\mathbf{C}_{\alpha\alpha}$ are referred to by their nuclide-reaction types together, then the energy group. This pair-up of isotope and reaction is more convenient and meaningful in terms of examining the uncertainty contributors as we will see in examples later. Expanding Equation (2.69) into a sum of elements:

$$\sigma_k^2 = \sum^{(I\times X)^2} V_{ix,i'x'} \tag{2.73}$$

The value of σ_k^2 is calculated from the sum of energy-integrated uncertainty contributions from all possible (and relevant) nuclide-reaction pairs (ix). When putting the energy-integrated contributions in a $(I \times X) \times (I \times X)$ matrix, the diagonal elements correspond to the variance $V_{ix,ix} = \sigma_{ix}^2$ of nuclide-reaction pair ix. The off-diagonal elements are equal to the covariance $V_{ix,i'x'}$ between nuclide-reaction pairs ix and $i'x'$. An important realization is that, when an off-diagonal element of the covariance matrix $\mathbf{C}_{\alpha\alpha}$ is negative, it will make the corresponding uncertainty contribution in σ_k^2 be negative. Therefore, some covariances are negative (denoted by V^-) and some are positive (V^+):

$$\sigma_k^2 = \sum V^+ - \sum |V^-| \tag{2.74}$$

Mathematically, the negative covariances are subtracted from the calculation of the σ_k^2. However, this operation does not mean such negative covariances are subtracted from the system uncertainty and should not be interpreted that they reduce the k_{eff} uncertainty. It should be taken simply as a result of the fact that the covariance of the two nuclide-reaction pairs ix and $i'x'$ is negative.

2.5 Generalized Linear Least-Squares Method

The need for GLLS method arises because the uncertainties in nuclear data affect the accuracy of the calculated k_{eff} values. Suppose a number of experiments were performed and their k_{eff} values were measured and represented by a vector $\vec{m} = \{m_i, i = 1, 2, \cdots, I\}$, where I is the number of experiments of interest. For each of these experiments, the value of k_{eff} could be calculated by computer codes and stored in a vector $\vec{k} = \{k_i, i = 1, 2, \cdots, I\}$ whose elements correspond in sequence to the ones of $\vec{m}$. The deviation of the measured k_{eff} from their corresponding calculated k_{eff} is $\vec{d} = \vec{k} - \vec{m}$. GLLS method utilizes the deviation vector $\vec{d}$ to find a unique set of nuclear data $\vec{\alpha'} = \{\alpha_n + \delta\alpha_n, n = 1, 2, \cdots, N\}$ where $\delta\alpha_n$ are the adjustments made by

GLLS method. Under linearity restriction and with the knowledge of *absolute* sensitivity coefficients $S_{\mathrm{k}} = \partial \mathrm{k}_i / \partial \alpha_n$, the adjusted k becomes:

$$\mathrm{k}'(\alpha') = \mathrm{k}'(\alpha + \delta\alpha) \approx \mathrm{k}(\alpha) + \delta\mathrm{k} \approx \mathrm{k}(\alpha) + S_{\mathrm{k}}\delta\alpha \tag{2.75}$$

If *relative* sensitivity coefficients from Equation (2.53) are used, the *relative* deviation vector $\vec{d_r}$ has the following definition shown in Equation (2.76). For simplicity, the derivation of GLLS method is illustrated only in the *absolute* terms here. The full derivation can be found in Appendix B of Broadhead *et al.* (1999) and the complete results for both *absolute* and *relative* derivations are summarized by Williams *et al.* (2009b).

$$\vec{d_r} = \left\{ d_i = \frac{\mathrm{k}_i(\vec{\alpha}) - \mathrm{m}_i}{\mathrm{k}_i(\vec{\alpha})}, i = 1, 2, \cdots, I \right\} \tag{2.76}$$

Now let the discrepancy between $\vec{\mathrm{k}'}$ and $\vec{\mathrm{m}}$ be denoted as:

$$\vec{y} = \vec{\mathrm{k}'} - \vec{\mathrm{m}} = \vec{\mathrm{k}} + S_{\mathrm{k}}\vec{\delta\alpha} - \vec{\mathrm{m}} = \vec{d} + S_{\mathrm{k}}\vec{\delta\alpha} \tag{2.77}$$

It is obvious that $\vec{y}$ can be controlled by choosing the $\delta\alpha$ values from the uncertainties in nuclear data. Recall the relative covariance of nuclear data from Equation (2.71):

$$\mathbf{C}_{\alpha\alpha} = \frac{\mathrm{COV}\left(\alpha_n, \alpha_p\right)}{\alpha_n \alpha_p} \tag{2.78}$$

To continue the *absolute* derivations, the absolute covariance of nuclear data is thus:

$$\mathrm{C}_{\alpha\alpha} = \mathrm{COV}\left(\alpha_n, \alpha_p\right) = \langle \delta\alpha_n, \delta\alpha_p \rangle \tag{2.79}$$

Similarly, the measured and calculated $\mathrm{k_{eff}}$ values (in vectors $\vec{\mathrm{m}}$ and $\vec{\mathrm{k}}$), as well as the deviation between them ($\vec{d}$) have uncertainties in covariance matrices in $\mathrm{C_{mm}}$, $\mathrm{C_{kk}}$ and $\mathrm{C_{dd}}$ respectively:

$$\mathrm{C_{mm}} = \mathrm{COV}\left(m_n, m_p\right) = \langle \delta m_n, \delta m_p \rangle \tag{2.80}$$

$$\mathrm{C_{kk}} = \mathrm{COV}\left(k_n, k_p\right) = \langle \delta k_n, \delta k_p \rangle \tag{2.81}$$

$$\mathrm{C_{dd}} = \mathrm{COV}\left(d_n, d_p\right) = \langle \delta(k-m)_n, \delta(k-m)_p \rangle \tag{2.82}$$

The covariances of mixed nuclear data and $\mathrm{k_{eff}}$ can also be defined: $\mathrm{C}_{\alpha\mathrm{m}} = \langle \delta\alpha_{\mathrm{n}}, \delta\mathrm{m_p} \rangle$. However, they are often assumed to be zero initially and then acquire values in the GLLS calculations (see Appendix B of Broadhead *et al.* (1999) and Williams *et al.* (2009b)). Here we follow the same assumption and neglect the cross term $\mathrm{C}_{\alpha\mathrm{m}}$. Therefore, the covariance matrix of $\vec{d}$ can be

simplified in the following manner:

$$\begin{aligned} \mathrm{C_{dd}} &= \langle \delta(k-m)_n, \delta(k-m)_p \rangle && (2.83)\\ &= \langle \delta(k-m)\delta(k-m)^{\mathrm{T}} \rangle && (2.84)\\ &= \langle \delta k \delta k^{\mathrm{T}} \rangle + \langle \delta m \delta m^{\mathrm{T}} \rangle - \langle \delta k \delta m^{\mathrm{T}} \rangle - \langle \delta m \delta k^{\mathrm{T}} \rangle && (2.85)\\ &= \mathrm{C_{kk}} + \mathrm{C_{mm}} - S_k \langle \delta\alpha \delta m^{\mathrm{T}} \rangle - \langle \delta m \delta \alpha^{\mathrm{T}} \rangle S_k^{\mathrm{T}} && (2.86)\\ &\approx \mathrm{C_{kk}} + \mathrm{C_{mm}} && (2.87) \end{aligned}$$

It should be noted that the goal of GLLS method is not simply to minimize the discrepancy $\vec{y}$. Since S_k has dimensions of I by M, it is not a square matrix and thus not invertible. In Equation (2.77), it is impossible to force $\vec{y} = \vec{0}$ and then to calculate $\vec{\delta\alpha}$ from $-S_k^{-1}\vec{d}$. What this means is that there can exist several sets of $\vec{\delta\alpha}$ that satisfy Equation (2.77). As its name suggests, GLLS is based on the least-squares fit method and it uses Equation (2.77) as a *forcing* condition. The term that should be minimized is:

$$Q = \delta\vec{\alpha}^{\mathrm{T}} \mathrm{C}_{\alpha\alpha}^{-1} \delta\vec{\alpha} + \vec{y}^{\mathrm{T}} \mathrm{C}_{\mathrm{mm}}^{-1} \vec{y} \qquad (2.88)$$

where $\mathrm{C}_{\alpha\alpha}^{-1}$ and $\mathrm{C}_{\mathrm{mm}}^{-1}$ are inverse of the symmetric matrices $\mathrm{C}_{\alpha\alpha}$ and C_{mm} and $\vec{y}$ is under the constraint of Equation (2.77). Note that the cross terms are ignored in the definition of Q here which will not (and should not) affect the result compared to the full derivation.

The unique set of $\{\delta\alpha_i\}$ such that the value of Q is minimized is determined using the Lagrange Multiplier method and the solution is shown by Wagschal and Yeivin (1980). Since there is only one constraint from Equation (2.77), only one Lagrange multiplier λ (dimension: $I \times 1$) is needed. The first step is to define the conditional-minimum formulation in the form:

$$\begin{aligned} \Lambda &= Q + 2\lambda^{\mathrm{T}}(S_{\mathrm{k}}\delta\alpha - y + d)\\ &= \delta\alpha^{\mathrm{T}} \mathrm{C}_{\alpha\alpha}^{-1} \delta\alpha + y^{\mathrm{T}} \mathrm{C}_{\mathrm{mm}}^{-1} y + 2\lambda^{\mathrm{T}}(S_{\mathrm{k}}\delta\alpha - y + d) \end{aligned} \qquad (2.89)$$

where the number 2 is included for the mathematical convenience as a common factor as shown in the following. Impose the condition $\nabla_{\delta\alpha,y,\lambda}\Lambda(\delta\alpha, y, \lambda) = 0$:

$$\frac{\partial\Lambda}{\partial(\delta\alpha)} = 2\delta\alpha^{\mathrm{T}} \mathrm{C}_{\alpha\alpha}^{-1} + 2\lambda^{\mathrm{T}} S_{\mathrm{k}} = 0 \qquad (2.90)$$

$$\frac{\partial\Lambda}{\partial y} = 2y^{\mathrm{T}} \mathrm{C}_{\mathrm{mm}}^{-1} - 2\lambda^{\mathrm{T}} = 0 \qquad (2.91)$$

$$\frac{\partial \Lambda}{\partial \lambda} = 2(S_{\mathrm{k}}\delta\alpha - y + d) = 0 \tag{2.92}$$

It is easy to solve for the three unknowns from the three equations above:

$$\lambda = (\mathrm{C_{mm}} + S_{\mathrm{k}}\mathrm{C}_{\alpha\alpha}S_{\mathrm{k}}^{\mathrm{T}})^{-1}d = \mathrm{C_{dd}^{-1}}d \tag{2.93}$$

$$\delta\alpha = (-\lambda^{\mathrm{T}}S_{\mathrm{k}}\mathrm{C}_{\alpha\alpha})^{\mathrm{T}} = -\mathrm{C}_{\alpha\alpha}^{\mathrm{T}}S_{\mathrm{k}}^{\mathrm{T}}\lambda = -\mathrm{C}_{\alpha\alpha}S_{\mathrm{k}}^{\mathrm{T}}\mathrm{C_{dd}^{-1}}d \tag{2.94}$$

$$y = \mathrm{C_{mm}C_{dd}^{-1}}d \tag{2.95}$$

Putting them back into Equation (2.88):

$$\begin{aligned} Q_{\min} &= \left(-\mathrm{C}_{\alpha\alpha}S_{\mathrm{k}}^{\mathrm{T}}\mathrm{C_{dd}^{-1}}d\right)^{\mathrm{T}}\mathrm{C}_{\alpha\alpha}^{-1}\left(-\mathrm{C}_{\alpha\alpha}S_{\mathrm{k}}^{\mathrm{T}}\mathrm{C_{dd}^{-1}}d\right) + \left(\mathrm{C_{mm}C_{dd}^{-1}}d\right)^{\mathrm{T}}\mathrm{C_{mm}^{-1}}\left(\mathrm{C_{mm}C_{dd}^{-1}}d\right) \\ &= d^{\mathrm{T}}\left\{\left(\mathrm{C}_{\alpha\alpha}S_{\mathrm{k}}^{\mathrm{T}}\mathrm{C_{dd}^{-1}}\right)^{\mathrm{T}}S_{\mathrm{k}}^{\mathrm{T}}\mathrm{C_{dd}^{-1}} + \left(\mathrm{C_{mm}C_{dd}^{-1}}\right)^{\mathrm{T}}\mathrm{C_{dd}^{-1}}\right\}d \\ &= d^{\mathrm{T}}\left\{\mathrm{C_{dd}^{-1^{\mathrm{T}}}}S_{\mathrm{k}}\mathrm{C}_{\alpha\alpha}{}^{\mathrm{T}}S_{\mathrm{k}}^{\mathrm{T}}\mathrm{C_{dd}^{-1}} + \mathrm{C_{dd}^{-1^{\mathrm{T}}}C_{mm}}{}^{\mathrm{T}}\mathrm{C_{dd}^{-1}}\right\}d \\ &= d^{\mathrm{T}}\mathrm{C_{dd}^{-1^{\mathrm{T}}}}\left(S_{\mathrm{k}}\mathrm{C}_{\alpha\alpha}{}^{\mathrm{T}}S_{\mathrm{k}}^{\mathrm{T}} + \mathrm{C_{mm}}{}^{\mathrm{T}}\right)\mathrm{C_{dd}^{-1}}d \qquad (2.96) \\ &= d^{\mathrm{T}}\mathrm{C_{dd}^{-1}}d \qquad (2.97) \end{aligned}$$

where we have used $(\mathrm{C_{dd}^{-1}})^{\mathrm{T}} = (\mathrm{C_{dd}^{T}})^{-1}$ and $\mathrm{C_{dd}^{T}} = \mathrm{C_{dd}}$. The result of $Q_{\min}$ is essentially the χ^2 of the fitted nuclear data with adjustments that are consistent within the nuclear data uncertainties (Williams *et al.*, 2009b). In the simplest case of a single system measurement, $Q_{\min}$ is easily found to have the expression of χ^2:

$$Q_{\min} = \frac{(\mathrm{k} - \mathrm{m})^2}{\sigma_{\mathrm{m}}^2 + \sigma_{\mathrm{k}}^2} = \chi^2 \tag{2.98}$$

The new covariances of nuclear data are derived in Appendix B of Broadhead *et al.* (1999), including the use of the cross terms:

$$\mathrm{C}_{\alpha'\alpha'} = \mathrm{C}_{\alpha\alpha} - (\mathrm{C}_{\alpha\mathrm{m}} - \mathrm{C}_{\alpha\alpha}S_{\mathrm{k}}^{\mathrm{T}})\mathrm{C_{dd}^{-1}}\left(\mathrm{C}_{\mathrm{m}\alpha} - S_{\mathrm{k}}\mathrm{C}_{\alpha\alpha}\right) \tag{2.99}$$

Finally the new set of nuclear data and adjusted $\mathrm{k_{eff}}$ can be calculated, where α, $\mathrm{C}_{\alpha\alpha}$ and S_{k} are known and $\mathrm{C_{dd}^{-1}}d$ is computed iteratively with the updated α' and k' after each iteration, until a minimized χ^2 per degree of freedom is achieved:

$$\alpha' = \alpha + \left(-\mathrm{C}_{\alpha\alpha}S_{\mathrm{k}}^{\mathrm{T}}\mathrm{C_{dd}^{-1}}d\right) \tag{2.100}$$

$$\mathrm{k}' = \mathrm{k} + S_{\mathrm{k}}\left(-\mathrm{C}_{\alpha\alpha}S_{\mathrm{k}}^{\mathrm{T}}\mathrm{C_{dd}^{-1}}d\right) \tag{2.101}$$

Chapter 3

TSUNAMI Codes

TSUNAMI stands for the Tools for Sensitivity and UNcertainty Methodology Implementation. It is part of the SCALE6 code package developed at the Oak Ridge National Laboratory. As a control module in SCALE6, TSUNAMI consists of several independent control modules and functional modules, which perform in sequence to determine k_{eff}, sensitivity and uncertainty information and etc. The classification of these modules (control or functional), their features and the detailed implementation of TSUNAMI are explained by Rearden (2004). As mentioned in Chapter 2, TSUNAMI was chosen because of its built-in and comprehensive capability of sensitivity and uncertainty analysis. In this chapter, the overall TSUNAMI sequence employed in our study will be presented and accompanied by the explanation of the role of each module.

3.1 Overall TSUNAMI Sequence

The TSUNAMI sequence starts with the control module TSUNAMI-3D. The main components of TSUNAMI-3D are the two functional modules:

1. KENO is a three-dimensional (3D) Monte Carlo code capable of calculating forward and adjoint fluxes and the system's k_{eff}.

2. SAMS (Sensitivity Analysis Module for SCALE) generates sensitivity coefficients (S_k) and the uncertainty of k_{eff} (σ_k^2) using the adjoint-based first-order linear perturbation theory presented in Chapter 2.3 and Chapter 2.4.

The sensitivity and uncertainty results from TSUNAMI-3D are stored in sensitivity data files which become the inputs for three TSUNAMI utility modules:

1. TSAR (Tool for Sensitivity Analysis of Reactivity): similar to TSUNAMI-3D, it generates sensitivity coefficients (S_ρ) and the uncertainty of reactivity response (σ_ρ) between two systems due to system parameter changes such as coolant void, fuel temperature, moderator purity, etc.

2. TSUNAMI-IP (Indices and Parameters): it generates specific indices to characterize the similarity and correlation among selected systems.

3. TSURFER (Tool for Sensitivity/Uncertainty analysis of Response Functionals using Experimental Results): it uses the method of Generalized Linear Least Squares to determine a unique set of nuclear data which would generate a computed k_{eff} value very close to its experimental value, thus reducing the bias in computational k_{eff} values.

The aforementioned modules, their inputs and outputs are illustrated in Figure 3.1.

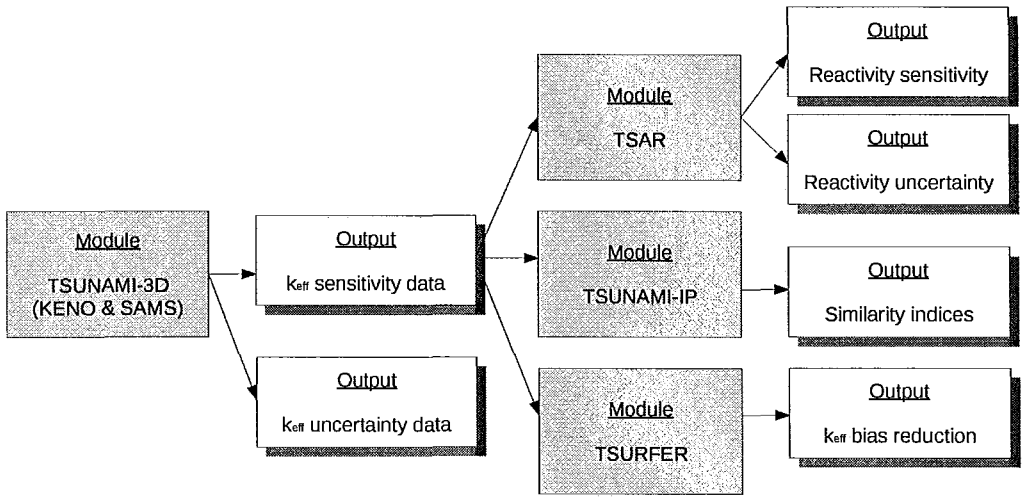

Figure 3.1: TSUNAMI work-flow sequence shows the connection among the modules.

3.2 TSUNAMI-3D Control Sequence

Figure 3.2 illustrates the sequence of modules that are involved in generating the neutron flux, the value of k_{eff} and the SAMS module outputs. In parallel on the right is the required information from a TSUNAMI-3D input file.

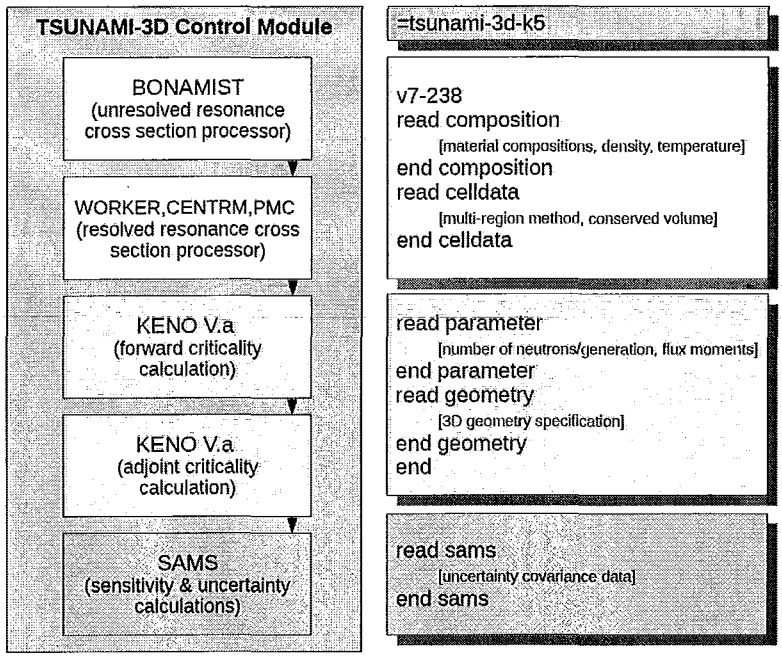

Figure 3.2: Components of TSUNAMI-3D control module on the left and the corresponding (coloured) parts of the input file on the right.

3.2.1 Call of Control Module

The identifier for the TSUNAMI-3D module call is: `=tsunami-3d-k5`. This line at the beginning of the input file informs SCALE6 that a TSUNAMI-3D control sequence is to be executed. In this work, the determination of k_{eff} and forward/adjoint fluxes has been done by KENO V.a. SCALE6 has both KENO V.a and KENO VI modules, the latter of which has several new options which are not required for the purpose of this work. KENO V.a is sufficient, meanwhile requiring much less memory and computation time than KENO VI.

3.2.2 Preparation of Cross Section Data

The nuclear cross section library used is `v7-238` which contains all ENDF/B-VII.0 nuclide data in a 238-group structure from 10^{-5}eV to 2×10^{7}eV (Bowman and Dunn, 2009). Following the specification of the nuclear cross section library, the precise compositions of materials used in the modelling of the reactor are input between `read composition` and `end composition`. Every material specified in this section has to have a unique material ID.

For each material mixture, the specification also requires density, temperature and weight percentages of the involved isotopes. The cross section values and multigroup structure for the isotopes are determined by the chosen nuclear cross section library (`v7-238` in this case).

A problem-dependent cross section data library needs to be prepared for KENO V.a. It is called the "working" library because it consists of only cross sections that are relevant for the specific problem and is processed to be group-averaged and self-shielded. In the `tsunami-3d-k5` module, the determination of the working library is automated using functional modules illustrated below:

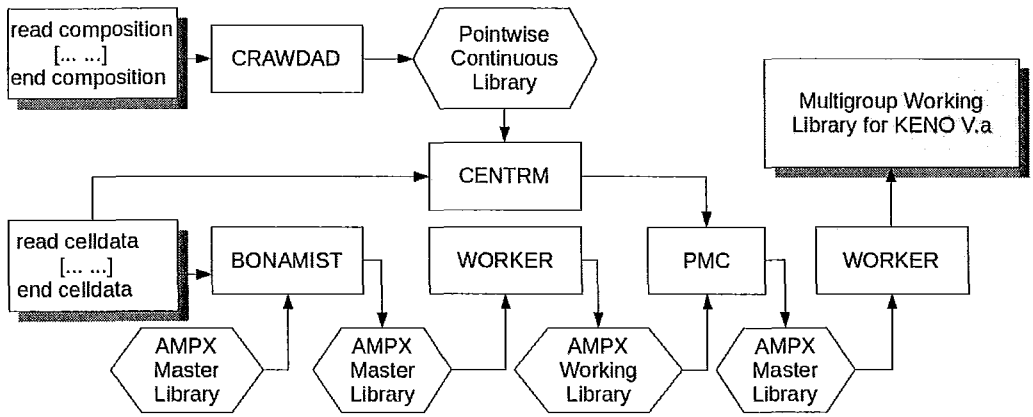

Figure 3.3: Flowchart of modules (in yellow blocks) used to generate problem-dependent multigroup data.

- CRAWDAD (Code to Read And Write DAta for Discretized solution) identifies all isotopes that are used to comprise material mixtures between `read composition` and `end composition` (see Petrie *et al.*, 2009). As the first step in the preparation of cross section data, it selects these problem-specific nuclear data from the general pointwise library files of SCALE6 and reformats them to create a pointwise continuous energy library suitable for the CENTRM and PMC modules.

- BONAMIST (BONdarenko AMPX Interpolator ST) is an expanded version of the BONAMI module (see Rearden and Jessee, 2009, p. 18.3.1). BONAMI reads information provided between `read celldata` and `end celldata` of the input file, and generates cross sections that are corrected for the unresolved resonances. As its name suggests, BONAMI is based on the Bondarenko method where Narrow Resonance approximation is used, implying the collision reaction rate is not affected by the

resonance: $\phi(u)\Sigma_t(u)$ is constant and $\phi(u) \sim \frac{1}{\Sigma_t(u)}$. The total macroscopic cross section Σ_t for each of the geometric zones in the celldata is defined as:

$$\Sigma_t = N_i\sigma_t^i(u) + \sum_{j\neq i} N_j\sigma_t^j(u) \tag{3.102}$$

where u is in the unit of lethargy, i denotes the resonance nuclide and j denotes individual nuclides other than i. N is the nuclide number density and σ_t is the microscopic total cross section. Hence the problem-dependent cross section of nuclide i of energy group g, with the adjustment for shielding effects in the unresolved resonance region becomes:

$$\overline{\sigma_g^i} = \frac{\int_g \sigma^i(u)\phi(u)du}{\int \phi(u)du} = \frac{\int_g \left(\frac{\sigma^i(u)}{\sigma_t^i(u)+\sigma_0^i(u)}\right) du}{\int_g \left(\frac{1}{\sigma_t^i(u)+\sigma_0^i(u)}\right) du} \tag{3.103}$$

given that σ_0^i is the so-called *background* cross section per atom of the nuclide i for all nuclides in the mixture other than nuclide i itself:

$$\sigma_0^i = \sum_{j\neq i} N_j\sigma_t^j(u)/N_i \tag{3.104}$$

The dependence of $\overline{\sigma_g^i}$ on σ_o^i is usually expressed in the form of a self-shielding factor, called the Bondarenko factor, or f-factor:

$$\overline{\sigma_g^i} = f_g^i(T, \sigma_o^i)\sigma_g^i(\infty) \tag{3.105}$$

where the f-factor is tabulated for different background cross sections and corresponding temperatures, and $\sigma_g^i(\infty)$ represents the infinitely diluted cross section value of isotope i at energy group g:

$$\sigma_g^i(\infty) = \frac{1}{\triangle u}\int_g \sigma_g^i(u)du \tag{3.106}$$

The reason for including the temperature dependence is to account for the Doppler broadening effect. Hence, the algorithm to generate problem-dependent self-shielded cross sections begins with the calculation of the background cross section σ_o^i, followed by the retrieval of the f-factor from pre-calculated tables. The shielded cross section can be efficiently calculated from the product of the f-factor and infinitely diluted cross section.

The output of BONAMI is an updated AMPX master library that is

problem-dependent but still not ready for direct use in KENO. Meanwhile, the BONAMIST module performs the same calculations. It then continues to generate implicit sensitivity coefficients and stores them in a `bonamist.sen` data file.

- WORKER generates an AMPX multigroup working library from an AMPX multigroup master library after both BONAMIST and CENTRM/PMC (see Goluoglu *et al.*, 2009b). The master library has a lot more details than the working library and is not structured for direct use in KENO calculations. On the other hand, a working library contains both group-averaged cross sections for relevant nuclide-reaction processes and total transfer matrices for neutron scattering and/or gamma scattering.

- CENTRM (Continuous ENergy TRansport Module) calculates the angular neutron flux spectrum using the method of S_n quadrature discrete-ordinate difference, which is a deterministic transport approximation (see Williams *et al.*, 2009a). When as part of the TSUNAMI sequence, CENTRM has default values for the S_n quadrature order (n=6), lowest and highest energy of pointwise calculation (0.1×10^{-2}eV and 0.02 MeV respectively). Using the geometry specified in the `celldata` section, it computes pointwise flux spectra using the S_n method which gives accurate results for determining the resolved-resonance cross section using the PMC module.

- PMC (Produce Multigroup Cross sections) uses the neutron spectra obtained from CENTRM to generate multigroup cross sections that are problem-dependent, zone-averaged, resonance self-shielding corrected (see Williams and Hollenbach, 2009). PMC prepares two types of multigroup data: (1) cross sections in 1-D vectors and (2) 2-D scatter matrices, both of which use the problem-dependent neutron spectra for determining the energy-dependent multigroup data:

$$(\sigma_{z,g})_{\text{new}} = \frac{\int_g \sigma_z(E)\Phi_z(E)dE}{\int_g \Phi_z(E)dE} \tag{3.107}$$

$$(\sigma_{z,gg})_{\text{new}} = \frac{\int_g \sigma(E)[1-p_r(E)]\Phi_z(E)dE}{\int_g \Phi_z(E)dE} \tag{3.108}$$

$$(\sigma_{z,gg'})_{\text{new}} = \frac{(\sigma_{z,g})_{\text{new}} - (\sigma_{z,gg})_{\text{new}}}{(\sigma^{\infty}_{z,g})_{\text{new}} - \sigma^{\infty}_{gg}} \times (\sigma_{gg'})_{\text{orig}} \tag{3.109}$$

where z denotes the zone, g the energy group and E the energy. Φ_z is the zone-averaged continuous flux from CENTRM, σ_{gg} is the within-group scattering cross section and $p_r(E)$ is the probability that a neutron at energy E within group g will scatter to an energy below the lower boundary of the group. In Equation (3.109), the superscript $^\infty$ denotes that the σ is the infinitely-diluted cross section.

3.2.3 Preparation of Monte Carlo Calculations

Between `read parameter` and `end parameter` in the input file, parameters are defined to customize the Monte Carlo calculation in KENO V.a. In Table 3.1, example values of the cut-off standard deviation (`sig`), the number of neutrons per generation (`npg`) and the number of generations (`gen`) are listed. Their values should be chosen carefully such that k_{eff} with a low variance can be calculated within a reasonable amount of time. Also, KENO V.a. terminates at the moment when either `gen` or `sig` is reached first. The forward and adjoint flux calculations are subject to the same criteria. However, the adjoint flux generally is more difficult to converge and reaches the end of `gen` before `sig`.

parameter	explanation	sample value
`sig`	cut-off standard deviation	0.2 mk
`npg`	number per generation	100000
`gen`	number of generations	3000

Table 3.1: Typical parameters specified in order to customize Monte Carlo calculations.

3.2.4 KENO V.a

With the knowledge of problem-dependent and self-shielded cross sections, and having specified the Monte Carlo parameters, KENO V.a can start the calculation of k_{eff} and neutron fluxes. Rearden (2004) defined the group-wise scalar flux within a region z of volume V_z to be:

$$\phi_{g,z} = \left(\sum_{k=1}^{K} W_{k,z} l_{k,z} \right) / \left(V_z \sum_{k=1}^{K} W_{k,0} \right) \tag{3.110}$$

where $W_{k,0}$ is the initial weight of the neutron k and $W_{k,z}$ is its weight while travelling in region z. Equation (3.110) is a variation of Equation (2.9) which

is based on the method of track length estimator. The flux is essentially the sum of the distances $l_{k,z}$ traversed by K number of neutrons within the region z and the energy group g in a unit time. The purpose of the weight function has been explained previously as a result of the *non-analog* (Russian roulette) method. The forward and adjoint steady state transport equations (2.29), (2.51) are solved by simulating the flight trajectories of neutrons and their collisions with materials inside the reactor model. After each generation, the value of k_{eff} is calculated as the ratio between the total number of neutrons at the end of the generation and the specified number of neutrons per generation (`npg`). When the total number of generations (`gen`) is achieved or k_{eff} has converged to the specified `sig`, KENO V.a (forward or adjoint case) is finished. The forward and adjoint fluxes of the last generation performed are taken as the steady state neutron transport solutions and saved for sensitivity and uncertainty analysis.

3.2.5 SAMS

SAMS is the sensitivity analysis module for SCALE6 and is used following the KENO V.a calculations in the TSUNAMI-3D control sequence (Figure 3.2). In Chapter 2.3, the calculations for explicit and implicit sensitivity coefficients are explained. As part of the TSUNAMI-3D control sequence, SAMS automatically takes the forward and adjoint fluxes from KENO V.a and records all problem-dependent nuclide-reaction pairs found in the KENO V.a calculations. The implicit sensitivity coefficients from resonance self-shielding calculations from BONAMIST are included by default. Therefore, the sensitivity outputs from SAMS include:

- implicit, explicit and total nuclide-reaction sensitivity coefficient, integrated over mixtures, energy groups and regions;
- implicit, explicit and total nuclide-reaction sensitivity coefficient for each mixture, integrated over energy groups and regions;
- groupwise total sensitivity coefficients for each nuclide-reaction pair, integrated over mixtures and regions.

The cross section covariance data used in this work has a 44-group structure. It is specified between `read sams` and `end sams` by the parameter `coverx`:

```
coverx = 44groupcov
```

Since the group-wise sensitivity coefficients have a 238-group structure, they are collapsed into 44 groups first. Then the calculation of the k_{eff} uncertainty due to cross section covariance is performed using Equation (2.69) from Chapter 2.4.

3.3 TSAR

For reactor safety analysis, the change in k_{eff} in response to a deviation of parameters such as coolant density, moderator purity or fuel temperature is of great importance. The TSAR module, shown in Figure (3.1) is capable of utilizing the k_{eff} sensitivity coefficients from TSUNAMI-3D for sensitivity and uncertainty analysis of reactivity[2].

Suppose the system's k_{eff} is changed from k_1 to k_2 and therefore the reactivity response is:

$$\rho_{1\to 2} = \rho_2 - \rho_1 = \left(1 - \frac{1}{k_2}\right) - \left(1 - \frac{1}{k_1}\right) = \frac{1}{k_1} - \frac{1}{k_2} = \lambda_1 - \lambda_2 \qquad (3.111)$$

where $\lambda = 1/k$. The relative sensitivity coefficient for reactivity response due to the change of the α parameter in the system is defined as:

$$S_{\rho,\alpha} = \frac{\alpha}{\rho_{1\to 2}} \frac{\partial \rho_{1\to 2}}{\partial \alpha} = \frac{\alpha}{\rho_{1\to 2}} \left[\frac{\partial \lambda_1}{\partial \alpha} - \frac{\partial \lambda_2}{\partial \alpha}\right] = \frac{\lambda_1 S_{\lambda_1,\alpha} - \lambda_2 S_{\lambda_2,\alpha}}{\rho_{1\to 2}} \qquad (3.112)$$

where $S_{\lambda,\alpha}$ has the same form as $S_{k,\Sigma}$:

$$S_{\lambda,\alpha} = \frac{\alpha}{\lambda} \frac{\partial \lambda}{\partial \alpha} \qquad (3.113)$$

It is easy to show that $S_{k,\alpha} = -S_{\lambda,\alpha}$:

$$S_{k,\alpha} = \frac{\alpha}{k} \frac{\partial k}{\partial \alpha} = (\alpha\lambda)\left(\frac{-1}{\lambda^2} \frac{\partial \lambda}{\partial \alpha}\right) = -\frac{\alpha}{\lambda} \frac{\partial \lambda}{\partial \alpha} = -S_{\lambda,\alpha} \qquad (3.114)$$

Therefore, Equation (3.112) becomes:

$$S_{\rho,\alpha} = \frac{\lambda_2 S_{k_2,\alpha} - \lambda_1 S_{k_1,\alpha}}{\rho_{1\to 2}} = \frac{k_1 S_{k_2,\alpha} - k_2 S_{k_1,\alpha}}{k_2 - k_1} \qquad (3.115)$$

On the other hand, the uncertainty of relative reactivity $\rho_{1\to 2}$ due to

[2] In TSAR analysis, the term reactivity actually refers to the reactivity difference or change between two states, as shown in Equation (3.111).

the nuclear data uncertainties can be computed the same way as the k_{eff} uncertainty:

$$\sigma_\rho^2 = \vec{S}_\rho \mathbf{C}_{\alpha\alpha} \vec{S}_\rho^{\mathrm{T}} \tag{3.116}$$

Interestingly, the uncertainty of $\rho_{1\to 2}$ can be expressed using the uncertainties of k_1 and k_2 as derived by Williams (2007):

$$\sigma_\rho^2 = \frac{\lambda_1^2}{(\lambda_1-\lambda_2)^2}\sigma_{k_1}^2 + \frac{\lambda_2^2}{(\lambda_1-\lambda_2)^2}\sigma_{k_2}^2 - 2\mathcal{C}_{1,2}\frac{\lambda_1\lambda_2}{(\lambda_1-\lambda_2)^2}\sigma_{k_1}\sigma_{k_2} \tag{3.117}$$

where $\mathcal{C}_{1,2}$ is called the correlation coefficient between the states 1 and 2 and can be computed as:

$$\mathcal{C}_{1,2} = \frac{S_{k_2}\mathsf{C}_{\alpha\alpha}S_{k_1}^{\mathrm{T}}}{\sqrt{S_{k_1}\mathsf{C}_{\alpha\alpha}S_{k_1}^{\mathrm{T}}}\sqrt{S_{k_2}\mathsf{C}_{\alpha\alpha}S_{k_2}^{\mathrm{T}}}} = \frac{\sigma_{k_1k_2}}{\sigma_{k_1}\sigma_{k_2}} \tag{3.118}$$

Therefore, there are two ways of calculating σ_ρ^2 using either the sensitivity coefficients of reactivity (S_ρ) or of the multiplication factor (S_k). Coincidentally, $\mathcal{C}_{1,2}$ will be calculated in the next TSUNAMI module and used to quantify the similarity between two systems.

3.4 TSUNAMI-IP

The goal of TSUNAMI-IP is to provide measurable quantities for describing how similar two or more systems are, in terms of the correlations of nuclear data uncertainties. And by doing so, it can help establish the degree of applicability of benchmark experiments to systems for which only simulations are available. Several indices can be computed by TSUNAMI using the sensitivity coefficients. Let S be a matrix of sensitivity coefficients that are row vectors $\vec{S}_i$ where $i = 1, 2, ..., I$ and I is the total number of systems (benchmark and simulation together):

$$\mathsf{S} = \begin{bmatrix} \vec{S}_1 \\ \vec{S}_2 \\ \vdots \\ \vec{S}_i \\ \vdots \\ \vec{S}_I \end{bmatrix} \tag{3.119}$$

The length of each $\vec{S}_i$ vector is M (the number of nuclide-reaction pairs

$\times$ the number of energy groups) and the nuclear data covariance matrix $\mathtt{C}_{\alpha\alpha}$ has a dimension of $M \times M$. Then Equation (3.120) has a dimension of $I \times I$ and each matrix element of $\mathtt{C}$ is $[\mathtt{C}]_{ij} = \sigma_{ij}^2$.

$$\mathtt{C} = \mathtt{S}\mathtt{C}_{\alpha\alpha}\mathtt{S}^{\mathrm{T}} \tag{3.120}$$

For a single system (implying $i = j$), the importance of σ_{ij}^2 has been illustrated in Equation (2.69), using the system's sensitivity coefficients (i-th row vector of $\mathtt{S}$):

$$\sigma_{\mathrm{k}}^2 = \vec{S}_{\mathrm{k}}\mathtt{C}_{\alpha\alpha}\vec{S}_{\mathrm{k}}^{\mathrm{T}} = [\mathtt{S}_{\mathrm{k}}]_i\mathtt{C}_{\alpha\alpha}[\mathtt{S}_{\mathrm{k}}]_i^{\mathrm{T}} = [\mathtt{C}_{\mathrm{k}}]_{ii} \tag{3.121}$$

TSUNAMI-IP defines the correlation coefficient between systems i and j as the integral index c_{k}, which is calculated from the corresponding matrix elements of $\mathtt{C}_{\mathrm{k}}$:

$$c_{\mathrm{k}} = \frac{[\mathtt{C}_{\mathrm{k}}]_{ij}}{\sqrt{[\mathtt{C}_{\mathrm{k}}]_{ii}}\sqrt{[\mathtt{C}_{\mathrm{k}}]_{jj}}} = \frac{\sigma_{ij}^2}{\sigma_i\sigma_j} \tag{3.122}$$

which has the same definition as Equation (3.118). In the case of $i = j$, the system is clearly correlated completely with itself and giving the maximum value of c_{k}:

$$c_{\mathrm{k}} = \frac{[\mathtt{C}_{\mathrm{k}}]_i}{\sqrt{[\mathtt{C}_{\mathrm{k}}]_i}\sqrt{[\mathtt{C}_{\mathrm{k}}]_i}} = 1$$

The integral index c_{k} may have a value from -1.0 to 1.0 where the former represents a full anti-correlation and the median 0.0 represents no correlation between the systems (see Rearden and Jessee, 2009, p. 18.1.3).

A second integral index G in TSUNAMI-IP is constructed based solely on the sensitivity data of fission (f), capture (c) and scattering (s) reactions. Index G represents the overlap of sensitivities between systems i and j, providing a measure of *coverage*:

$$G = 1 - \frac{\sum_n \sum_x \sum_g \left(S_{x,g}^{i,n} - \bar{S}_{x,g}^{j,n}\right)}{\sum_n \sum_x \sum_g S_{x,g}^{i,n}} \tag{3.123}$$

where g is the energy group, n the nuclide type and x is summed over fission, capture and scattering reactions. The value of $\bar{S}_{x,g}^{j,n}$ is chosen according to the following three conditions:

$$\bar{S}_{x,g}^{j,n} = \begin{cases} S_{x,g}^{j,n} & \text{where} \quad |S_{x,g}^{i,n}| \geq |S_{x,g}^{j,n}| \quad \text{and} \quad S_{x,g}^{i,n}/|S_{x,g}^{i,n}| = S_{x,g}^{j,n}/|S_{x,g}^{j,n}| \\ S_{x,g}^{i,n} & \text{where} \quad |S_{x,g}^{i,n}| < |S_{x,g}^{j,n}| \quad \text{and} \quad S_{x,g}^{i,n}/|S_{x,g}^{i,n}| = S_{x,g}^{j,n}/|S_{x,g}^{j,n}| \\ 0 & \text{otherwise} \end{cases}$$

The three cases restrict the *coverage* to include only the sensitivities of system i that are larger than those of system j in absolute terms. The value of $S/|S|$ is either 1 or -1. The third condition ensures that when $S^{i,n}_{x,g}/|S^{i,n}_{x,g}| = -S^{j,n}_{x,g}/|S^{j,n}_{x,g}|$, G becomes 0, meaning there is completely zero coverage. On the other hand, when the second condition is satisfied, $G = 1$ means systems i and j completely overlap, giving 100% coverage. The reaction-specific integral G value can be calculated by integrating over a single reaction:

$$G_x = 1 - \frac{\sum_n \sum_g \left(S^{i,n}_{x,g} - \bar{S}^{j,n}_{x,g}\right)}{\sum_n \sum_g S^{i,n}_{x,g}} \tag{3.124}$$

where x = fission, capture or scattering.

3.5 TSURFER

As the last module of the TSUNAMI sequence for sensitivity and uncertainty analysis, the TSURFER module requires input information from the TSUNAMI-3D and TSUNAMI-IP modules:

1. sensitivity coefficients (S_k) from TSUNAMI-3D;
2. correlation coefficients for the various systems of interest (c_k) from TSUNAMI-IP.

There are other essential inputs in TSURFER depending on the type of system being investigated. TSURFER considers benchmark experiments to be *active responses* and applications (aka. simulations without experimental results) as *passive responses*. The distinction is that an *active* response has both calculated and measured key parameters such as k_{eff} while a *passive* response only has calculated ones. Hence in the TSURFER's input for specifying the *active* response, the KENO-calculated experimental value (cv), the corresponding experimentally measured value (ev) and their associated uncertainty value (uv) are required. In contrast, only cv is needed for the *passive* response (because an application does not have experimental measurements).

As described in Chapter 2.5, TSURFER uses the GLLS method to adjust the nuclear data within the consistency of their uncertainties such that the discrepancy between cv and ev is minimized. Indicated in Equation (2.94), the adjustments in nuclear data uncertainties ($\delta\alpha$) are driven by the bias in k_{eff} (a.k.a. the discrepancy vector $\vec{d}$) and its covariance matrix (C_{dd}). The covariance matrix for the discrepancy is a combination of calculated and measured

data covariances as shown in Equation (2.87). The former (C_{kk}) can be obtained from TSUNAMI-IP using Equation (3.122). However the latter (C_{mm}) has to be determined prior to TSURFER calculation. In TSURFER calculations, the covariance matrix C_{mm} is calculated as (Williams *et al.*, 2009b):

$$C_{mm}(i,j) = \sum_{\theta} \left(\sigma^{\theta}_{m,i} \rho^{\theta}_{i,j} \sigma^{\theta}_{m,j}\right) \tag{3.125}$$

where m denotes the systems under investigation and parameter θ represents the individual experimental uncertainty contributor which could be enrichment, density, impurities, etc. σ^{θ}_{m} is the experimental uncertainty for parameter θ of the measured experiment and is labelled by uv in the TSURFER input file. $\rho^{\theta}_{i,j}$ is the correlation coefficient of systems m_i and m_j due to uncertainty component θ and is input in the CORR section in the TSURFER input file.

The measured uncertainties can sometimes be acquired from recorded uncertainties in the benchmark experiment reports. The values of σ^{θ}_{m} and C_{mm} can have non-negligible impact on the goodness of the adjusted nuclear data, evaluated by the value of χ^2 per degree of freedom (dof) that TSURFER generates. The ideal χ^2/dof should be within $\pm$ 20% of unity. If χ^2/dof is too small (or big), it is resulted from overestimating (or underestimating) the experimental uncertainties. Furthermore, it is advised that: "correlation values [of experimental measurements] usually should be limited to a maximum of 0.95, suggesting that a small random component is always present".

Once the new set of adjusted nuclear data ($\vec{\alpha'}$) is obtained from GLLS method, they can be used to predict the k_{eff} of a design system. Since the design system does not have experimental measurements, the application bias β is defined as the difference between the original k_{eff} value and the best-estimate of the k_{eff} obtained using the new nuclear data (proof is given by Williams *et al.* (2009b)):

$$\beta = k_{orig}(\alpha) - k_{est}(\alpha') \approx -\vec{S}_{k,orig} \cdot (\vec{\alpha'} - \vec{\alpha}) \tag{3.126}$$

where $\vec{S}_{k,orig}$ is the row vector of the relative sensitivities of the original nuclear data for the design system. It is also of a great interest to calculate the isotopic contributions to the application bias in terms of their relative percentages:

$$\frac{\beta_{\alpha}}{k_{orig}} \times 100\% = -\frac{S_{k,\alpha}(\alpha' - \alpha)}{k_{orig}} \times 100\% \tag{3.127}$$

From this information, the top application bias contributors can be identified.

Chapter 4

Models of the ZED-2 Experiments

The ZED-2 (Zero Energy Deuterium) critical facility operated by AECL put forward a number of irradiation experiments for the study of $(Th, Pu)O_2$ fuel bundles. ZED-2 is a 50-year-old, vertical, tank-type reactor operated at low power (less than 300W) and it uses heavy water moderator. In this chapter, the performed experiments by Jones (1984) are the focus of our attention. Even though the modelling of the experiments included a few approximations, with the help of KENO3D (Horwedel and Bowman, 2000) which is a visualization tool accompanying SCALE6, as well as the calculated k_{eff} results by KENO, the precision of the models can be ensured.

4.1 Types of Fuels

There are two types of fuels involved in the $(Th, Pu)O_2$ experiments. The first and foremost is the $(Th, Pu)O_2$ fuel with its compositions summarized in Table 4.2.

Nuclide	^{232}Th	^{239}Pu	^{240}Pu	^{241}Pu	^{242}Pu	^{238}Pu	^{16}O
wt %	86.051	1.181	0.303	0.045	0.008	0.002	12.410

Table 4.2: Composition of $(Th, Pu)O_2$ fuel pellet and the density is 9.46 g/cm^3.

Thirty-six $(Th, Pu)O_2$ fuel pellets are oriented in concentric rings surrounding a hollow central support tube as shown in Figure 4.4. The central support tube (CST), the calandria and pressure tubes are made of aluminum. Zircaloy tie-rods are used to separate the zircaloy endplates of each $(Th, Pu)O_2$ bundle. The configuration and geometric specifications are identified as the BDL-422 fuel design.

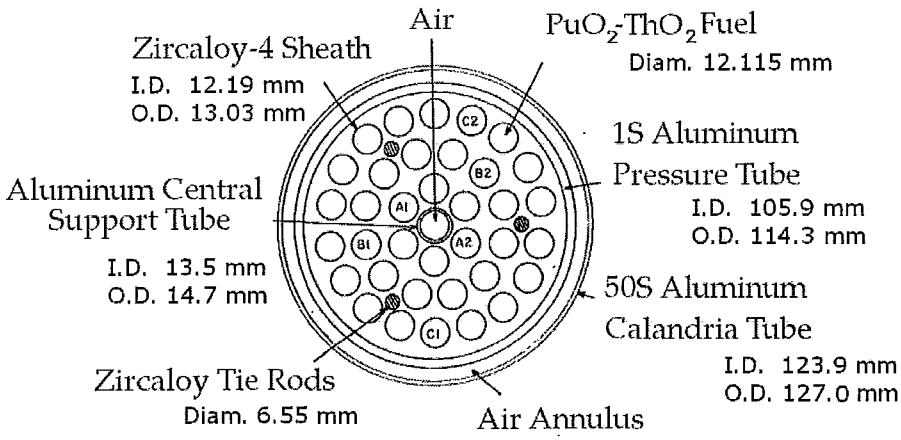

Figure 4.4: Cross section of the $(Th, Pu)O_2$ fuel bundle where labels I.D. and O.D. stand for inner and outer diameter respectively.

The second type of fuel is the natural uranium metal ZEEP rods. Natural uranium can be directly referred to in SCALE/KENO and it is assumed to have a density of 19.05 g/cm^3, consisting of 99.284% of ^{238}U, 0.711% of ^{235}U and 0.005% of ^{234}U. Each ZEEP rod is 3.25 cm in diameter and 15 cm long. There are 19 ZEEP rods stacked inside a single 2S aluminum alloy tube of 1 mm wall thickness. We assumed that the ZEEP aluminum cylinder is made of the same aluminum as the calandria tube. As a comparison, the outer diameter of the calandria tube is about 3.7 times that of the ZEEP aluminum cylinder.

4.2 Locations of Fuels

Figure 4.5 shows the side view of the ZED-2 reactor (Hagberg, 2009). The reactivity control for ZED-2 is achieved by adjusting the height of the moderator. Hence fuel bundles are often partially covered by heavy water at criticality. Even though ZED-2 operates at very low power, it is still equipped with 12 shut-off rods held by magnetic clutches (not shown here). The discharge of the moderator from three dump lines situated below the calandria tank can also achieve shut-down. ZED-2 has a graphite reflector, which should be included in the full core model to better represent the true configuration of the reactor. It can be seen in Figure 4.5 that the fuel bundles are suspended in the reactor core by steel beams and immersed in the heavy water moderator. The level of the moderator is measured from the bottom of the calandria tank. The height of moderator that is needed to achieve criticality is called

the critical height (H_c).

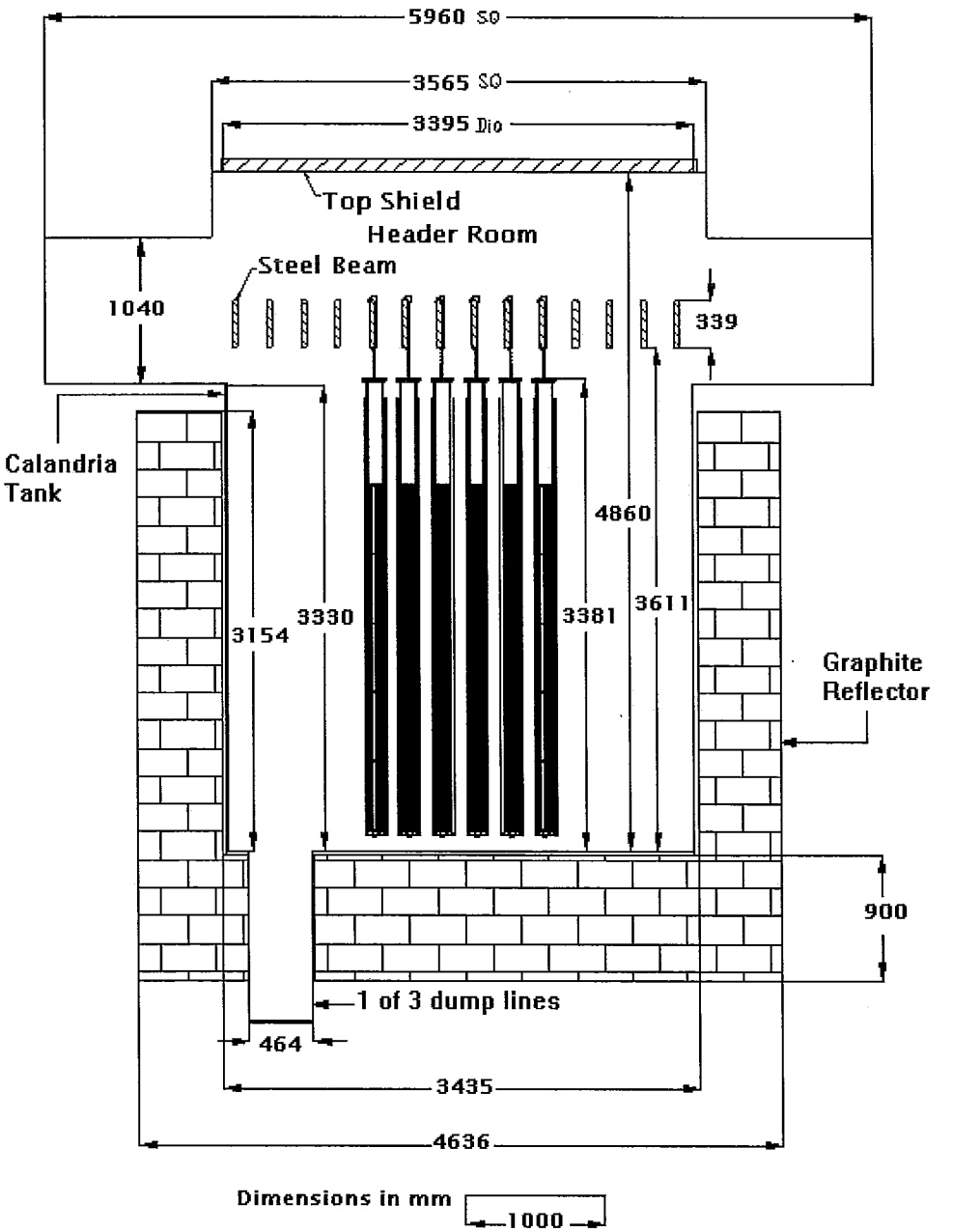

Figure 4.5: Side view of the ZED-2 reactor, showing the fuel rods are suspended inside the calandria tank.

A reference lattice is defined for the particular experiment which has 64 ZEEP rods distributed in "a non-uniform hexagonal array". Figure 4.6 shows the locations of ZEEP rods in the reactor, with respect to the three dump lines, the calandria tank and the graphite reflector. The centre of the core is referred to as the **K0** site by Jones (1984). A modified lattice for the $(Th, Pu)O_2$ experiments has five $(Th, Pu)O_2$ bundles stacked at the centre of the lattice, replacing the ZEEP rod in the K0 site in the reference lattice.

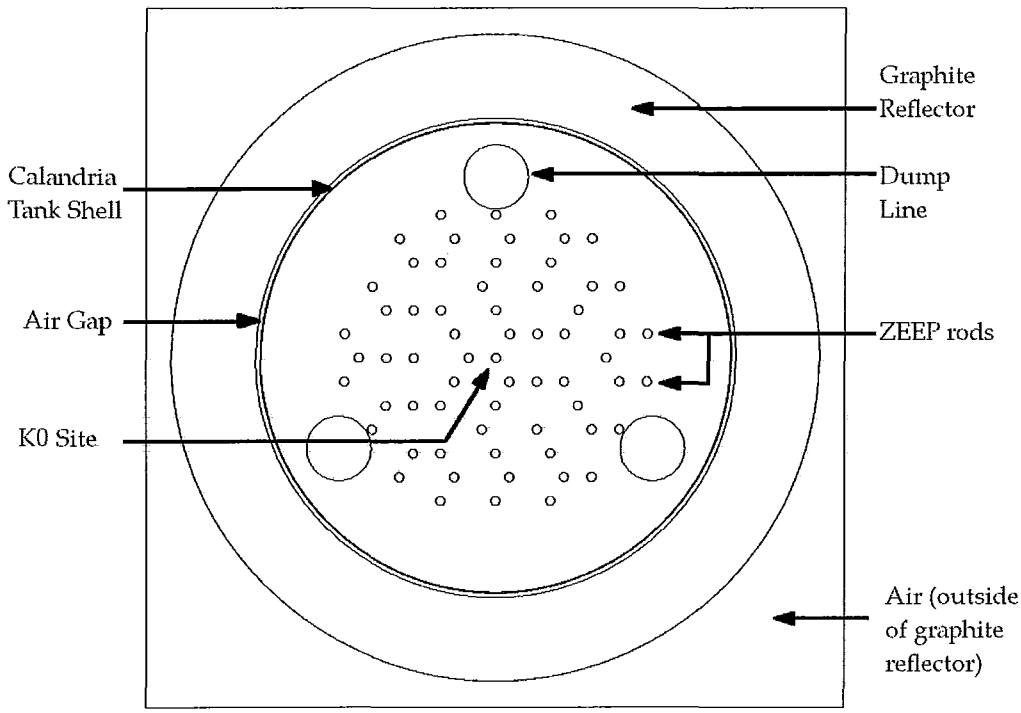

Figure 4.6: Plan view of the reference lattice, superimposed with the three moderator dump lines, the calandria tank and the graphite reflector. The inner and outer diameters of the calandria tank are 336 cm and 337.28 cm respectively. The outer diameter of the graphite reflector is 463.5 cm.

This lattice is said to have an "NRU pitch" of 19.685 cm. It is illustrated in Figure 4.7 that the lattice is both triangular and hexagonal. The pitch is measured as the side length of the equilateral triangle or as the distance between the centres of two hexagons.

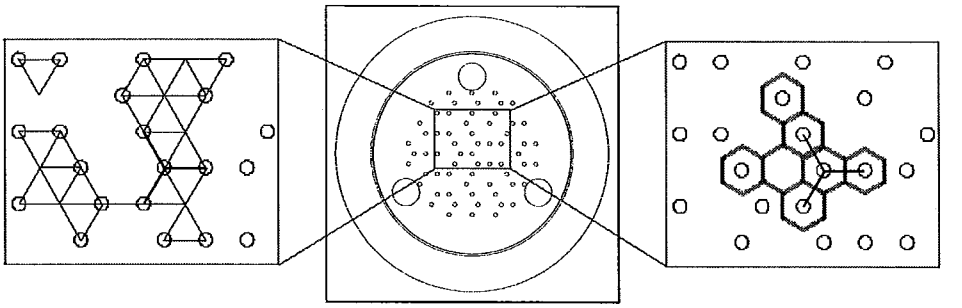

Figure 4.7: An illustration of the "NRU pitch" represented by the black straight lines in both the triangular and hexagonal lattices.

Figure 4.6 was created by the KENO3D software which was also used to generate the following two styles of the ZED-2 model representation. Similar to Figure 4.5, Figure 4.8 provides a centre slice of the reactor model, viewing from the side and showing different material components as labelled. Figure 4.9 presents the model in a wire-frame mode and in a rotated orientation.

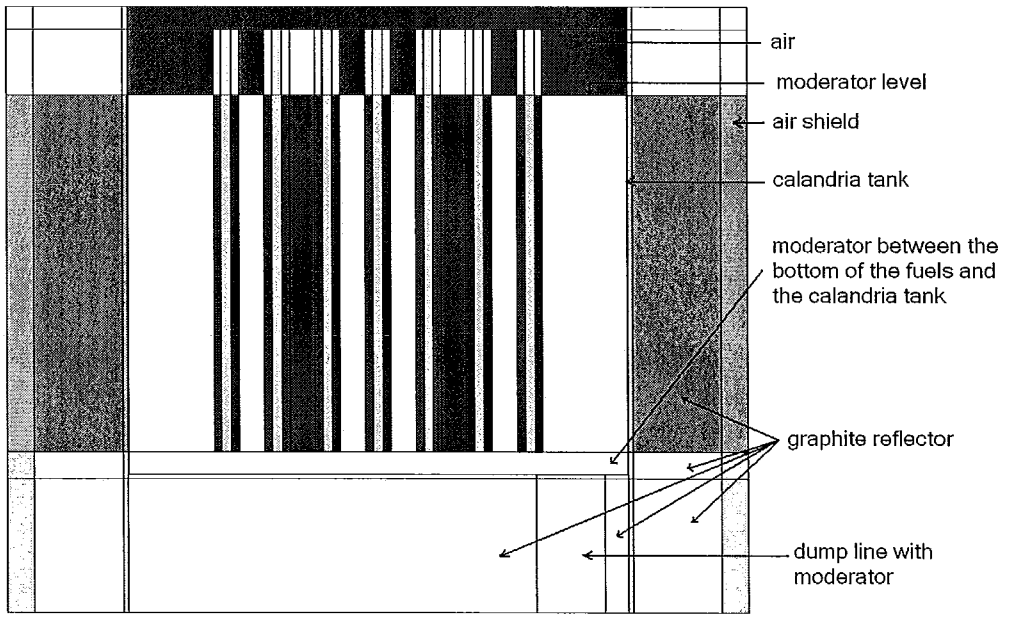

Figure 4.8: KENO3D was used to generate and display a vertical slice of the ZED-2 reactor model.

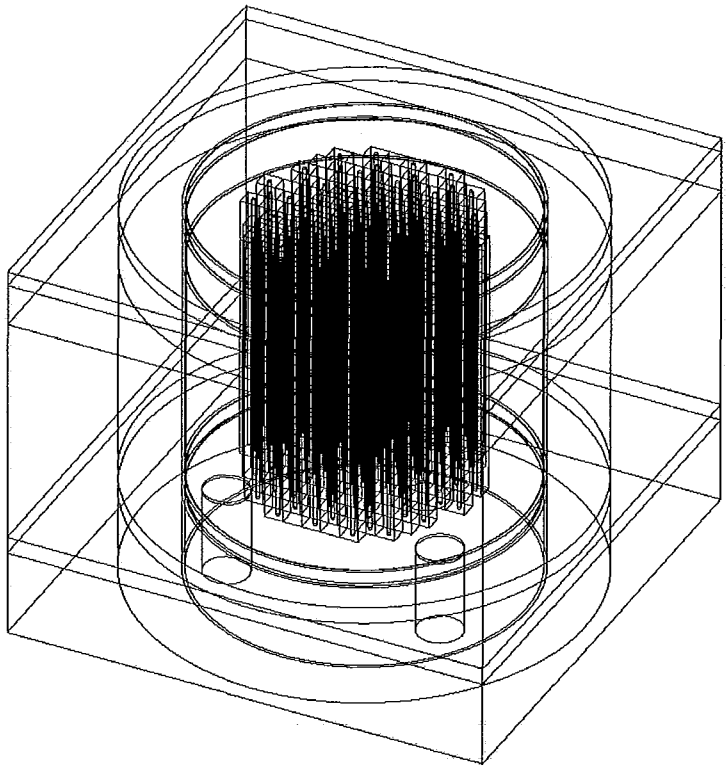

Figure 4.9: KENO3D was used to generate and display the ZED-2 reactor model in the wire-frame mode and in a rotated orientation.

4.3 Experiments and Critical Heights

Table 4.3 lists the six experiments conducted in ZED-2, along with the temperature and critical height measurements. The "Core" column describes the situation at the centre of the reactor core, which is also the K0 site. When there is no fuel at K0, it means the K0 location is simply filled with D_2O moderator. The "Temperature" and the "H_c" columns show moderator data recorded after 20 minutes of running at a constant low power in ZED-2 (Jones, 1984). This ensured the measurements indeed correspond to the criticality conditions of the reactor. Because of the low power operation of ZED-2, it is assumed that the fuels did not heat up enough to cause temperature gradient between the fuels, the coolant and the moderator. The moderator temperature is taken as the uniform temperature of all materials in each of the experiments.

Case	Core	Temperature (°C)	H_c (cm)
1	No fuel at K0	21.15	265.394(10)[a.]
2	No fuel at K0	21.14	265.411(10)
3	ZEEP rod at K0	21.12	252.376(10)
4	Air-cooled $(Th, Pu)O_2$ at K0	21.18	243.961(10)
5	Air-cooled $(Th, Pu)O_2$ at K0	21.11	243.968(10)
6	H_2O-cooled $(Th, Pu)O_2$ at K0	21.10	256.209(10)

[a.] Read as: 265.411 ± 0.010 cm

Table 4.3: Experimental measurements of temperatures and critical heights (H_c). The 0.010 cm uncertainty is the estimated accuracy of a measured height change.

Since cases 1 and 2 have the fewest fuel rods out of the six experiments, their critical heights of D_2O are the largest to cover more available fuels. Simple calculations can show that the total amount of fuel covered by the moderator is not the determining factor in achieving criticality. Let $V_{\mathrm{i}}^{\mathrm{f}}$ and $V_{\mathrm{ii}}^{\mathrm{f}}$ denote the volume of fuel materials in the "No fuel at K0" and "ZEEP rod at K0" cases respectively. They can be calculated in the following way:

$$V_{\mathrm{i}}^{\mathrm{f}} = (H_{c,\mathrm{i}} - 15) \times (\pi r^2) \times 63 \text{ rods} \approx 0.1309\mathrm{m}^3$$
$$V_{\mathrm{ii}}^{\mathrm{f}} = (H_{c,\mathrm{ii}} - 15) \times (\pi r^2) \times 64 \text{ rods} \approx 0.1260\mathrm{m}^3$$

where $H_{c,\mathrm{i}}$ is the average of the critical heights of cases 1 and 2 in Table 4.3, $H_{c,\mathrm{ii}}$ is the critical height of case 3. The radius of each ZEEP rod, r is equal to 1.625 cm. 15 cm is subtracted for the distance between the bottom of the fuel rods and the calandria tank. Further calculations show that the amount of moderator is different as well:

$$V_{\mathrm{i}}^{\mathrm{m}} = H_{c,\mathrm{i}} \times (\pi R^2) - V_{\mathrm{i}}^{\mathrm{f}} \approx 23.4\mathrm{m}^3$$
$$V_{\mathrm{ii}}^{\mathrm{m}} = H_{c,\mathrm{ii}} \times (\pi R^2) - V_{\mathrm{ii}}^{\mathrm{f}} \approx 22.3\mathrm{m}^3$$

where R is the calandria tank radius (1.68 m). These calculations show that even though there is an extra fuel rod in the "ZEEP rod at K0" case, the actual amount of fuel materials that is under D_2O is less due to the decrease in critical height. Also, a lower critical height is sufficient in order to achieve and maintain criticality when there is less fuel materials under the moderator.

The ratio of moderator and fuel has about 1% difference:

$$\text{Ratio}_{\text{i}} = \frac{V_{\text{i}}^{\text{m}}}{V_{\text{i}}^{\text{f}}} \approx 179$$

$$\text{Ratio}_{\text{ii}} = \frac{V_{\text{ii}}^{\text{m}}}{V_{\text{ii}}^{\text{f}}} \approx 177$$

For cases 4/5 and 6, there are same number ZEEP rods and the same $(\text{Th}, \text{Pu})\text{O}_2$ bundle. However, a voided $(\text{Th}, \text{Pu})\text{O}_2$ fuel channel at K0 (case 4/5) was able to insert a large amount of positive reactivity, thus the critical height is the lowest, equivalent to *subtracting* some fuel materials from being immersed under D_2O. The system is able to go critical with the smallest amount of ZEEP rod fuel materials when the coolant in the $(\text{Th}, \text{Pu})\text{O}_2$ is voided.

Chapter 5

Results and Analysis

The KENO V.a. simulations of the $(Th, Pu)O_2$ ZED-2 experiments proved to be accurate, up to a k_{eff} bias of less than 3mk. In Section 5.1 of this chapter, k_{eff} results will be presented which give us good confidence in the four KENO V.a models constructed for forward and adjoint flux calculations. Keeping in mind that the sensitivity coefficients are a property of the reactor system, not of the code used to compute them, we are ensured that the SAMS sensitivity coefficient results (Section 5.2) truly reflect the model's (and system's) k_{eff} sensitivity to isotopic perturbation, with the same degree of accuracy as the Monte Carlo-calculated fluxes. The major nuclide-reaction uncertainty contributors and the total k_{eff} uncertainties will be presented in Section 5.3. The TSUNAMI-3D module (consisting of KENO V.a. and SAMS) generated sensitivity data files which were the inputs for the TSAR, TSUNAMI-IP and TSURFER modules. Their results will be examined in Sections 5.4, 5.5 and 5.6 respectively.

5.1 Values of k_{eff}

The KENO V.a. module in TSUNAMI-3D solved the neutron transport equation by Monte Carlo simulation using 100,000 neutrons per generation and the k_{eff} convergence was subject to a standard deviation of 0.2 mk (Table 3.1 from Chapter 3.2.3). Even though there were six ZED-2 experiments performed on two consecutive days, only the four distinct ones done on the same day were simulated. Their k_{eff} results are summarized in Table 5.4.

Case	Core	Calculated k_{eff}
1	No fuel at K0	1.000188(119)[a.]
2	ZEEP rod at K0	1.000485(162)
3	Air-cooled $(Th, Pu)O_2$ at K0	1.001517(131)
4	H_2O-cooled $(Th, Pu)O_2$ at K0	1.002310(128)

[a.] Read as: 1.000188 ± 0.000119

Table 5.4: KENO V.a. k_{eff} results of the four ZED-2 experiments.

The statistical standard deviations of the k_{eff} values are presented in

brackets. It is important to keep in mind that they were calculated by assuming the Monte Carlo-calculated k_{eff} values have a normal distribution and they are not to be confused with the k_{eff} uncertainty due to nuclear data uncertainties (Chapter 2.4). It is interesting to see the k_{eff} bias (from unity) increases with the ascending complexity of the models (from case 1 to case 4). This suggests the biases are influenced by the addition of ^{238}U in the 64^{th} ZEEP rod (from case 1 to 2), ^{232}Th and ^{239}Pu in the $(Th, Pu)O_2$ bundles (from case 1 to 3) and ^{1}H in the coolant (from case 3 to 4). Since the rest of fuel and moderator materials remains the same, the nuclear data uncertainties of the aforementioned isotopes are most likely the main source of Type-(3) k_{eff} uncertainty (Chapter 2.4).

5.1.1 Reaction Rates

Here the three important reactions rates: (1) fission, (2) absorption and (3) leakage are examined. First taking case 2 (ZEEP rod at K0) as an illustration, Figure 5.10 shows two large peaks at the low and high energy ranges due to thermal and fast fission respectively. Since ZED-2 is heavy water-moderated, thermal fission is expected to be the dominant neutron production mechanism. Absorption becomes the most prominent reaction out of the three between energies 1 eV and 10^6 eV which cover the resonance range of many isotopes.

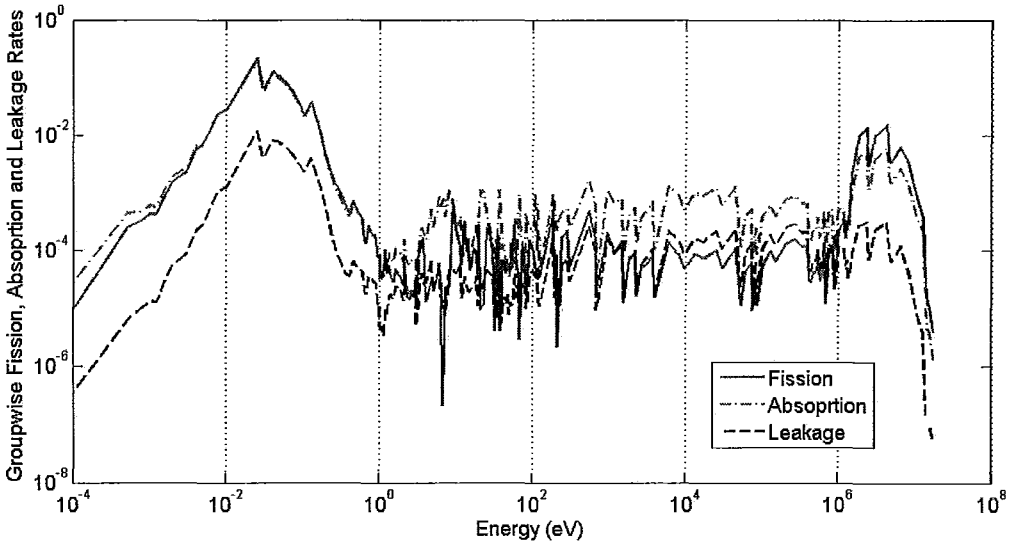

Figure 5.10: Fission production, absorption and leakage rates of case 2 "ZEEP rod at K0 site" in 238 energy groups.

Compared with case 2 where the fuel material is solely natural uranium metal, case 4 which has introduced five H_2O-cooled $(Th, Pu)O_2$ bundles no longer has a drop of fission rate at the 6.75 eV energy group, as shown in Figure 5.11. The lack of fission reaction rate in that energy group is replenished with one of the ^{239}Pu (fission) resonances. At thermal and fast energies, their fission rates are very similar as a result of the large amount of U^{235} and U^{238} in both cases.

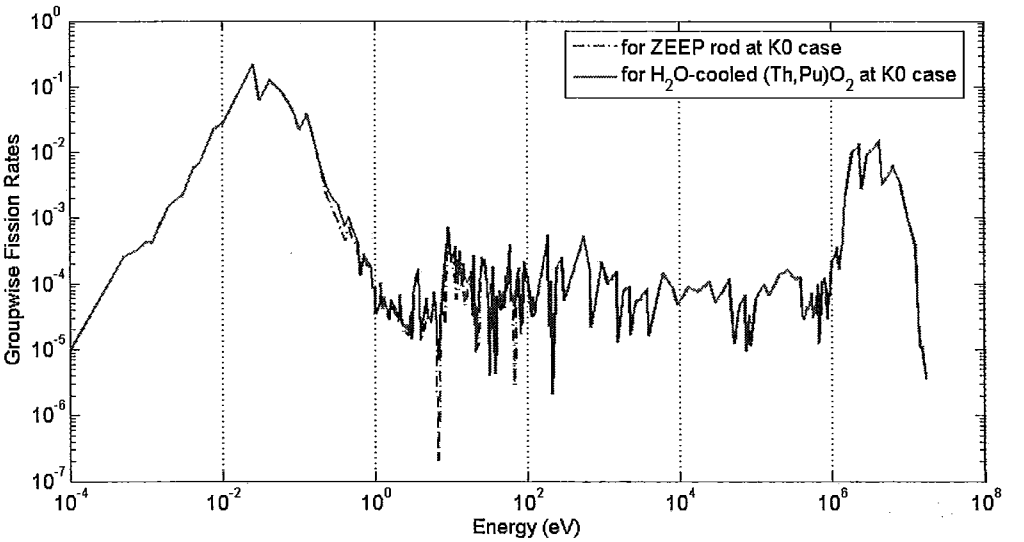

Figure 5.11: Comparison for fission production rates of cases 2 and 4 in 238 energy groups.

In Figure 5.12, the percentage differences in the three reaction rates between cases 3 and 4 are plotted and can illustrate the effect of coolant voiding. It is observed that voiding the coolant resulted in a 0.2% decrease in fission rate at about 0.325 eV and 22.5 eV, which correspond to the known ^{239}Pu resonances. There is also a 3.5% drop in absorption rate at 1 eV which is a prominent resonance of ^{240}Pu and we will see its effect again later. On the other hand, there is overall increase in leakage rate when the coolant is voided. At high energies (above 10^4 eV), the percentage increase in leakage is more than twice the fission and absorption rates.

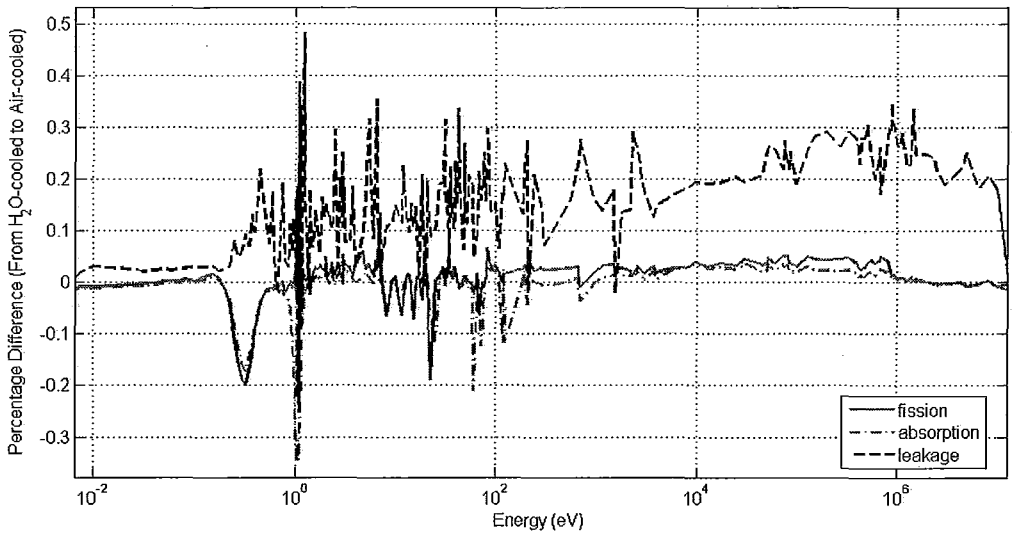

Figure 5.12: Percentage differences in fission, absorption and leakage rates from H_2O-cooled $(Th, Pu)O_2$ (case 4) to air-cooled $(Th, Pu)O_2$ (case 3): (case 3 - case 4)/case 4.

5.1.2 Fission Density Inside Fuel Pins

The $(Th, Pu)O_2$ bundle has three rings of fuel pins, as already shown in Figure 4.4. Table 5.5 lists the fission density in the inner, middle and outer rings of the $(Th, Pu)O_2$ bundles. The comparison shows that due to spatial self-shielding, fission densities decrease as the ring radius decreases. When the coolant is changed from H_2O to air, fuel pins in the inner ring have the largest increase in fission density. This is resulted from a higher fast fission rate in pins that are closer to the bundle centre where leakage is the smallest. Between fuel pins, the direct neutron paths from one fission to another are more probable without coolant absorption. If there had been a centre pin, it would have the highest fission density increase. There is about 1.2% of ^{239}Pu in the $(Th, Pu)O_2$ fuel pins, comparable to the slightly ^{235}U-enriched grade. For this reason, burnable poison such as dysprosium in the centre pin is usually employed to balance and adjust coolant void reactivity (Assawaroongruengchota and Marleau, 2008).

Ring	Fission Density ($\times 10^{-6}$) H_2O-cooled	Fission Density ($\times 10^{-6}$) air-cooled	$\triangle$ F.D. ($\times 10^{-6}$)
Inner	3.619	5.273	1.654
Middle	5.228	6.775	1.547
Outer	10.45	10.34	-0.11

Table 5.5: Fission density in $(Th, Pu)O_2$ pins cooled by H_2O or air. Also shown is the change in fission density ($\triangle$ F.D.)=F.D.$_{air}$ - F.D.$_{H_2O}$

5.2 Sensitivity Coefficients of k_{eff}

Using the adjoint-based first-order linear perturbation method, the SAMS module has calculated k_{eff} sensitivity coefficients for the four models (cases 1 to 4). One of the merits of sensitivity analysis as a reactor physics tool lies in its clear indication of the positive or negative impact on k_{eff} caused by the (uniform) change of any isotope in the system. The value of sensitivity coefficients offers a quantitative measure of the change in k_{eff} , ∂k. Recall Equation (2.53), which can be written as the ratio between the fractional changes of cross section Σ and k_{eff} :

$$S_{k,\Sigma} = \frac{\Sigma}{k}\frac{\partial k}{\partial \Sigma} = \frac{\partial k/k}{\partial \Sigma/\Sigma} \tag{5.128}$$

Here $S_{k,\Sigma}$ can be the total (reaction-, energy- and space-integrated) sensitivity coefficient of cross section Σ. If it is a positive number, we expect an increase in k_{eff} when the change of Σ is positive, and $\partial k/\partial \Sigma > 0$. If $S_{k,\Sigma} < 0$, then k_{eff} is reduced as Σ increases and $\partial k/\partial \Sigma < 0$. Quantitatively, if there is a 1% change in Σ uniformly throughout the system, it is expected to produce a percentage change in k that is: $\partial k/k = 1\% \times S_{k,\Sigma}$.

The usefulness of sensitivity coefficients is also demonstrated in the clear comparison of nuclide-reaction pairs between systems. For example, even though case 1 and case 2 differ in the number of ZEEP rods and the moderator critical heights (temperature difference is negligible), they have the same reactor state (at criticality) and identical material compositions. Figure 5.13 shows that the groupwise ^{235}U (fission) sensitivity profiles for cases 1 and 2 appear to overlap extensively. Figure 5.14 presents a similar result that ^{238}U (capture) has very small differences in its groupwise sensitivity coefficients.

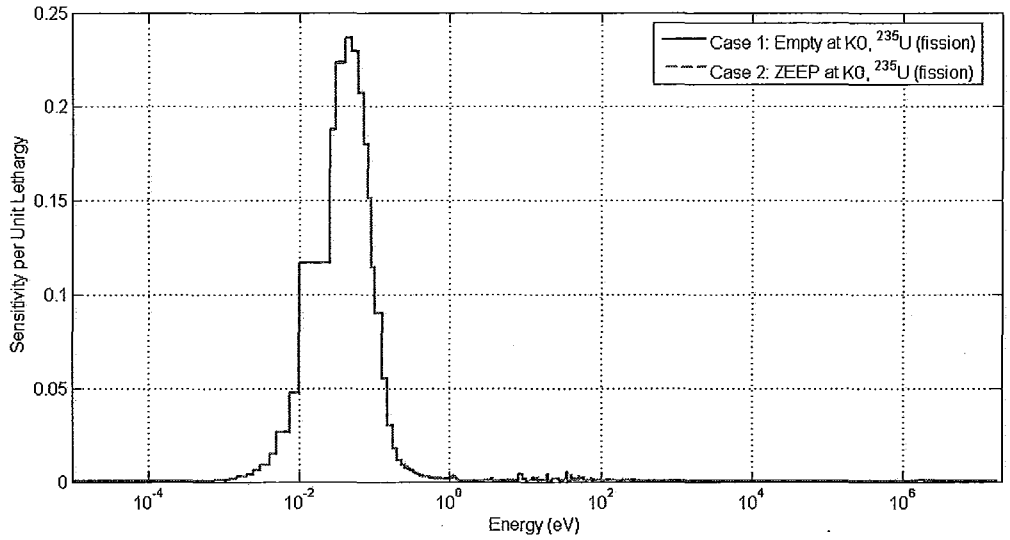

Figure 5.13: The groupwise ^{235}U (fission) sensitivity profiles for cases 1 and 2.

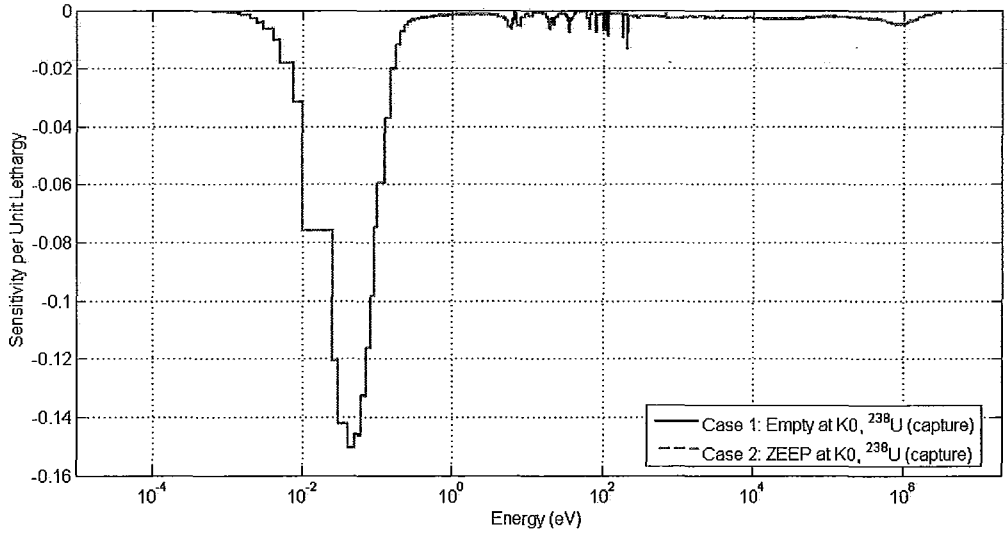

Figure 5.14: The groupwise ^{238}U (capture) sensitivity profiles for cases 1 and 2.

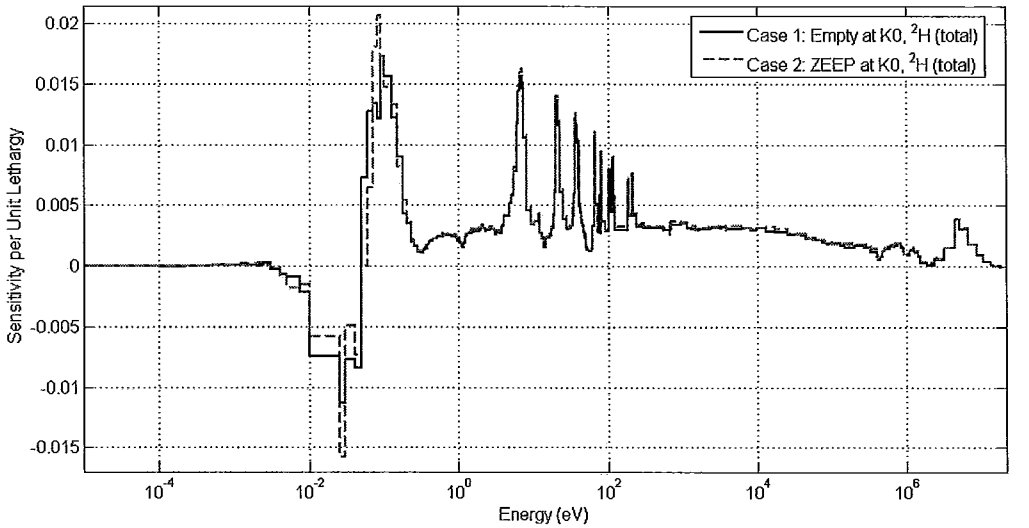

Figure 5.15: The groupwise ^{2}H (total) sensitivity profiles for case 1 and 2.

In Chapter 4.2 we have mentioned that the reactivity control of ZED-2 is by adjusting the moderator critical height and it is no surprise that the system's k_{eff} is very sensitive to the perturbation of the D_2O moderator. It is shown in Figure 5.15 that the ^{2}H (total) sensitivity profiles have noticeable differences between 10^{-1} eV and 10^{-2} eV, where the ^{2}H (total) sensitivity per unit lethargy is sharper and of larger magnitude in case 2 which has less D_2O. To examine this seemingly counter-intuitive result, we first break up the ^{2}H (total) into ^{2}H (scatter) and ^{2}H (capture) coefficients as shown in Table 5.6. Furthermore, they can be separated into explicit and implicit portions.

		total	scatter	capture
Case 1	Explicit ($\times 10^{-2}$)	5.4778	6.9963	-1.5184
	Implicit ($\times 10^{-6}$)	8.1047	8.1045	2.5530×10^{-4}
	Sum ($\times 10^{-2}$)	5.4786	6.9971	-1.5184
Case 2	Explicit ($\times 10^{-2}$)	5.7958	7.2571	-1.4613
	Implicit ($\times 10^{-6}$)	8.6589	8.6587	2.4684×10^{-4}
	Sum ($\times 10^{-2}$)	5.7966	7.2579	-1.4613

Table 5.6: Explicit sensitivity, implicit sensitivity and their sums for the three dominant reactions pertained to ^{2}H in case 1 and case 2.

First observation is that ^{2}H (total) and ^{2}H (scatter) have larger sensitivities (of both explicit and implicit parts) in case 2. This implies, in order to achieve the same amount of change in k_{eff} :

$$\triangle k \approx S_1 \frac{k}{\Sigma} \triangle \Sigma_1 = S_2 \frac{k}{\Sigma} \triangle \Sigma_2 \tag{5.129}$$

$\triangle \Sigma_1$ has to be larger than $\triangle \Sigma_2$ because S_1 of case 1 is less than S_2 of case 2. This can be attributed to the extra ZEEP rod in case 2 such that less ^{2}H perturbation (in either scatter or total) can cause a reactivity change which would otherwise be obtained only with a larger ^{2}H perturbation in case 1. Second observation is that ^{2}H (capture) is more negative in case 1. This suggests the capturing sensitivity is mainly related to the amount of moderator (i.e. critical height). Furthermore, it should be noted that increasing moderator purity is not the same as raising moderator height when the action of the latter will inevitably increase the amount of fuel under moderation and reduce the leakage of the system.

Having demonstrated the kind of useful information sensitivity coefficients can offer, we now turn our attention to the two $(Th, Pu)O_2$ experiments of cases 3 and 4 from Table 5.4. These two experiments have the identical orientation of fuel rods, but they differ in the coolant types and moderator critical heights. When the $(Th, Pu)O_2$ bundles were cooled by air in case 3, they needed a lower critical height to achieve criticality. This is partly resulted from a hardened neutron spectrum from fast fission in the absence of H_2O coolant inside the $(Th, Pu)O_2$ bundles. Figure 5.16 shows the groupwise sensitivity profiles of ^{1}H (scatter). Compared to the curve for case 3 which solely reflects the presence of H_2O molecules as a result of moderator impurity, the drastic increase in sensitivity for case 4 is clearly caused by neutron scattering in the coolant in fuel bundles. The two distinct peaks at around 1 eV and 0.3 eV are clear deviations from the flat sensitivity profiles of case 3 and therefore unique to case 4. The positive peak at 1 eV corresponds to the ^{240}Pu resonance even though there is only a small amount of it in the fuel (0.303% wt). Figure 5.17 shows the cross section data for ^{240}Pu (n,total fission) and (n,γ) from NNDC. When fast fission neutrons are down-scattered by the coolant until 1 eV, neutrons at this energy are very likely absorbed by the large ^{240}Pu (n,γ) resonance, resulting in flux depression around this resonance. But some of the absorbed neutrons have also caused fission via ^{240}Pu (fission). Since neither ^{239}Pu nor ^{241}Pu have resonances at 10^0 eV, the ^{240}Pu (fission) resonance has to be responsible for the positive k_{eff} sensitivity peak there in Figure 5.16. Here we have seen a good demonstration of the implicit k_{eff} sensitivity in ^{1}H (scatter) whose perturbation also affects other isotopes.

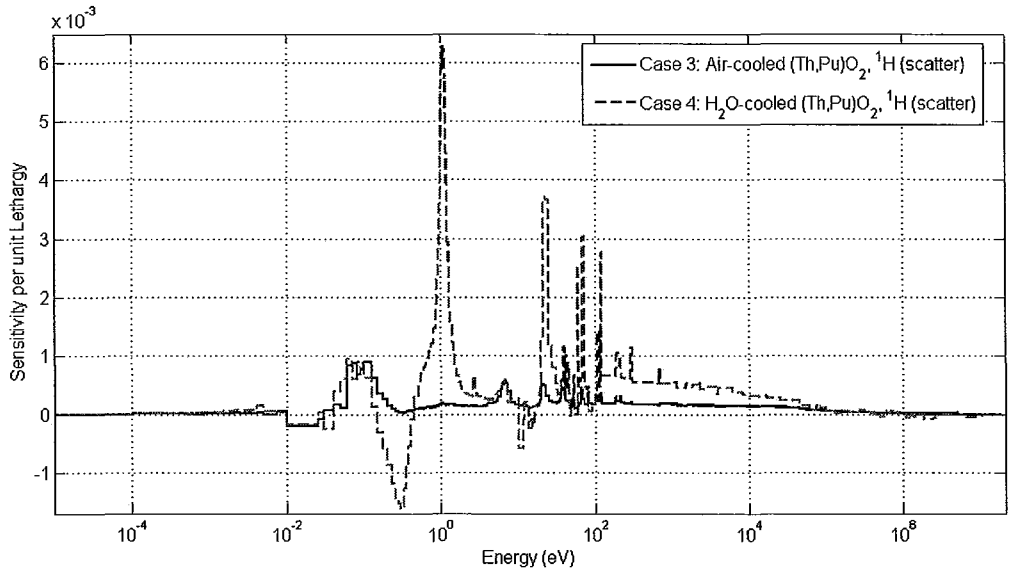

Figure 5.16: The groupwise ^{1}H (scatter) sensitivity profiles for cases 3 and 4.

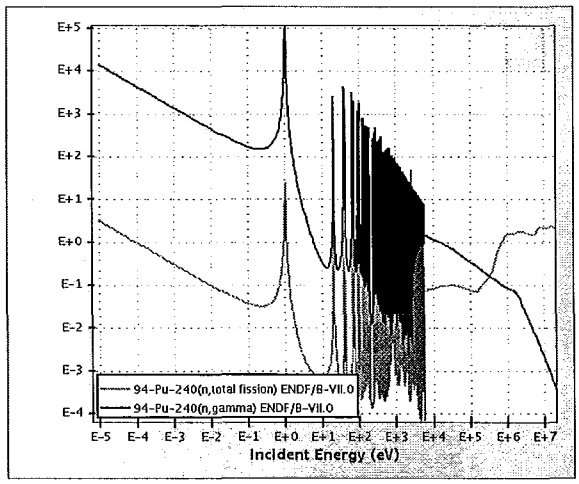

Figure 5.17: ENDF/B-VII.0 cross section data for ^{240}Pu (n,total fission) and (n,γ), taken from National Nuclear Data Centre (NNDC).

The groupwise sensitivity profiles for ^{2}H (total) are presented in Figure 5.18. Around the epithermal resonances and above, the profiles look mostly overlapping. However, there are noticeable differences in lower energy groups starting from the left edge of the first resonance peak at around 3 eV. They could be affected by a combination of several factors. Table 5.7 shows that case

3 has a more positive sensitivity coefficient for ^{2}H (scatter) than case 4 does, even though it has less D_2O in quantity (lower critical height). Also shown is that k_{eff} sensitivity for ^{2}H (capture) has a smaller absolute magnitude in case 3 than in case 4. These results can be interpreted in a similar way as we did for the Table 5.6 results. When the difference in moderator height between case 1 and 2 is caused by the insertion of the 64th ZEEP rod, the voiding of the coolant in the $(Th, Pu)O_2$ bundles also acts as an insertion of positive reactivity, thus allowing a lower critical height in case 3. It is by the same reasoning illustrated through Equation (5.129) that scattering sensitivity is increased by the more positive reactivity and capture sensitivity is more negative due to a larger D_2O quantity.

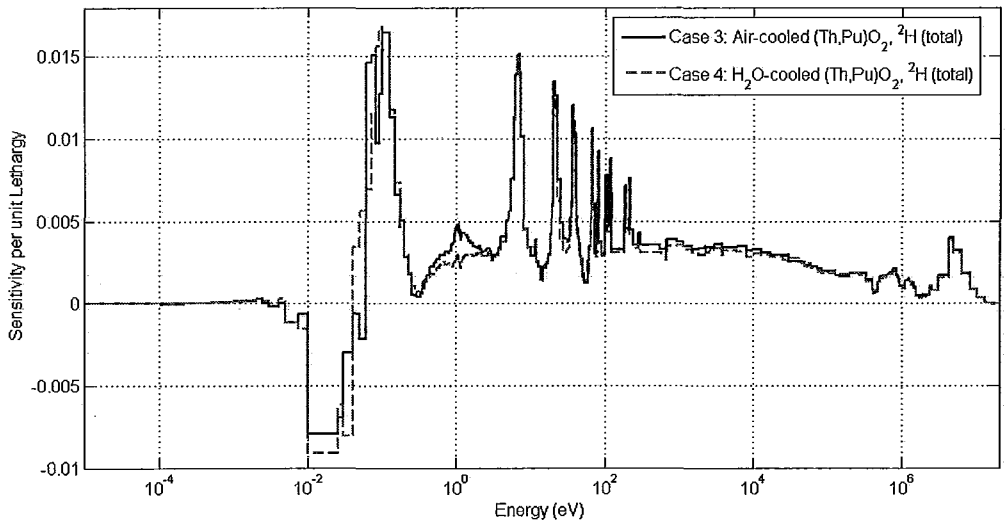

Figure 5.18: The groupwise ^{2}H (total) sensitivity profiles for cases 3 and 4.

	^{2}H (total)	^{2}H (scatter)	^{2}H (capture)
Case 3 ($\times 10^{-2}$)	6.0253	7.3745	-1.3492
Case 4 ($\times 10^{-2}$)	5.5396	6.9036	-1.3640

Table 5.7: Integrated sensitivity coefficients for ^{2}H (total), ^{2}H (scatter) and ^{2}H (capture) in case 3 (air-cooled $(Th, Pu)O_2$) and case 4 (H_2O-cooled $(Th, Pu)O_2$).

Cases 3's and 4's groupwise sensitivity profiles for ^{235}U (fission) are presented in the top graph of Figure 5.19. Their difference is calculated and

plotted in the bottom graph for closer examination. Since all of ^{235}U and ^{238}U isotopes are inside ZEEP rods, the voiding of H_2O coolant is not relevant. The increase in k_{eff} sensitivity for ^{235}U (fission) is due to the higher moderator critical height in case 4. Similarly, Figure 5.20 shows the ^{238}U (total) sensitivity profiles in the top graph, and their sensitivity coefficients difference in the bottom. ^{238}U (total) cross section consists of ^{238}U (fission) at energies above 1 MeV, and the large ^{238}U (capture) at the thermal energy range. For the same reason as before, the sensitivity magnitudes of ^{238}U (capture) and ^{238}U (fission) are larger in case 4 because a larger portion of the ZEEP rods are immersed in D_2O.

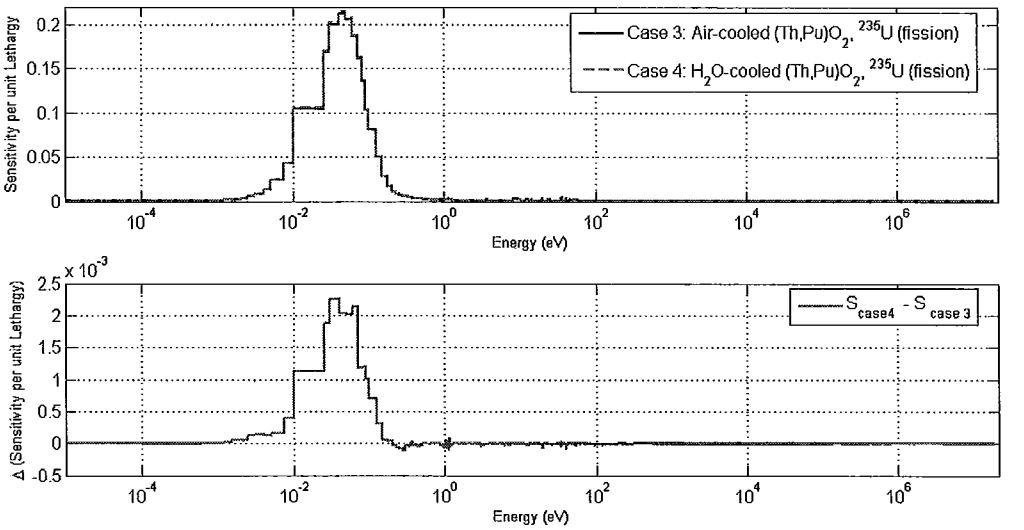

Figure 5.19: The groupwise ^{235}U (fission) sensitivity profiles for cases 3 and 4.

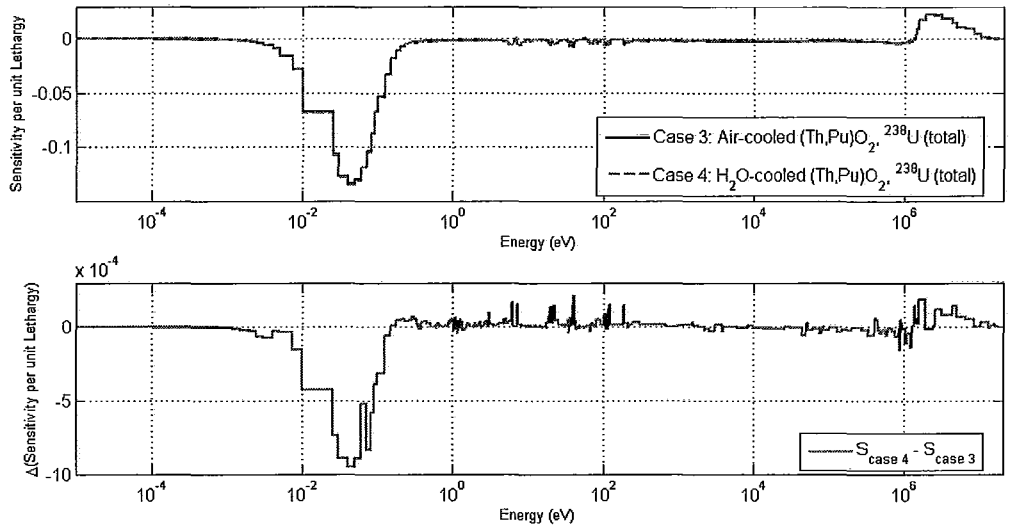

Figure 5.20: The groupwise ^{238}U (total) sensitivity profiles for cases 3 and 4.

Finally, we are going to look at the k_{eff} sensitivities coefficients for ^{232}Th and ^{239}Pu. The cross section data for ^{232}Th (capture) are shown in Figure 5.21. The groupwise sensitivity coefficients for ^{232}Th (capture) are plotted in Figure 5.22. Both sensitivity profiles are negative over the entire 238-group energy range. When the coolant is voided in case 3, fast flux from ^{239}Pu (fission) cannot get down-scattered by the missing coolant inside the $(Th, Pu)O_2$ bundles, resulting in less capture by ^{232}Th resonances in the epithermal energy range. In the thermal energy range, thermal neutrons coming into the $(Th, Pu)O_2$ bundles from the moderator can no longer be up-scattered in the absence of coolant, thus unable to escape the ^{232}Th (capture) and exhibiting a larger sensitivity in case 3 than case 4.

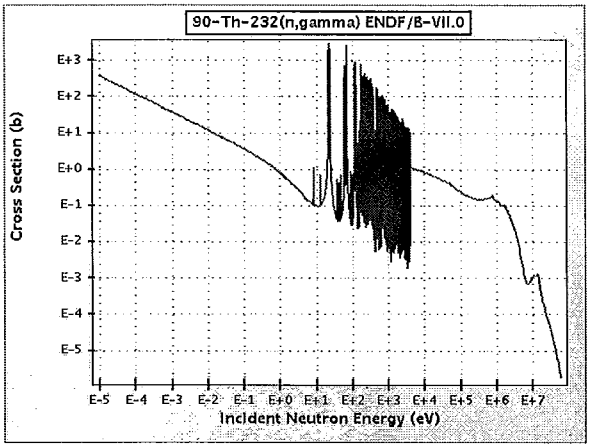

Figure 5.21: NNDF/V-II.0 cross section data for ^{232}Th (n,γ) from NNDC. Note that ^{232}Th (n,γ) is equivalent to ^{232}Th (capture) here.

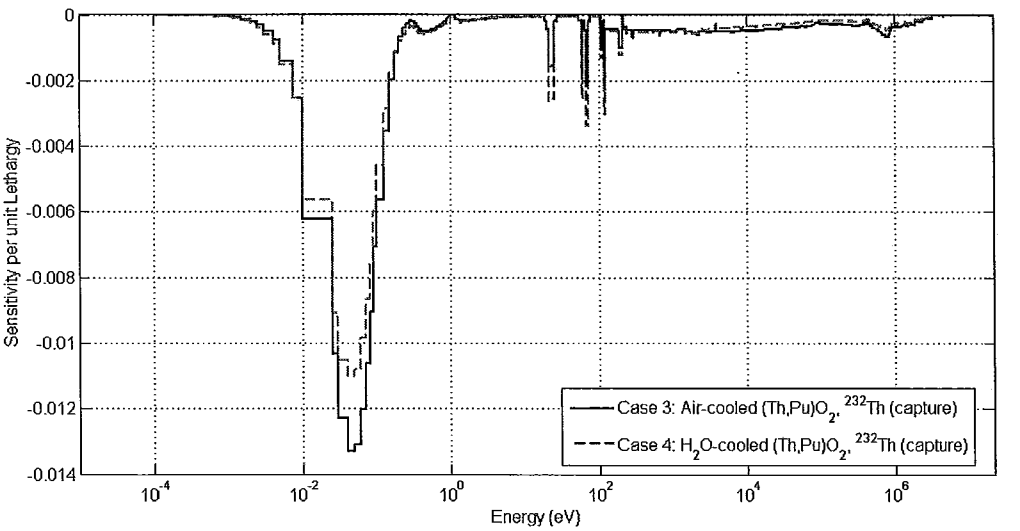

Figure 5.22: The groupwise ^{232}Th (capture) sensitivity profiles for cases 3 and 4.

The cross section data for ^{239}Pu (fission) are shown in Figure 5.23 and the groupwise sensitivity coefficients for ^{239}Pu (fission) are plotted in Figure 5.24. The peaks centred around 0.04 eV correspond to the average energy of thermalized neutrons entering the (Th, Pu)O_2 bundles. In the absence of a coolant, these neutrons cause ^{239}Pu (fission) reaction to also centre around

0.04 eV. When there is the coolant, obviously some of these neutrons are up-scattered to cause ^{239}Pu (fission) at about 0.3 eV which is the well-known ^{239}Pu (fission) resonance in the thermal energy range.

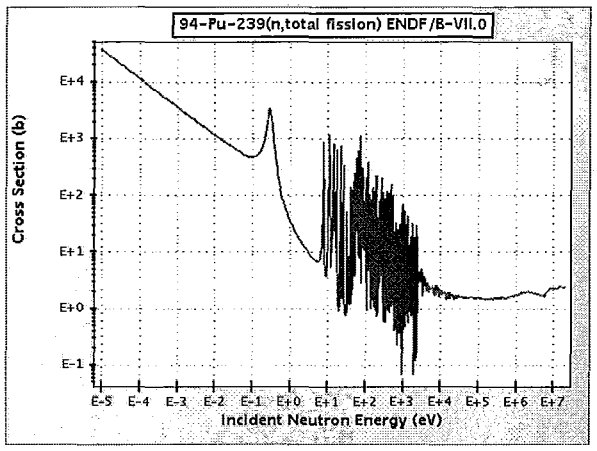

Figure 5.23: NNDF/V-II.0 cross section data for ^{239}Pu (fission) NNDC.

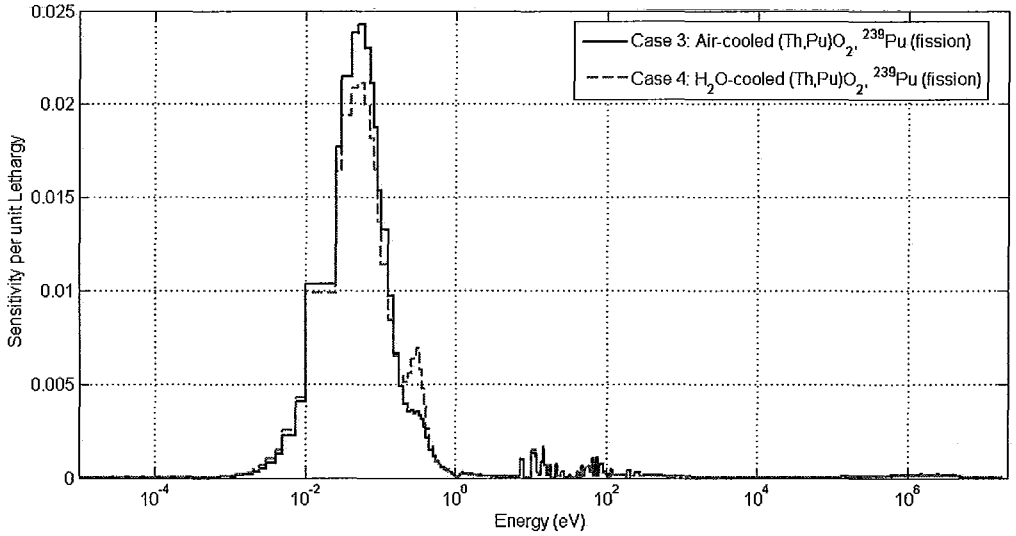

Figure 5.24: The groupwise ^{239}Pu (fission) sensitivity profiles for cases 3 and 4.

5.3 k_{eff} Uncertainty and Major Contributors

When the sensitivity of k_{eff} is coupled with the uncertainty in the cross section data, the SAMS module can compute the uncertainty in k_{eff} due to uncertainties in the nuclear data:

$$\sigma_k^2 = S_k \mathbf{C}_{\alpha\alpha} S_k^T \tag{5.130}$$

It is important to keep in mind that a large sensitivity coefficient does not warrant a large uncertainty component from the same nuclide-reaction. First of all, the magnitude of the sensitivity to a particular pair of isotope-reaction depends on both the cross section value and the total physical quantity that is present in the model. Secondly, if the uncertainty in the cross section value of this particular isotope is small, its contribution to the overall k_{eff} uncertainty can be small even though its sensitivity coefficient is big. In the following tables, there are several nuclide-reaction pairs whose integrated sensitivities do not stand out, but have made in the list of top k_{eff} uncertainty contributors.

Table 5.8 shows that the top five uncertainty contributors for case 1 and case 2 are identical. Even though the largest k_{eff} uncertainty contributor is ^{238}U (n,γ), its integrated sensitivity (by absolute magnitude) is less than that of ^{235}U ($\bar{\nu}$) or ^{235}U (fission). This means, its cross section uncertainty has to be larger than those of ^{235}U ($\bar{\nu}$) and ^{235}U (fission) in order to generate the biggest contribution into k_{eff} uncertainty. Similarly, even though the value of k_{eff} is very sensitive to ^{235}U ($\bar{\nu}$) and ^{235}U (fission), they contribute to about 20% of the overall k_{eff} uncertainty (15% + 5%) because their respective nuclear data are better known (smaller uncertainty).

Table 5.9 shows the same lists of top five uncertainty contributors for case 3 and case 4. This is not surprising in that it will be pointed out in Section 5.5 that cases 1 to 4 have a high degree of similarity in terms of the correlations in the uncertainties inherent in all systems. On the other hand, it can be seen from Table 5.10 that the uncertainty contribution from isotopes such as ^{232}Th and ^{239}Pu are less than 1mk. In terms of percentage of variance, they do not have significant contributions. This is because of their much smaller quantities in the models and the small sensitivities limit their uncertainty contributions.

Case	k_{eff} $\pm\sigma_k$(mk)	Nuclide-Reaction	σ_k^i(mk)	V%	S_I
1: Empty K0	1.00018 ±7.5mk	^{238}U (n,γ)	5.72	58%	-0.34
		^{235}U ($\bar{\nu}$)	2.86	15%	0.93
		^{2}H (n,2n)	2.17	8%	0.003
		^{238}U (n,n')	1.71	5%	-0.009
		^{235}U (fission)	1.65	5%	0.48
2: ZEEP K0	1.00048 ±7.5mk	^{238}U (n,γ)	5.73	58%	-0.34
		^{235}U ($\bar{\nu}$)	2.87	15%	0.93
		^{2}H (n,2n)	2.17	8%	0.003
		^{238}U (n,n')	1.71	5%	-0.009
		^{235}U (fission)	1.65	5%	0.47

Table 5.8: For cases 1 and 2, the top five contributors to the k_{eff} uncertainty are listed, in addition to the k_{eff} standard deviation σ_k. For each nuclide-reaction, σ_k^i is the corresponding standard deviation. The value of $V\%$ is calculated as $(\sigma_k^i)^2/(\sigma_k)^2$, the percentage of the total k_{eff} variance. S_I is the integrated sensitivity.

Case	k_{eff} $\pm\sigma_k$(mk)	Nuclide-Reaction	σ_k^i(mk)	V%	S_I
3: Air-cooled $(Th, Pu)O_2$	1.00151 ±6.9mk	^{238}U (n,γ)	5.14	56%	-0.30
		^{235}U ($\bar{\nu}$)	2.57	14%	0.83
		^{2}H (n,2n)	2.15	10%	0.003
		^{238}U (n,n')	1.52	5%	-0.008
		^{235}U (fission)	1.49	5%	0.42
4: H_2O-cooled $(Th, Pu)O_2$	1.0023 ±6.9mk	^{238}U (n,γ)	5.17	56%	-0.30
		^{235}U ($\bar{\nu}$)	2.60	14%	0.84
		^{2}H (n,2n)	2.12	9%	0.003
		^{238}U (n,n')	1.54	5%	-0.008
		^{235}U (fission)	1.50	5%	0.43

Table 5.9: For cases 3 and 4, the top five contributors to the k_{eff} uncertainty are listed, in addition to the k_{eff} standard deviation σ_k. For each nuclide-reaction, σ_k^i is the corresponding standard deviation. The value of $V\%$ is calculated as $(\sigma_k^i)^2/(\sigma_k)^2$, the percentage of the total k_{eff} variance. S_I is the integrated sensitivity.

Case	Nuclide-Reaction	σ_k^i(mk)	V%	S_I
3: Air-cooled $(Th, Pu)O_2$	^{239}Pu $(\bar{\nu})$	0.996	2.1%	0.097
	^{239}Pu (fission)	0.535	0.60%	0.053
	^{232}Th (n,γ)	0.340	0.243%	-0.0315
	^{1}H (n,γ)	0.259	0.132%	-0.050
4: H_2O-cooled $(Th, Pu)O_2$	^{239}Pu $(\bar{\nu})$	0.935	1.8%	0.0905
	^{239}Pu (fission)	0.494	0.51%	0.051
	^{232}Th (n,γ)	0.303	0.190%	-0.028
	^{1}H (n,γ)	0.280	0.164%	-0.056

Table 5.10: The values of uncertainty contribution from $(Th, Pu)O_2$ isotopes and ^{1}H (n,γ) are listed.

5.4 TSAR

The need for studying reactivity arises from reactor operation during which control rod movements, fuel temperature change, moderator purity fluctuation can all cause reactor state instability. The definition of reactivity ρ in the TSAR module was given by Equation (3.111):

$$\rho_{1\to 2} = \rho_2 - \rho_1 = \left(1 - \frac{1}{k_2}\right) - \left(1 - \frac{1}{k_1}\right) = \frac{1}{k_1} - \frac{1}{k_2} = \lambda_1 - \lambda_2$$

Utilizing the results from TSUNAMI-3D, TSAR calculates the sensitivity coefficients and uncertainty of reactivity in terms of the k_{eff} sensitivity coefficients, as shown in Equation (3.115):

$$S_{\rho,\alpha} = \frac{\lambda_2 S_{k_2,\alpha} - \lambda_1 S_{k_1,\alpha}}{\rho_{1\to 2}} = \frac{k_1 S_{k_2,\alpha} - k_2 S_{k_1,\alpha}}{k_2 - k_1}$$

If there had not been biases in the calculated k_{eff} due to nuclear data uncertainties, the reactivity of our four critical simulations would be zero. It is due to these biases that the reactivity result calculated by TSAR should be considered the reactivity bias:

$$\rho_{1\to 2} = \rho_2 - \rho_1 = (\rho_{2(crit.)} + \triangle\rho_2) - (\rho_{1(crit.)} + \triangle\rho_1) = \triangle\rho_2 - \triangle\rho_1 \quad (5.131)$$

where $\rho_{2(crit.)} = \rho_{1(crit.)} = 0$ when they are both at criticality. Since the values of calculated k_{eff} are known from Table 5.4, Equation (3.111) can be used to calculated the absolute reactivity biases which are summarized in Table 5.11.

Case	1	2	3	4
1: Empty at K0	0	0.297	1.327	2.117
2: ZEEP rod at K0	-	0	1.030	1.820
3: Air-cooled $(Th, Pu)O_2$	-	-	0	0.790
4: H_2O-cooled $(Th, Pu)O_2$	-	-	-	0

Table 5.11: Absolute values of the reactivity bias (in mk) for all four experiments in relation to each other.

It is expected that the biggest (smallest) bias comes from the pair of cases whose difference in calculated-k_{eff} is the greatest (smallest). Out of all four simulations, cases 3 and 4 are the closest scenario to a coolant void reactivity (CVR) change. As listed in Table 5.11, the absolute value of CVR bias is 0.790mk. From the H_2O-cooled state to the air-cooled state, the sign of the CVR bias becomes negative.

CVR bias is not to be confused with CVR worth, which is determined by:

$$\tilde{\rho}_{1\to 2} = \frac{1}{k^{cooled}} - \frac{1}{k^{voided}} \tag{5.132}$$

where we are interested in the value k^{voided}, given that $k^{cooled} = 1$ at criticality. In our case, a $(Th, Pu)O_2$ bundle with D_2O moderator and H_2O coolant, k^{voided} should be supercritical and the CVR worth $\tilde{\rho}_{1\to 2}$ is positive. Indeed, when a KENO simulation was performed using a H_2O density that was 0.1% of the original, while keeping all other materials and dimensions the same, the calculated-k_{eff} is 1.00767 and the CVR worth is about 5.31 mk, calculated according to Equation (5.132). Since there is no experimental k_{eff} measurement for this voided case, the bias in the calculated-k_{eff} is unknown.

From the point of view of code validation, CVR bias is important since the magnitude of the bias indicates the accuracy of the simulations. On the other hand, the value of CVR worth is more useful in reactor safety analysis in that we should be able to predict the amount of reactivity increase or decrease in a loss of coolant accident for power reactors. Even though the bias in k^{voided} is unknown experimentally, CVR bias can provide an approximated margin on the CVR worth's uncertainty due to uncertainties from nuclear data, modelling approximations and numerical errors.

Regardless of CVR bias or CVR worth, the TSAR module can generate reactivity sensitivity coefficients $S_{\rho,\alpha}$ in the same way. There are two conventions defined by TSAR which are *relative* and *absolute* sensitivity coefficients.

In Equation (3.115), the value of $\rho_{1\to 2}$ can be either positive or negative, making the interpretation of the sensitivity S_ρ more complicated. Therefore, by convention, the absolute value of $\rho_{1\to 2}$ is used in Equation (3.115) instead, which becomes:

$$S_{\rho,\alpha} = \frac{\lambda_2 S_{k_2,\alpha} - \lambda_1 S_{k_1,\alpha}}{|\rho_{1\to 2}|} \tag{5.133}$$

Equivalently, the *relative* sensitivity coefficient is:

$$S_{\rho,\alpha} = \frac{\alpha}{|\rho_{1\to 2}|}\frac{\partial \rho_{1\to 2}}{\partial \alpha} \tag{5.134}$$

This way, a negative $S_{\rho,\alpha}$ clearly indicates that a positive $\partial\alpha$ would imply a negative $\partial\rho_{1\to 2}$. In the case of extremely small reactivity difference, $|\rho_{1\to 2}|$ can be very small and the sensitivity coefficients very large. Hence the *absolute* sensitivity coefficient has also been defined:

$$S_{\rho,\alpha} = \lambda_2 S_{k_2,\alpha} - \lambda_1 S_{k_1,\alpha} \tag{5.135}$$

Since the CVR worth is positive in our case, the *relative* and *absolute* sensitivities are proportional with a factor of the value of $\tilde{\rho}_{1\to 2}$. Our emphasis is going to be put in the CVR worth's sensitivities in this work and will look at the *absolute* sensitivity without loss of generality.

Figure 5.25 shows the absolute reactivity sensitivity profiles for ^{239}Pu(fission) and ^{232}Th(capture). The negative peak centred at 0.3 eV for ^{239}Pu(fission) indicates that an increase in ^{239}Pu can result in a decrease in CVR worth. If we write out the change in CVR worth as the following:

$$\begin{aligned}
\mathrm{CVR^f} - \mathrm{CVR^i} &= \left(\frac{1}{k_c^f} - \frac{1}{k_v^f}\right) - \left(\frac{1}{k_c^i} - \frac{1}{k_v^i}\right) \\
&= \left(\frac{1}{k_c^f} - \frac{1}{k_c^i}\right) - \left(\frac{1}{k_v^f} - \frac{1}{k_v^i}\right) \\
&= \frac{k_c^i - k_c^f}{k_c^f k_c^i} - \frac{k_v^i - k_v^f}{k_v^f k_v^i} \\
&= \frac{k_v^f - k_v^i}{k_v^f k_v^i} - \frac{k_c^f - k_c^i}{k_c^f k_c^i}
\end{aligned} \tag{5.136}$$

where the subscripts c and v denote cooled and voided and superscript i, f denote the initial and final k_{eff} values due to an increase in isotope cross section value. First, we are certain that in the denominators in Equation (5.136), $k_c^f k_c^i$ is less than $k_v^f k_v^i$ for k_{eff} values which are supercritical. Let us now recall Figure 5.24. We see that in the same energy range in the vicinity

of 0.3 eV, S_k for ^{239}Pu(fission) is more positive in the cooled case than in the voided case, meaning $k_c^f - k_c^i$ is larger than $k_v^f - k_v^i$. Putting this result back into Equation (5.136), we can see that $CVR^f - CVR^i$ is indeed negative about 0.3 eV of the ^{239}Pu resonance. The same mathematical reasoning can be applied to explain the S_ρ profile for ^{232}Th(capture) in Figure 5.25.

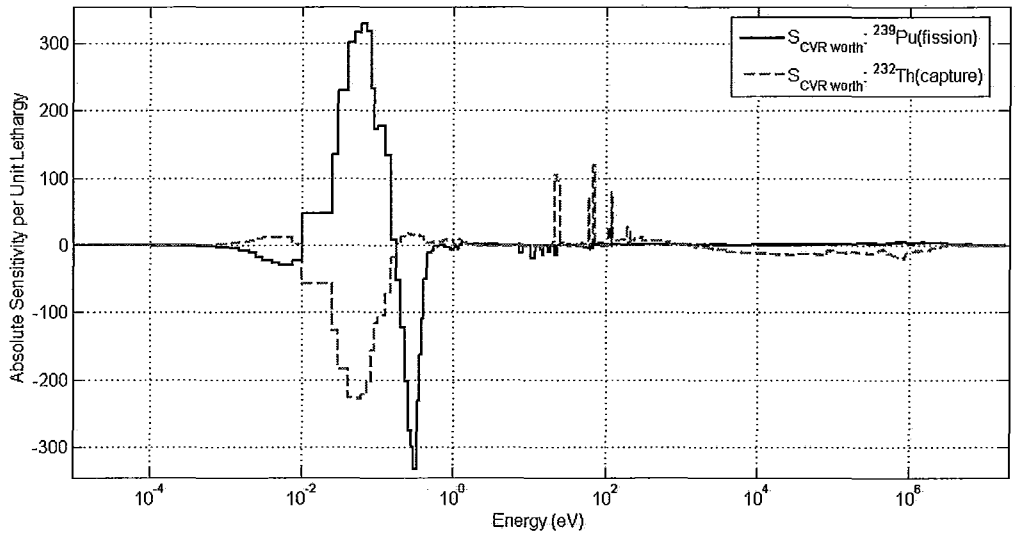

Figure 5.25: ^{239}Pu(fission) and ^{232}Th(capture) absolute sensitivity profiles for CVR worth.

Similar to the k_{eff} uncertainty calculated by SAMS, the uncertainty in CVR worth can also be calculated by TSAR using Equation (3.116), whose results are presented in Table 5.12. The top contributor in the CVR worth uncertainty is ^{239}Pu ($\bar{\nu}$) which also has the third highest integrated sensitivity coefficient (by magnitude), after ^{235}U ($\bar{\nu}$), and ^{235}U (fission). It is also interesting to find ^{27}Al (n,γ) as the third top uncertainty contributor. Aluminum is the main material of the central support tube and calandria and pressure tubes. Contributing about 7% in the CVR worth uncertainty, ^{232}Th (n,γ) is the only nuclide-reaction pair in Table 5.12 that has a negative integrated sensitivity coefficient.

Nuclide - Reaction		σ_ρ^i(mk)	V%	S_I
^{239}Pu	($\bar{\nu}$)	0.065	18.1%	645
^{238}U	(n,γ)	0.054	12.5%	307
^{27}Al	(n,γ)	0.050	12%	118
^{2}H	(elastic)	0.049	10.3%	235
^{239}Pu	(fission)	0.047	9.6%	271
^{238}U	(n,n')	0.044	8.3%	23.4
^{232}Th	(n,γ)	0.040	7%	-347

Table 5.12: Top contributors in the CVR worth standard deviation (σ_ρ) which is 0.15mk. The value of $V\%$ is calculated as $(\sigma_\rho^i)^2/(\sigma_\rho)^2$, the percentage of the total CVR worth variance. S_I is the integrated *absolute* sensitivity.

5.5 Similarity by TSUNAMI-IP

The TSUNAMI-IP module can generate the integral c_k index to quantify the similarity between systems, one of which can be a benchmark experiment, the other can be but is not limited to an application. Even though we have four benchmark experiments and we can still use TSUNAMI-IP to examine their similarity. The values of their c_k set the admissible criterion for the TSURFER module.

Case	1	2	3	4
1: Empty at K0	1.0	1.0	0.9828	0.9852
2: ZEEP rod at K0	-	1.0	0.9828	0.9852
3: Air-cooled (Th, Pu)O_2	-	-	1.0	0.9998
4: H_2O-cooled (Th, Pu)O_2	-	-	-	1.0

Table 5.13: Values of the integral c_k indices for all four experiments in relation to each other.

Recall equation (3.120), (3.121) and (3.122):

$$c_k = \frac{[C_k]_{ij}}{\sqrt{[C_k]_{ii}}\sqrt{[C_k]_{jj}}} = \frac{\sigma_{ij}^2}{\sigma_i \sigma_j} = \frac{S_i C_{\alpha\alpha} S_j^T}{\sqrt{S_i C_{\alpha\alpha} S_i^T}\sqrt{S_j C_{\alpha\alpha} S_j^T}} \tag{5.137}$$

The entries along the diagonal in Table 5.13 represent the condition when $i = j$ in Equation (5.137). Hence they have the maximum value of 1,

meaning a full correlation. Interestingly, the c_k between the two ZEEP cases is also equal to 1, which suggests they have extremely similar k_{eff} sensitivity coefficients (it was not feasible to compare *all* k_{eff} sensitivity coefficients in Section 5.2). But this c_k value (equal to 1) does not conclude the equality of the k_{eff} sensitivity coefficients. On the contrary, σ_{ij} is cumulative by definition:

$$\sigma_{ij}^2 = \sum_{\alpha} (S_{i,\alpha} C_{\alpha\alpha} S_{j,\alpha}) \tag{5.138}$$

Individual sensitivity coefficients $S_{i,\alpha}$, $S_{j,\alpha}$ do not have to be identical. Their c_k number which is both the correlation coefficient and similarity index implies the two ZEEP cases (1 and 2) are fully correlated in terms of the summed correlations in the uncertainties shared by both systems. This is the case mainly because the material compositions are the same and both systems are at criticality. This also resulted in the same c_k values for case pairs 1/3 and 2/3, 1/4 and 2/4 when cases 1 and 2 are seen as fully correlated.

On the other hand, the $(Th, Pu)O_2$ bundles and the ZEEP rod are made of very different materials. But this difference is small in physical proportions compared to the rest of the system (63 ZEEP rods vs. 1 $(Th, Pu)O_2$ channel). The deviation of the c_k value from unity is less than 2% and is obviously the result of the materials in the $(Th, Pu)O_2$ bundles, such as the fuel materials and zircaloy in the cladding, as well as aluminum in the central support tube, calandria and pressure tubes.

In Table 5.13 we also observe that case 1 (or 2) is more similar to case 4 than case 3. It appears that the addition of H_2O coolant which is not present in case 1, 2 or 3 actually increases the correlation in uncertainty between ZEEP rods and $(Th, Pu)O_2$ bundles. The possible explanation is that H_2O is more correlated in uncertainty than air is, because of the large D_2O quantity as the moderator in the systems. Air is clearly far less *"similar"* to D_2O than H_2O is, in ways from cross section data to physical properties (eg. density). Furthermore, voiding the coolant affects the flux spectra and sensitivity coefficients of ^{232}Th and ^{239}Pu. These differences consequently decrease the uncertainty correlations with the ZEEP cases.

Furthermore, the c_k value between case 3 and case 4 is the second highest in Table 5.13. This is not unexpected since the fuel materials are the same and the difference in the coolant type is limited in a single channel (vs. 63 identical ZEEP rods). From all c_k values, it seems that the critical height is not a big factor even though it is closely related to the reactivity of the K0 site, whether it is a ZEEP rod or a $(Th, Pu)O_2$ bundle or there is no fuel present. The evidence is the strongest in the case pair 1 and 2 where the critical height difference is about 13 cm and their c_k can still be 1.

So far, only the similarity of experiments has been compared. TSUNAMI-IP can also be used to assess the similarity between experiments and applications. The coolant void simulation is an application which does not have experimental measurements. Its sensitivity coefficients have been calculated in the same manner as the experiments by TSUNAMI-3D and they can be input to TSUNAMI-IP to obtain both the similarity c_k and the integral G indices. Recall Equation (3.123), the G index represents the total overlapping of sensitivities between the experiment and the application. Index G can be further categorized into fission, capture and scattering reactions. They are listed in Table 5.14

CVR simulation	Empty at K0	ZEEP rod at K0	Air-cooled $(Th, Pu)O_2$	H_2O-cooled $(Th, Pu)O_2$
c_k	0.9825	0.9825	1	0.9998
G	0.8854	0.8849	0.9926	0.9803
$G_{fission}$	0.8893	0.8893	0.9988	0.9892
$G_{capture}$	0.8852	0.8854	0.9979	0.9849
$G_{scatter}$	0.8698	0.8639	0.9435	0.9227

Table 5.14: Integral c_k, total and reaction-specific G indices for the CVR simulation in relation to the four experiments.

It is interesting to find a full correlation between the air-cooled case and the CVR simulation, even though the CVR simulation has 7.67 mk excess and the air-cooled case has a k_{eff} bias of 1.517 mk. This suggests, in terms of sensitivities, the approach where the coolant density is reduced to 0.1% of the original, is equivalent to simulating air coolant in a real experiment. The values of G indices are above 0.92 for cases 3 and 4 while they are only above 0.86 for cases 1 and 2. The $G_{scatter}$ index has the smallest value of all three reactions for cases 1 to 4.

5.6 Bias Adjustment by TSURFER

At the last stage in the TSUNAMI sequence, the TSURFER module uses the sensitivity data and the method of Generalized Linear Least Squares (GLLS) to determine a set of nuclear data which will generate a computed k_{eff} value very close to it experimental value. For the four ZED-2 experiments we have been studying, the experimental k_{eff} values should be equal to 1 for

critical experiments. But they have computed k_{eff} values with biases ranging from 0.188 mk (case 1) to 2.3 mk (case 4).

The goodness of the TSURFER adjusted nuclear data is evaluated based on the value of χ^2 per degree of freedom (dof). In order to calculate χ^2, the TSURFER module requires both experimental and nuclear data uncertainties as explained in Chapter 2.5. The challenge of using TSURFER in our work is the lack of experimental uncertainty measurements. The reason is very much its little relevance in the actual experiments. In order to achieve criticality in ZED-2, the moderator level was raised to reduce the neutron leakage. Since ZED-2 does not have any reactivity control devices (it has shut-off rods though), its criticality state is entirely controlled by the moderator height. Therefore, in reality once ZED-2 reaches criticality, it is at an equilibrium state which means the power level is constant. This makes the estimation of experimental uncertainties extremely difficult. An alternative approach is to utilize a physical quantity (q) which has a known uncertainty ($\triangle q$) and assume that the bias in k_{eff} ($\triangle k$) due to the nuclear data uncertainties (σ_α) remains unchanged upon varying this quantity within its uncertainty:

$$\mathrm{k} = \mathbf{k}(q) + \triangle k(\sigma_\alpha) \tag{5.139}$$

$$\mathrm{k}' = \mathbf{k}'(q + \triangle\, q) + \triangle k(\sigma_\alpha) \tag{5.140}$$

$$\triangle \mathbf{k} = \mathbf{k}'(\alpha_m + \triangle \alpha_m) - \mathbf{k}(\alpha_m) = \mathrm{k}' - \mathrm{k} \tag{5.141}$$

which simply derives the experimental k_{eff} uncertainty ($\triangle \mathbf{k}$) to be the difference between the simulated k_{eff} values, k′ and k.

5.6.1 Source of Experimental Uncertainty

It is known that the greatest uncertainty comes from the moderator purity in ZED-2. The moderator purity was measured to be 99.495 wt% (Jones, 1984), and we assume it has a common uncertainty of 0.005 wt%. This can be interpreted that if the moderator purity is measured experimentally for a large number of times, the sample has a normal probability density function with a mean at 99.495 wt% and 0.005 w% is one standard deviation (shown in Figure 5.26).

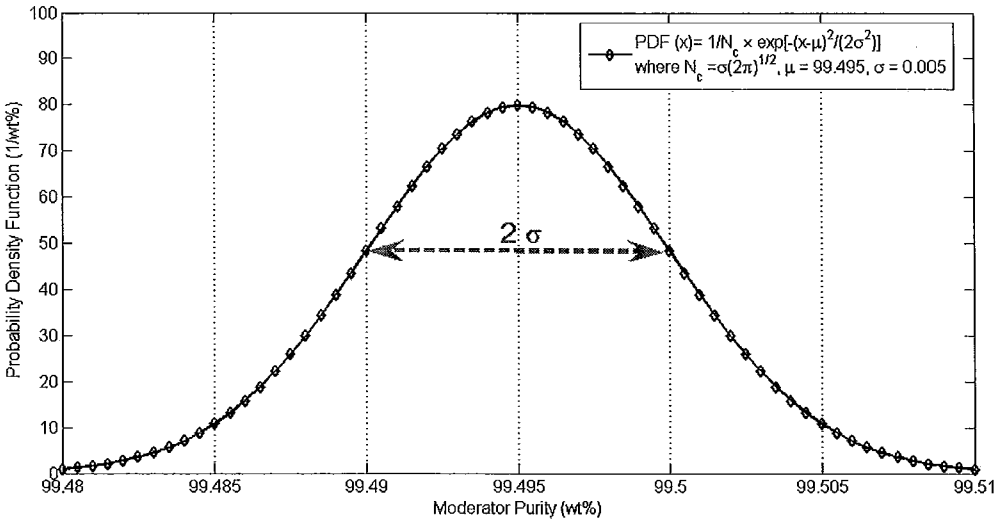

Figure 5.26: Probability density function for the moderator purity is assumed to be a normal distribution with a mean at 99.495 wt% and one standard deviation of 0.005 wt%.

The value of k_{eff} is sensitive to the change in moderator purity and therefore its uncertainty can contribute to the k_{eff} experimental uncertainty as well. In reality, the k_{eff} measurements would always be unity since ZED-2 is a critical reactor. This is why it is very difficult to specify and record the exact k_{eff} experimental uncertainties. Without the ability to actually perform these measurements, we had to rely on simulations. As a start, we used the CSAS5 module (Goluoglu *et al.*, 2009a) in SCALE6 to simulate case 1 ("No fuel at K0") using moderator purity values from 99.49 wt% to 99.50 wt% ($\pm\sigma$ from the mean). We obtained the calculated $k_{eff} \pm 1\ \sigma$ and plotted the corresponding reactivity values in Figure 5.27. The CSAS5 module runs KENO V.a Monte Carlo code to obtain the k_{eff} value of the model.

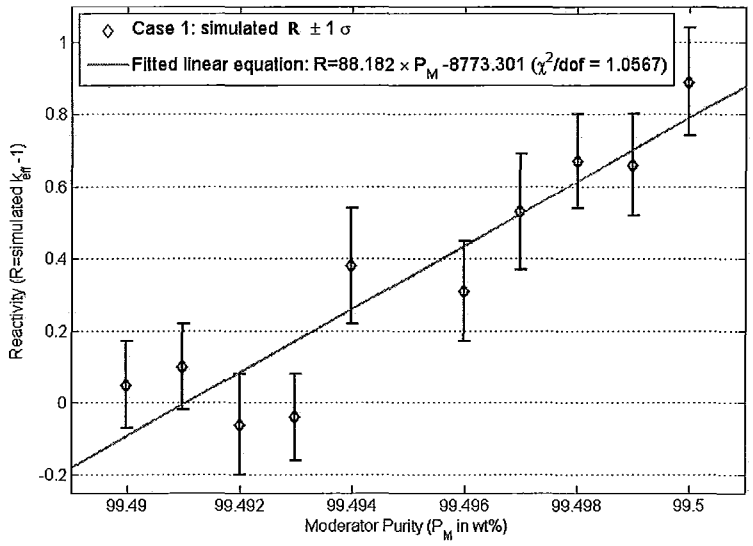

Figure 5.27: k_{eff} values and standard deviations were computed using the CSAS5 module. A linear equation is fitted for Reactivity (in mk) vs. Moderator Purity. Reactivity is defined as $(k_{eff}\text{-}1)\times 10^3$.

First observation is that the simulated k_{eff} values do not increase in a perfectly linear fashion in response to the increase in moderator purity. This illustrates the drawback of using Monte Carlo (as opposed to deterministic methods) to examine small direct perturbations for large, three-dimensional systems. All Monte Carlo results have statistical standard deviation for the mean values, the size of which is directly influenced by the initial parameter set-up for the Monte Carlo simulation, such as `sig` (k_{eff} convergence), `npg` (neutron per generation) and `gen` (number of generations). In theory, the smaller the `sig` and the larger the `npg` and `gen` values are, the smaller the statistical fluctuations in k_{eff} are, compared to the reactivity effect due to direct perturbation (Dean and Blackwood, 2007). For these simulations, the `sig` convergence was set as 0.2 mk which is about the magnitude of the reactivity difference between two successive cases. We could have selected a smaller convergence but that would cost us the expense of time consuming calculations (for 40 CSAS5 runs and about 3.5 hours each). In our case, we are more interested in the *spread* of the k_{eff} values around its mean than the exact k_{eff} values individually. When a linear equation was fitted to the data points, we do observe a linear trend by the scattered data points. The choice of linearity (by the means of a linear χ^2 fitting) is based on the assumption that the perturbations are small enough so that the linear dependence of k_{eff} within the range is valid. Furthermore, the goodness of the fit is determined

by χ^2/dof:

$$\chi^2/dof = \left(\sum_i^N \frac{(R_f(i) - R(i))^2}{\sigma(i)^2} \right) /(N-2) \tag{5.142}$$

where $R_f(i)$ is the value of the i^{th} fitted reactivity, $R(i)$ is the i^{th} calculated value and $\sigma(i)$ is the standard deviation of the i^{th} reactivity. The degree of freedom is equal to the total number of data points (N) minus the number of fitted parameters which is 2 for the linear fit. The linear fit in Figure 5.27 gives a χ^2/dof of 1.056 and hence it is a good representation of the reactivity data within the data's uncertainties.

Before we continue, we recognize there could exist other experimental uncertainty sources such as moderator temperature and critical height. However, neither of them contribute noticeably for the following reasons. The ZED-2 reactor operates at very low power and the experiments were conducted at a temperature about 21°C (Jones, 1984). At such a low temperature and low power, reactivity effects associated with fuel temperature coefficient and Doppler effect are all negligible. The critical height measurements have an estimated accuracy of ±0.1 mm (Jones, 1984) which is very precise for the purpose of controlling reactivity. However KENO simulations using the value of ±0.1 mm as the critical height uncertainty showed unchanged k_{eff} values, therefore eliminating it as a significant experimental uncertainty contributor.

5.6.2 Extrapolation of k_{eff} Experimental Uncertainty

So far we have assumed that (1) experimental k_{eff} uncertainty is primarily affected by a single parameter, moderator purity (2) the probability density distribution of the moderator purity is normal and (3) k_{eff} variation is approximately linear within the uncertainty range of the moderator purity. According to Dean and Blackwood (2007, chapt. 1.3), the standard deviation of k_{eff} can be obtained from the standard deviation of the moderator purity and it represents an approximate 68% level of confidence. The contribution to the standard deviation of k_{eff} from the standard deviation of moderator purity can be obtained as (Dean and Blackwood, 2007, chapt. 4.1.5):

$$\sigma_{\mathrm{k,exp}} = \frac{\sigma_P}{\delta P}\left(\mathrm{k(P_{ref} + \delta P) - k(P_{ref})}\right) = \frac{\sigma_P}{\delta P}\delta \mathrm{k} = \left(\frac{\delta \mathrm{k}}{\delta P}\right)\sigma_P \tag{5.143}$$

where $\delta \mathrm{k} = \mathrm{k(P_{ref} + \delta P) - k(P_{ref})}$ is the change in k_{eff} caused by the change in purity δP, and σ_P is the standard deviation of moderator purity. Now let

us recall Equation (2.66) in Chapter 2.4:

$$\sigma_{\mathcal{F}}^2 = \left(\frac{\partial \mathcal{F}}{\partial a}\right)^2 \sigma_a^2 + \left(\frac{\partial \mathcal{F}}{\partial b}\right)^2 \sigma_b^2 + 2\left(\frac{\partial \mathcal{F}}{\partial a}\right)\left(\frac{\partial \mathcal{F}}{\partial b}\right)\sigma_{ab}^2$$

If now $\mathcal{F}$ is a function of a single parameter (such as P), the variance of $\mathcal{F}$ due to the variance of P can be simplified to be:

$$\sigma_{\mathcal{F}}^2 = \left(\frac{\partial \mathcal{F}}{\partial P}\right)^2 \sigma_P^2 \quad or \quad \sigma_{\mathcal{F}} = \left(\frac{\partial \mathcal{F}}{\partial P}\right)\sigma_P \tag{5.144}$$

Notice that Equation (5.143) has the same mathematical form and this shows the derivation of Equation (5.143) follows the same error propagation rule as Equation (2.66) using the above assumptions.

The factor $\left(\frac{\delta k}{\delta P}\right)$ can be easily obtained since we have determined the slope of the linear fit in Figure (5.27):

$$R_f(P) = A \cdot P + B \tag{5.145}$$

$$\frac{dk}{dP} \approx \frac{d}{dP}(R_f + 1) = \frac{dR_f(P)}{dP} = A = \text{slope} \tag{5.146}$$

Factor A for case 1 was found to be 88.182 mk/wt%. For cases 2, 3 and 4, CSAS5-computed k_{eff} data were also obtained by varying the moderator purity from 99.49% to 99.50%. They were fitted using the same linear χ^2 fitting technique and the results are shown in Figure 5.28, Figure 5.29 and Figure 5.30 respectively.

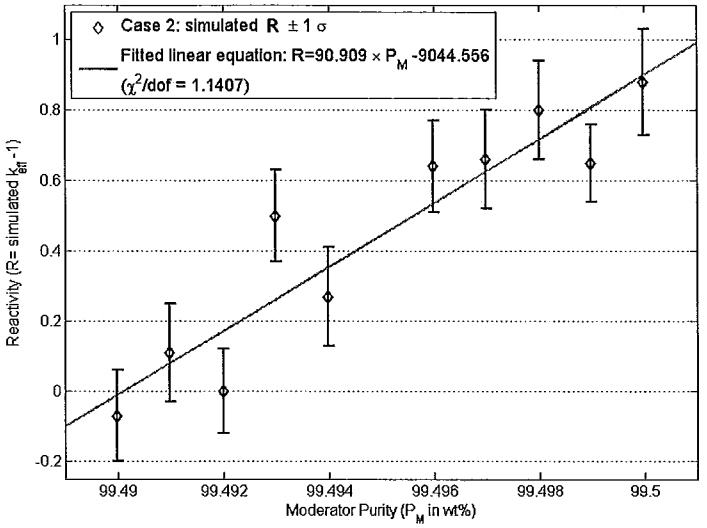

Figure 5.28: Case 2 k_{eff} $\pm\sigma$ values were computed using the CSAS5 module. A linear equation is fitted for Reactivity (in mk) vs. Moderator Purity. Reactivity is defined as $(k_{eff}\text{-}1)\times 10^3$.

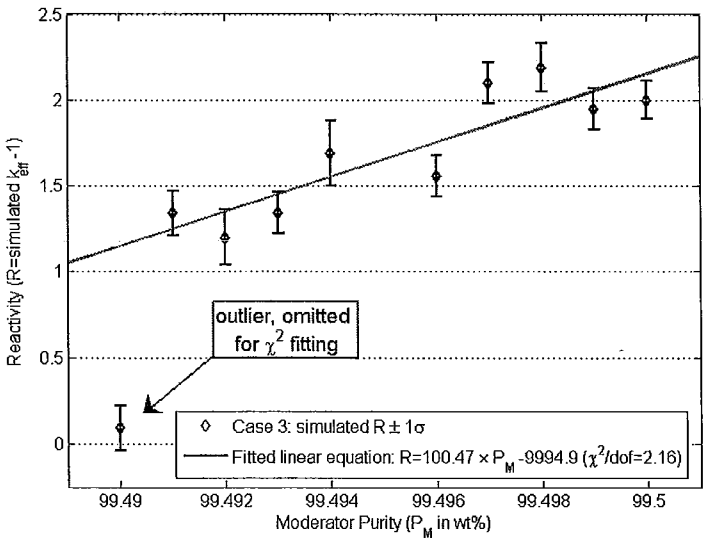

Figure 5.29: Case 3 k_{eff} $\pm\sigma$ values were computed using the CSAS5 module. A linear equation is fitted for Reactivity (in mk) vs. Moderator Purity. Reactivity is defined as $(k_{eff}\text{-}1)\times 10^3$.

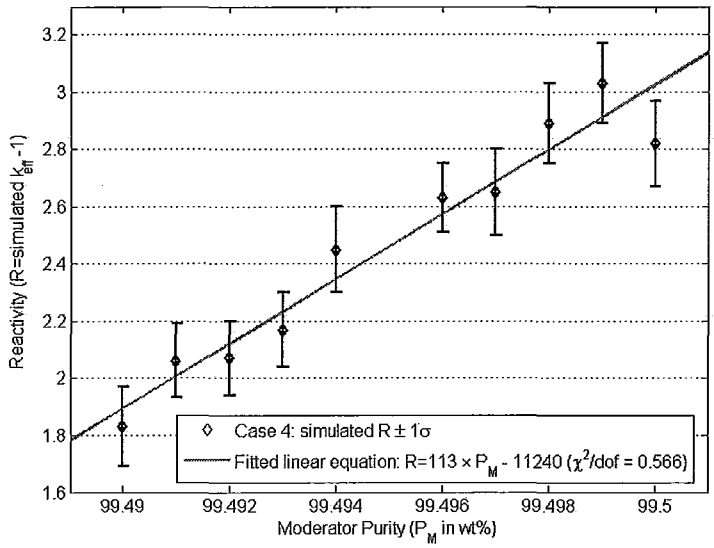

Figure 5.30: Case 4 k_{eff} $\pm\sigma$ values were computed using the CSAS5 module. A linear equation is fitted for Reactivity (in mk) vs. Moderator Purity. Reactivity is defined as $(k_{eff}\text{-}1)\times 10^3$.

Table 5.15 summarizes the four slope values as well as the k_{eff} uncertainty values due to moderator purity uncertainties, as calculated using Equation (5.143).

Cases	1	2	3	4
A (mk/wt%)	88.182	90.909	100.47	113
σ_k (mk)	0.441	0.455	0.502	0.565

Table 5.15: Value of A in Equation (5.146) is the ratio between changes in k_{eff} due to changes in moderator purity in the linear region. The values of σ_k are obtained from multiplying the corresponding A by σ_P which equals 0.005 wt%.

5.6.3 Extrapolation of Experiment Correlation

The uncertainty values have to be included in the TSURFER input file, using parameter uv. In addition to uv, the correlation coefficient $\rho_{i,j}$ for (active) responses i and j due to moderator purity uncertainty is the other parameter TSURFER input file requires. It was shown in Chapter 3.5, the relative covariance matrix $C_{mm}(i,j)$ which is required in the GLLS method is

calculated from the σ_k values (Table 5.15) and $\rho_{i,j}$ (in the case of a single uncertainty parameter) as:

$$C_{mm}(i,j) = \sigma_i \rho_{i,j} \sigma_j \tag{5.147}$$

The definition of correlation coefficient is the same throughout our work, whether it is in TSUNAMI-IP (Equation (3.122)), or here:

$$\rho_{i,j} = \frac{COV(k_i, k_j)}{\sqrt{VAR(k_i)VAR(k_j)}} = \frac{\sum(k_i - \bar{k}_i)(k_j - \bar{k}_j)}{\sigma_i \sigma_j} \tag{5.148}$$

It is emphasized here that we are using simulation results to estimate experimental correlations due to the shared moderator purity uncertainty, based on the three assumptions discussed previously. Table 5.16 lists the correlation coefficients and they should be included between the `read corr` and `end corr` block in the TSURFER input file.

Case	1	2	3	4
1: Empty at K0	1.0	0.81747	0.75141	0.89811
2: ZEEP rod at K0	-	1.0	0.82495	0.89121
3: Air-cooled $(Th, Pu)O_2$	-	-	1.0	0.86919
4: H_2O-cooled $(Th, Pu)O_2$	-	-	-	1.0

Table 5.16: Correlation coefficients $\rho_{i,j}$ for all four experiments in relation to each other, due to the shared moderator purity uncertainty.

5.6.4 Experiments and Application in TSURFER

While cases 1 to 4 were input in TSURFER as the *active responses* with their respective k_{eff} values from KENO V.a., a fifth case was also included as the *passive response*. It is the coolant void simulation by which the value of $(Th, Pu)O_2$ bundle CVR worth was derived. Originally, the reactivity (still defined as k_{eff} - 1) is 7.67 mk. Since it is a simulation only without experimental measurements, the experimental uncertainty is set internally by TSURFER to 10^{10}, a large value to approximate the "infinite" uncertainty. The correlation to other active responses is set to zero (Williams *et al.*, 2009b). In Table 5.14, the similarity indices between this case and the other four experiments were listed. A high degree of correlations among them is required in order for TSURFER to apply GLLS fit on the four experiments.

The χ^2/dof is found to be 3.684 where dof is equal to 4, the number

of experiments. Though the χ^2/dof value we obtained from TSURFER is not the ideal $\pm$ 2% from unity, theoretically χ^2/dof can be improved by including more of similar ZED-2 $(Th, Pu)O_2$ experiments in TSURFER in future work. In our case, the advanced thorium fuel program did not have the opportunity to continue or expand after the publication by Jones (1984). For now we can only use the available $(Th, Pu)O_2$ experiments in ZED-2 to demonstrate the capabilities of TSUNAMI analysis.

5.6.5 k_{eff} Results by TSURFER

Table 5.17 lists the original (before), adjusted (after) k_{eff} and corresponding k_{eff} uncertainties (σ_k) due to nuclear data uncertainties. Also presented is the new k_{eff} for the CVR application (case 5) after the nuclear data adjustment by GLLS. It is observed that the k_{eff} biases for cases 1 and 2 have increased after the adjustment. On the other hand k_{eff} biases for cases 3 and 4 are both reduced. At first glance, the results for cases 1 and 2 are worse by the evaluation of k_{eff} values alone. However, after the nuclear data GLLS adjustments, the k_{eff} uncertainties σ_k are drastically decreased (from 6, 7 mk to less than 0.5 mk). The significance of this result is that nuclear engineers and physicists can be more confident with these calculated k_{eff} values than before. Prior to the TSURFER GLLS adjustments, k_{eff} uncertainties were more than 6.9 mk for all four experiments and the CVR application. This implies that even though the biases of case 1 and case 2 were smaller (less than 0.5 mk), the large k_{eff} uncertainties gave error bars 10 times more than the bias values. However, after the GLLS adjustments, k_{eff} uncertainties of cases 1, 2, and 4 are all smaller than the new biases respectively. In terms of reactor safety, the new k_{eff} uncertainties can give more confidence in the calculated values for the nuclear engineers and reactor physicists.

Cases:		1	2	3	4	5
k_{eff}-1	before	0.18	0.48	1.51	2.3	7.67
	after	0.53	0.85	0.24	1.05	6.36
σ_k	before	7.5	7.5	6.9	6.9	6.9
	after	0.387	0.382	0.490	0.489	0.495

Table 5.17: Comparison between the k_{eff}-1 and k_{eff} uncertainty due to nuclear data uncertainty, before and after the TSURFER (GLLS) calculations. The values are all in mk.

5.6.6 Application Bias and CVR Worth

The difference between k_{eff} values before and after GLLS adjustment is called the application bias. For the simulation of case 5 which was created by reducing the H_2O coolant density to 0.1%, the application bias was found to be 1.3079 mk. But it should be used with caution because unlike cases 1 to 4, case 5 does not have experimental k_{eff} data to verify the simulation results. TSURFER also calculated the isotopic contributions to the application bias using Equation (3.127). The top five contributors to the application bias are listed in Table 5.18. The same list of nuclide-reactions also appeared in Table 5.12 as the CVR worth uncertainty contributors before TSURFER GLLS adjustment.

Nuclide - Reaction		$\Delta k/k$ (%)
^{239}Pu	($\bar{\nu}$)	0.112
^{2}H	(elastic)	-0.0669
^{27}Al	(n,γ)	0.0342
^{239}Pu	(fission)	0.0299
^{238}U	(n,γ)	-0.027

Table 5.18: Top contributors in the application bias and the respective contribution in relative percentage ($\Delta k/k\%$).

Once again, using Equation (5.132) and the new k_{eff} values in Table 5.17, we can calculate the new CVR worth to be:

$$\rho_{\text{worth}} = \frac{1}{k^{\text{cooled}}} - \frac{1}{k^{\text{voided}}} = \frac{1}{1.00105} - \frac{1}{1.00636} = 5.2709\text{mk} \qquad (5.149)$$

The new CVR worth value is slightly smaller than the original value of 5.3079 mk.

5.6.7 Cross Section Adjustments

Nuclide-reaction cross sections were adjusted using Equation (2.100) such that new k_{eff} values could have smaller biases. The adjustments in the cross sections have the same energy group structure as `44groupcov`, the 44-group covariance matrix. Figure 5.31 shows the relative cross section adjustments for the top five σ_k uncertainty contributors in the application bias.

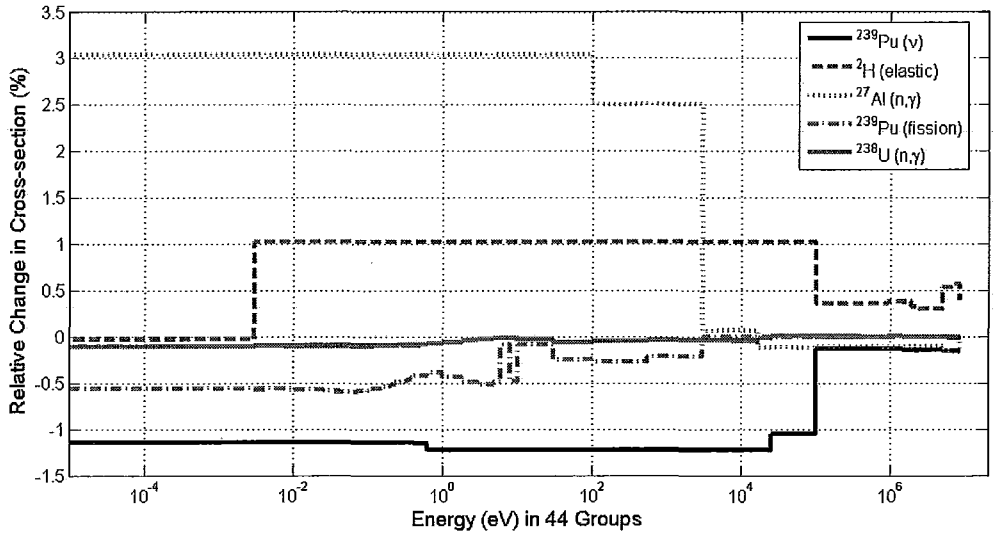

Figure 5.31: Relative cross section adjustments for the five nuclide-reaction pairs that contribute the most to the application bias.

It is clear from the graphs that the nuclear data of both ^{239}Pu ($\bar{\nu}$) and ^{239}Pu (fission) are reduced over the 44 energy groups, shown by the negative relative cross section percentages. These observations were expected since both reactions have positive k_{eff} sensitivities. In order to reduce the positive k_{eff} biases, their cross section values have to become smaller. In comparison, the adjustment of ^{238}U (n,γ) cross section was close to zero. However, the small fractional change in the cross section can affect k_{eff} substantially considering the large physical presence of ^{238}U throughout all experiments in the 63 ZEEP rods. It was found to be the top k_{eff} uncertainty contributor in all cases (Tables 5.8 and 5.9) therefore the bias and uncertainty it contributes to the k_{eff} as a whole are quite large.

For ^{2}H (elastic), the relative cross section adjustment is about 1% over a large energy range from 10^{-2} eV to 10^{5} eV. An examination of the ^{2}H (elastic) cross section data from NNDC, Figure 5.32 reveals that its value is also constant over the same energy range. Thus the absolute adjustments are uniform from 10^{-2} eV to 10^{5} eV.

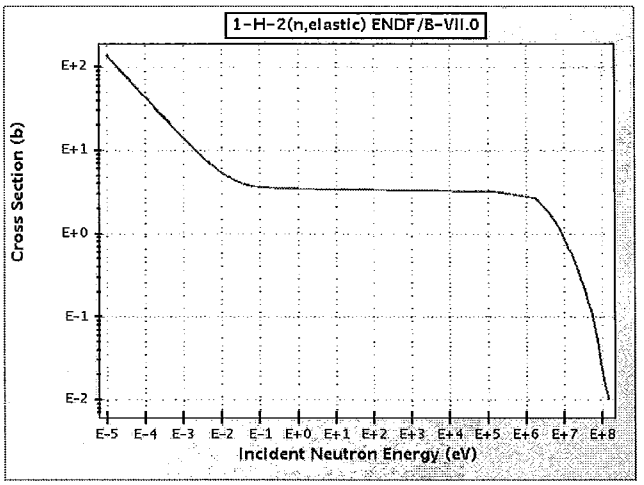

Figure 5.32: ENDF/B-VII.0 cross section data for ^{2}H (elastic), taken from NNDC.

Finally, ^{27}Al (n,γ) is found to have 2.5% to 3% adjustments from thermal energy up to 10^3 eV, which are larger than the other four nuclide-reaction pairs. It suggests the accuracy of the ^{27}Al (n,γ) cross section value is put in question when a 3% increase would be needed in order to reduce k_{eff} bias. Aluminum mainly comes from the central support tube, the pressure tube, the calandria tube and the calandria tank. Though it is neither fuel nor moderating material, we already saw that ^{27}Al (n,γ) contributed 12% of the total variance to the CVR worth uncertainty (Table 5.12). Therefore, the uncertainty of ^{27}Al data should be investigated, in that the adjustment results indicate the accuracy of existing experimental ^{27}Al data is questionable.

Chapter 6

Conclusion

In this work, the sensitivity and uncertainty (S/U) analysis methodology has been applied to study four benchmark experiments of the irradiation of $(Th, Pu)O_2$ fuel bundles. Rigorous analyses were carried out by TSUNAMI which is a series of computer code modules executed in sequence. The ultimate goal of TSUNAMI is to establish a consistent and systematic procedure to compare benchmark experiments and design systems (applications that have not been measured). The results from the S/U analysis of the $(Th, Pu)O_2$ benchmark experiments in this work serve as the basis for the future application studies of $(Th, Pu)O_2$ in CANDU-type reactors.

The first step of the S/U TSUNAMI analysis was to generate sensitivity coefficients which reveal how the changes in nuclide-reaction cross sections can explicitly and implicitly affect the system's k_{eff} value. Based on the first-order linear perturbation theory, the computation of sensitivity coefficients requires forward and adjoint neutron fluxes to be calculated by the three-dimensional Monte Carlo code KENO. Full core simulations of the benchmark experiments gave k_{eff} values which had biases ranging from 0.188 mk to 2.3 mk. The sensitivity coefficients were computed by SAMS which then performed the second part of the S/U analysis: the determination of uncertainties in the calculated k_{eff} values due to uncertainties in the nuclear data. It is found that the uncertainties range from 6.9 mk to 7.5 mk, and the main contributors are consistently ^{238}U (n,γ) (56% to 58%), ^{235}U ($\bar{\nu}$) (14% to 15%) and ^{2}H (n,2n) (8% to 10%) for the four benchmark experiments.

For illustrative purposes, an application was constructed to simulate the loss of coolant effects on reactivity, by reducing the coolant density in the $(Th, Pu)O_2$ fuel bundles to 0.1 wt% of the original. The voiding of coolant resulted in a system state with 7.67 mk above criticality. The TSAR module of TSUNAMI was used to calculate the coolant void reactivity (CVR) worth and its uncertainty to be 5.3 mk and 0.15 mk respectively. Similar to the k_{eff} uncertainty, the CVR worth uncertainty was calculated by taking into account the nuclear data uncertainties and TSAR identified ^{239}Pu ($\bar{\nu}$) (18%), ^{238}U (n,γ) (12.5%) and ^{27}Al (n,γ) (12%) to be the top uncertainty contributors.

As indicated by the identical list of top k_{eff} uncertainty contributors, the four simulations share a high degree of similarity in terms of the correlation in the uncertainties. The similarity index c_k was calculated using sensitivity coefficients and nuclear data uncertainty covariances. The values of c_k are

found to be 0.985 and higher among the experiments. In the case of the coolant void simulation, it is found to produce a c_k value of 1 when compared with the critical air-cooled experiment. This means the two cases are fully correlated in nuclear data uncertainties. A high degree of similarity among experiments and the application is an indicator for the desired applicability of these benchmark experiments to the application.

Without experimental measurement for the coolant void simulation to be verified, the question to how much confidence one has in the calculated k_{eff} was tackled by the TSURFER module of the S/U TSUNAMI analysis. Given the propagation of nuclear data uncertainty in the calculated k_{eff} values for the benchmark critical experiments, TSURFER adjusts the nuclear data using the method of Generalized Linear Least Squares (GLLS) such that the calculated k_{eff} matches the corresponding experimental value within uncertainties from applicable sources: experimental and nuclear data. From the known experimental uncertainty of moderator purity, k_{eff} experimental uncertainties were extrapolated assuming linear dependence within the studied window of the moderator purity uncertainty. The extrapolated experimental uncertainties and correlations of k_{eff} were input to the TSURFER, along with the nuclear data covariances and correlations. The goodness of final nuclear data adjustments was evaluated by the value of χ^2/dof, which was obtained to be 3.7. Theoretically the χ^2/dof value can be improved by including more of the similar $(Th, Pu)O_2$ experiments, hence increasing the dof value. Once again as an illustrative example, the predicted k_{eff} of the coolant void (reduced coolant density) simulation became 6.36 mk above criticality, as opposed to 7.67 mk before the GLLS nuclear data adjustments. The difference between the 7.67 mk and 6.36 mk was denoted as the application bias and contributed mostly by ^{239}Pu ($\bar{\nu}$), ^{2}H (elastic), and ^{27}Al (n,γ). Similar reductions in k_{eff} bias before and after the GLLS adjustment were also observed in the air-cooled and H_2O-cooled $(Th, Pu)O_2$ cases, from 1.51 mk to 0.24 mk and from 2.3 mk to 1.05 mk respectively. Furthermore, the calculated k_{eff} uncertainties due to nuclear data uncertainties are reduced as well, in response to the adjustment in the nuclear data covariance matrix. They dropped from 6.9 mk to 0.49 mk and lower, very close to the extrapolated k_{eff} experimental uncertainties.

Through the TSUNAMI modules, we have seen some, but not all of the S/U information they can provide. More functions of the TSUNAMI S/U analysis have to be left in future work due to the finite scope of this work. TSUNAMI is a rigorous and effective methodology that addresses the calculated k_{eff} bias due to nuclear data uncertainty. Using the example case of the coolant void simulation, the GLLS method also demonstrated to be quite

useful for predicting the calculated-versus-measured k_{eff} difference for an application system. Since the more practical application is the $(Th, Pu)O_2$ bundles in CANDU-type reactors, the S/U results from the $(Th, Pu)O_2$ benchmark experiments shall provide preliminary data for further TSUNAMI similarity and applicability analyses.

Chapter 7

Future Work

From the present work, we have the k_{eff} results and the associated uncertainties (both before and after GLLS adjustment) of the suite of $(Th, Pu)O_2$ bundle irradiation experiments in ZED-2, whose purpose is to provide benchmark experiments for the future applications of $(Th, Pu)O_2$ in CANDU. Admittedly, the number of available experiments in this work, being four is very small. One consequence of this is the large χ^2/dof generated from the GLLS method. Therefore, the value of benchmark experiments is very obvious. Even with the most powerful computer simulation, an adequate number of benchmark experiments is more important for providing confidence in the computer simulations. In the future work, there should be an emphasis on conducting more $(Th, Pu)O_2$ -related benchmark experiments such that there is a larger number of candidates to choose from for an appropriate suite of benchmark experiments for the complete TSUNAMI similarity and GLLS analyses. Furthermore, the applicability of benchmark experiments to design systems relies on the similarity and correlations in nuclear data uncertainties. In our work, the correlations were found to be extremely high but the materials we wanted to investigate do not contribute significantly to the correlations, because of their small physical presence in the systems. This revelation once again stresses the importance of the benchmark experiment design. Hence, it is proposed that TSUNAMI can be used to assist in the design of benchmark experiments. Their applicability will become the driving force for the design of benchmark experiments that provide experimental measurements for thorium-fueled CANDU reactors.

Once a suite of highly applicable benchmark experiments are designed and conducted, the following considerations are necessary for the development of the thorium-fueld CANDU reactor simulations. First of all, the primary compositions of the $(Th, Pu)O_2$ pellets may not be very different but the $(Th, Pu)O_2$ bundle designs certainly will not be of 36-element and with a hollow centre. In addition, the $(Th, Pu)O_2$ pellets in the ZED-2 experiments are considered fresh fuel. Therefore a burn-up study will be useful for determining the appropriate compositions of the $(Th, Pu)O_2$ fuel in CANDU, such that excessive reactivity can be avoided. Since the main attraction of thorium is its breeding capability for U^{233}, a burn-up study is required to calculate the amount of U^{233} bred and how it will affect the k_{eff} once it is included in the fuel compositions. There are also two approaches worth of investigation: (1)

$(Th, Pu)O_2$ bundles in the entire CANDU core, (2) $(Th, Pu)O_2$ bundles and Natural Uranium (NU) fuels together. Both approaches can further branch out to fuel bundles of different burn-up levels at different zones. The ultimate goal is to determine the fuel bundle and lattice configuration such that the system is able to achieve criticality and have a desirable flux profile.

Compared to the research reactor ZED-2, CANDU is much larger and is a horizontally oriented, heavy water moderated power reactor. It has complex control systems using absorber rods for reactivity control and flux profile shaping. The challenge of simulating a full core CANDU-6 reactor, even more complicated than ZED-2, necessitates the use of 3D reactor physics codes. In this work, KENO was used because it is conveniently part of the TSUNAMI analysis. In Canada, MCNP is the more widely used than KENO, but it has not the built-in sensitivity and uncertainty analysis capabilities at the moment. It is said that sensitivity is dictated by the reactor system, not by the code used to simulate it. Following this assumption, the sensitivity coefficients should be the same whether they are calculated using KENO or MCNP fluxes. In future work, the same suite of ZED-2 $(Th, Pu)O_2$ experiments should be simulated using MCNP to compare the computed k_{eff} biases. It would also be instructive to substitute the GLLS-adjusted nuclear data from TSUNAMI TSURFER, into the MCNP calculations and analyze the effect of the new nuclear data on k_{eff} biases from MCNP.

Finally, the TSUNAMI methodology currently uses ENDF libraries. However, differences exist among different libraries such as ENDF, JEFF and JENDL. It would be interesting to see the extent of their effects on the k_{eff} sensitivity and uncertainty.

Bibliography

Assawaroongruengchota, M. and Marleau, G. (2008). Coolant void reactivity adjustments in advanced CANDU lattices using adjoint sensitivity technique. *Annals of Nuclear Energy*, **35**(3), 377–394.

Bowman, S. M. and Dunn, M. E. (2009). *SCALE Cross-Section Libraries*, volume III of *ORNL/TM-2005/39*, chapter M4, pages M4.2.3–M4.2.4. Oak Ridge National Laboratory, 6th edition.

Broadhead, B. L., C. M. Hopper, R. L. C., and Parks, C. V. (1999). Sensitivity and uncertainty analyses applied to criticality safety validation: Methods development. Report, Oak Ridge National Laboratory.

Brown, F. and Martin, W. R. (2003). Direct sampling of monte carlo flight paths in media with continuously varying cross-sections. In *Nuclear Mathematical and Computational Sciences: A Century in Review, A Century Anew*, Gatlinburg, Tennessee. Los Alamos National Laboratory.

Carter, L. L. and Cashwell, E. D. (1975). *Particle Transport Simulation with the Monte Carlo Method*. ERDA Critical Review Series. National Technical Information Service, Springfield MA.

CNSC (2009). GD-327 Guidance for Nuclear Criticality Safety. Canadian Nuclear Safety Commission Draft Guidance Document. For public consultation.

Dean, V. F. and Blackwood, L. G. (2007). International criticality safety benchmark evaluation project (ICSBEP) guide to the expression of uncertainties. Technical report, Idaho National Laboratory.

Goluoglu, S., Landers, N. F., Petrie, L. M., and Hollenbach, D. F. (2009a). *CSAS5: Control Module for Enhanced Criticality Safety Analysis Sequences with KENOV.a*, volume I of *ORNL/TM-2005/39*, chapter C5. Oak Ridge National Laboratory, 6th edition.

Goluoglu, S., Hollenbach, D. F., and Petrie, L. M. (2009b). *WORKER: SCALE System Module for Creating and Modifying Working Format Libraries*, volume II of *ORNL/TM-2005/39*, chapter F20. Oak Ridge National Laboratory, 6th edition.

Hagberg, E. (2009). ZED-2 side view. Private communication via email. (Reactor Physics Branch, AECL).

Hébert, A. (2009). *Applied Reactor Physics.* Presses Internationales Polytechnique.

Horwedel, J. E. and Bowman, S. M. (2000). KENO3D visualization tool for KENO V.a and KENO-VI geometry models. Technical report, Oak Ridge National Laboratory.

IAEA, editor (2005). *Thorium fuel cycle - Potential benefits and challenges*, Vienna, Austria. Division of Nuclear Fuel Cycle and Waste Technology, IAEA. IAEA-TECDOC-1450.

Irving, D. C. (1971). The adjoint boltzmann equation and its simulation by monte carlo. *Nuclear Engineering and Design*, **15**, 273–292.

Jones, R. T. (1984). Experiments performed in ZED-2 in support of the irradiation of $(Th, Pu)O_2$ fuel (BDL-422) in NRU. Technical report, Atomic Energy of Canada Limited, Chalk River Nuclear Laboratories.

Lewins, J. (1965). *Importance, The Adjoint Function.* Pergamon Press, first edition.

Lewis, E. E. and Miller, W. F. J. (1984). *Computational Methods of Neutron Transport.* A Wiley-Interscience Publication, John Wiley & Sons.

Petrie, L. M., Williams, M. L., and Hollenbach, D. F. (2009). *Miscellaneous SCALE Utility Modules*, volume III of *ORNL/TM-2005/39*, chapter M17, pages M17.4.1–M.17.4.4. Oak Ridge National Laboratory, 3rd edition.

Rearden, B. T. (2004). Perturbation theory eigenvalue sensitivity analysis with monte carlo techniques. *Nuclear Science and Engineering*, **146**, 367–382.

Rearden, B. T. and Jessee, M. A. (2009). *TSUNAMI Utility Modules*, volume III of *ORNL/TM-2005/39*, chapter M18. Oak Ridge National Laboratory, 6th edition.

Rozon, D. (1996-1998). Introduction to nuclear reactor kinetics. Éditions de l'École Polytechnique de Montréal. Lecture notes.

Spanier, J. and Gelbard, E. M. (1969). *Monte Carlo Principles and Neutron Transport Problems.* Addison-Wesley Publishing Company.

Wagschal, J. J. and Yeivin, Y. (1980). The significance of lagrange multipliers in cross-section adjustment. Technical report, Oak Ridge National Laboratory. Research sponsored by Reactor Research and Technology Division

under Union Carbide Corporation contract W-7405-eng-26 with the U.S. Department of Energy.

Williams, M. L. (2007). Sensitivity and uncertainty analysis for eigenvalue-difference responses. *Nuclear Science and Engineering*, **155**, 18–36.

Williams, M. L. and Hollenbach, D. F. (2009). *PMC: A Program to Produce Multigroup Cross Sections Using Pointwise Energy Spectra from CENTRM*, volume II, chapter F19, pages F.19.3.1–F.19.3.5. Oak Ridge National Laboratory, 6th edition.

Williams, M. L., Broadhead, B. L., and Parks, C. V. (2001). Eigenvalue sensitivity theory for resonance-shielded cross sections. *Nuclear Science and Engineering*, **138**, 177–191.

Williams, M. L., Asgari, M., and Hollenbach, D. F. (2009a). *CENTRM: A One-Dimensional Neutron Transport Code for Computing Pointwise Energy Spectra*, volume II of *ORNL/TM-2005/39*, chapter F18. Oak Ridge National Laboratory, 6th edition.

Williams, M. L., Broadhead, B. L., Jessee, M. A., and Wagschal, J. J. (2009b). *TSURFER: An Adjustment Code to Determine Biases and Uncertainties in Nuclear System Responses by Consolidating Differential Data and Benchmark Integral Experiments*, volume III of *ORNL/TM-2005/39*, chapter M21, pages M21.4.4–M21.4.13. Oak Ridge National Laboratory, 6th edition.